Trifluoromethylation of Electron-Rich Alkenyl Iodides with Fluoroform-Derived "Ligandless" $CuCF_3$

Jordi Mestre,[†,‡] Anton Lishchynskyi,[‡] Sergio Castillón,[†] and Omar Boutureira*[,†]

[†]*Departament de Química Analítica i Química Orgànica, Universitat Rovira i Virgili chMarcel·lí Domingo 1, 43007 Tarragona, Spain*
[‡]*Institute of Chemical Research of Catalonia (ICIQ), The Barcelona Institute of Science and Technology (BIST), Av. Països Catalans 16, 43007 Tarragona, Spain*

**E-mail: omar.boutureira@urv.cat*

Table of Contents

1. Optimization of the trifluoromethylation of 3-iodoindole 1q

General procedure: in a glove box, the corresponding $CuCF_3$-nHF reagent solution in DMF (0.67 mL, 0.2 mmol) was added to 3-iodoindole **1q** (24 mg, 0.2 mmol). The vial was sealed, brought out of the glove box, and stirred overnight at the temperature indicated. The reaction was quenched by extraction with Et_2O/H_2O. The solvent was evaporated under reduced pressure and the crude analyzed by ^1H NMR to determine the hydrodehalogenation/trifluoromethylation (H/CF_3) ratio. **Note:** When old reagent batches were used, more hydrodehalogenated product was produced.

Table S1. Optimization of the trifluoromethylation of 3-iodoindole **1q** and control experiments

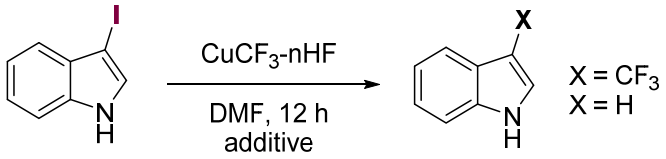

Entry[a]	$CuCF_3$-nHF	$Et_3N{\cdot}3HF$ ("extra" equiv)[b]	Additive (equiv)	*T* [ºC]	Conv. [%][c]	H/CF_3 ratio[d]
1[e]	$CuCF_3$	–	–	rt	>99	0.05
2[e]	$CuCF_3$	–	–	35	>99	0.04
3	$CuCF_3$-0.3HF	0.3	–	rt	>99	0.12
4	$CuCF_3$-0.3HF	0.3	–	35	>99	0.11
5	$CuCF_3$-0.6HF	0.6	–	rt	>99	0.19
6	$CuCF_3$-0.6HF	0.6	–	35	>99	0.17
7[e,f]	$CuCF_3$	–	–	rt	>99	0.06
8	–	–	CuI (1)	rt	<1	–
9[g]	–	–	Et_3N (1.2)	rt	<1	–

[a]Reactions were performed in a sealed vial with $CuCF_3$-nHF (1 equiv) in DMF and 3-iodoindole **1q** (1 equiv) unless otherwise indicated. [b]mol $Et_3N{\cdot}3HF$/mol CuCl. [c]Determined by ^1H NMR of the crude reaction mixture. [d]Determined by integration of H-5 protons. [e]So-called stabilized $CuCF_3$. [f]Reaction conducted in the darkness. [g]Reaction analyzed after 6 h.

Discussion: hydrodehalogenation processes can be promoted/favored by the addition of *N*-containing bases and/or phosphines,[1] which are able to stabilize iodonium species, by the presence of potential SET catalysts such as CuX salts[2] (produced during the course of the trifluoromethylation with $CuCF_3$), or initiated/promoted by light-driven processes. Moreover,

the presence of proton abstraction sources (including polar protic solvents) favors the hydrodehalogenation reaction and, although DMF has proven to be a good proton source,[3] the effect of HF has to be considered. Table S1 shows the hydrodehalogenation/trifluoromethylation (H/CF_3) ratio is directly proportional to the increasing amount of $Et_3N{\cdot}3HF$ (TREAT-HF) whereas the temperature has a negligible effect (entries 1–6). The formation of hydrodehalogenation product is not appreciably favored by exposure to light (entries 1 *vs.* 7) and is not produced when 3-iodoindole **1q** is stirred alone in the presence of CuI or Et_3N (entries 8 and 9).

2. Cu(I) coordination of 3-iodoindole 1q

Trifluoromethylation of unprotected 3-iodoindoles proceeds under milder conditions as compared to those with 2-iodoglycals since no additives neither heating is required. Striking differences were also observed with such substrates including an abnormal color-change to a greenish-blue immediately after mixing. Nonetheless, the most noteworthy remark was probably noticed by the *in situ* ^{19}F NMR monitoring of the reaction course (Scheme S1). Two signals appeared at –56.5 ppm, assigned to 3-(trifluoromethyl)indole **2q** and –54.3 ppm, tentatively assigned to a transient intermediate exhibiting N–Cu coordination that after quenching with water, converged to the same peak at –56.5 ppm. Meaningfully, only one signal was observed in the reaction with the corresponding *N*-Boc indole **2u**, which indeed reacted noticeably slower. The improved reaction rate resembles the enhancement observed during the trifluoromethylation of iodoarenes due to the *ortho*-effect[4] although in this case *via* a completely different mechanism. Collectively, the apparent N–Cu coordination probably enhances the trifluoromethylation rate by lowering the electronic density of the indole and increasing that of the metallic center, thus, facilitating the oxidative addition.

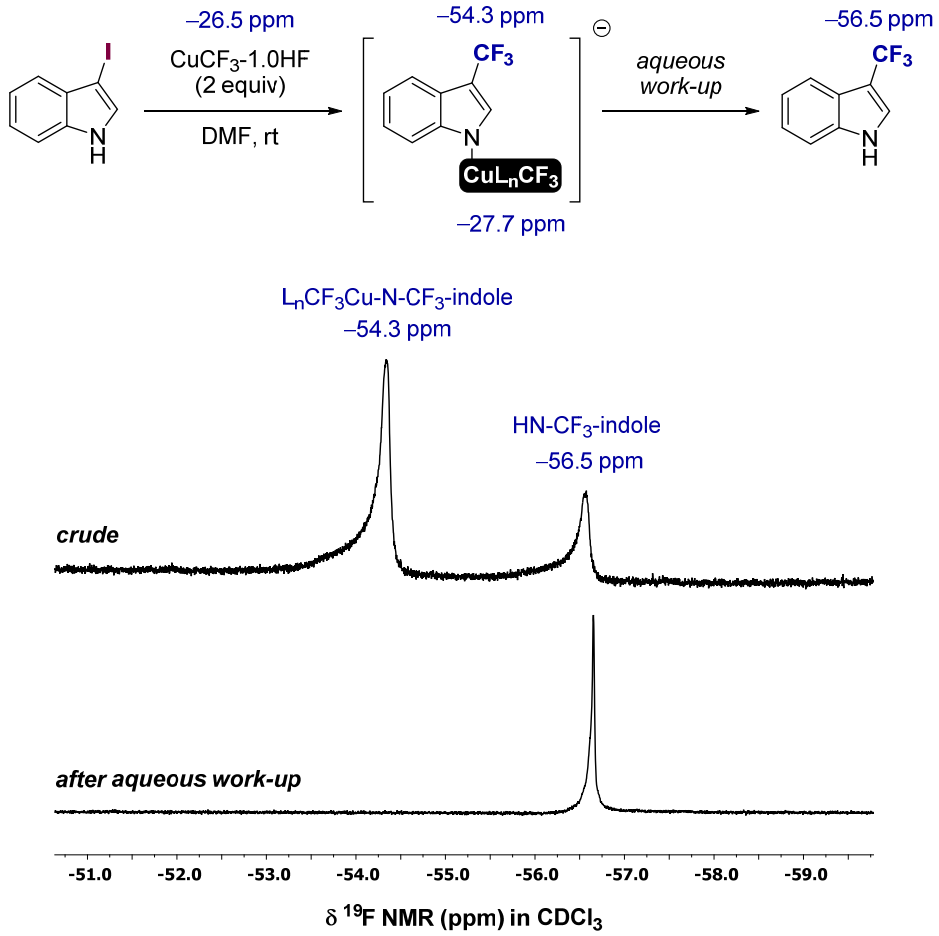

Scheme S1. Selected region of the ^{19}F NMR spectra showing Cu(I) coordination of unprotected 3-iodoindole **1q**

3. NMR Spectra

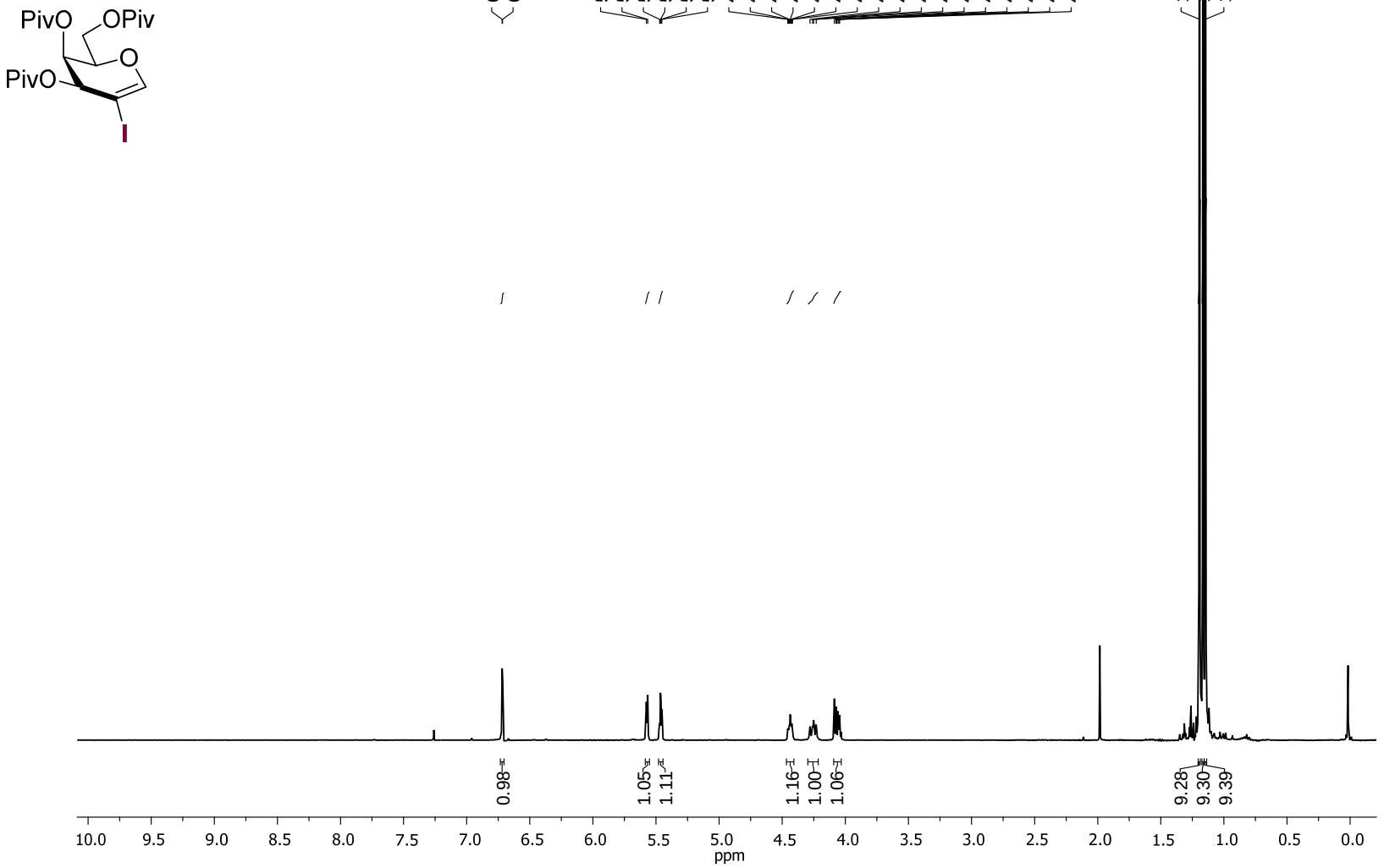

Figure S1. ^{1}H NMR ($CDCl_3$, 400 MHz) of **1c**

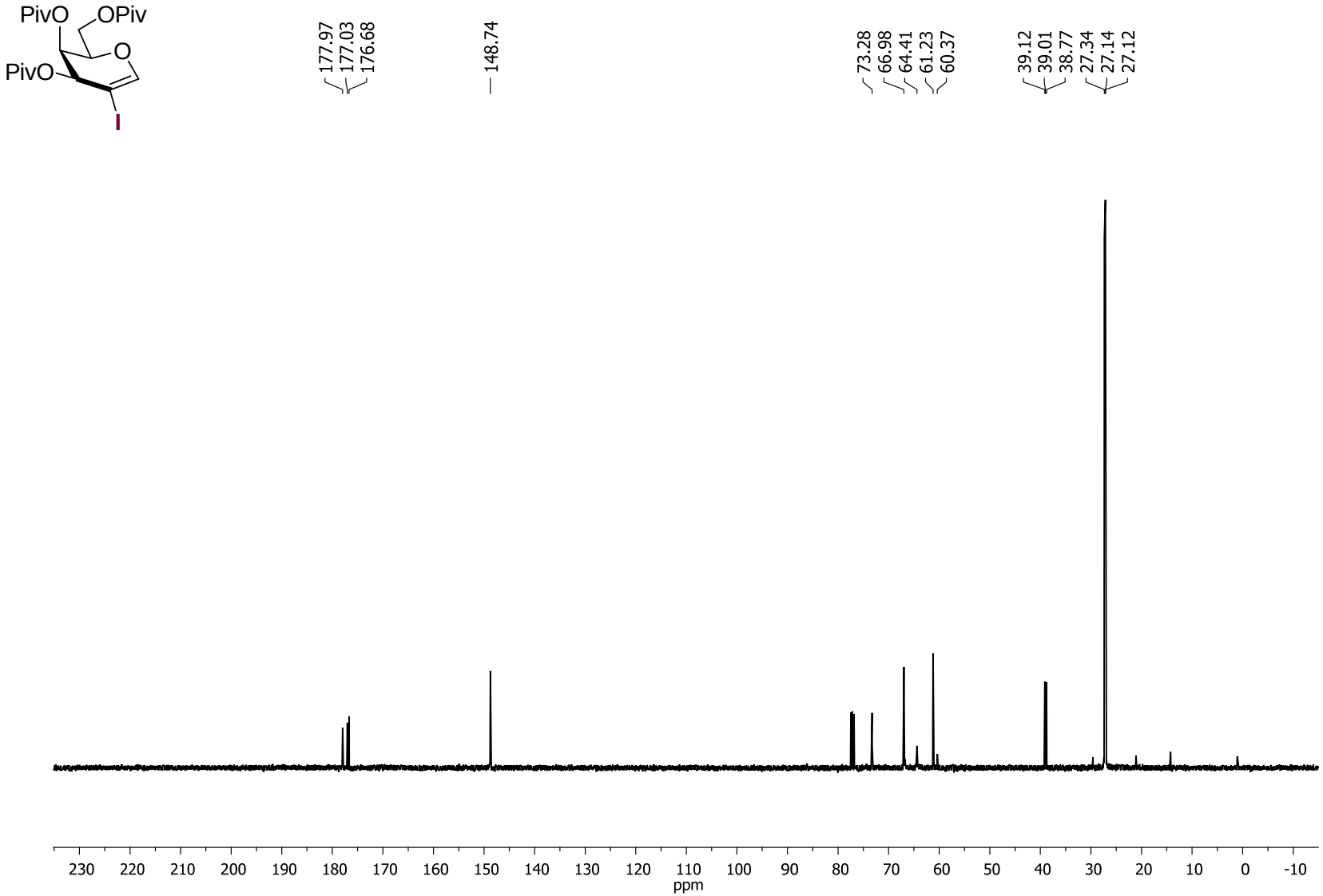

Figure S2. ^{13}C NMR ($CDCl_3$, 100.6 MHz) of **1c**

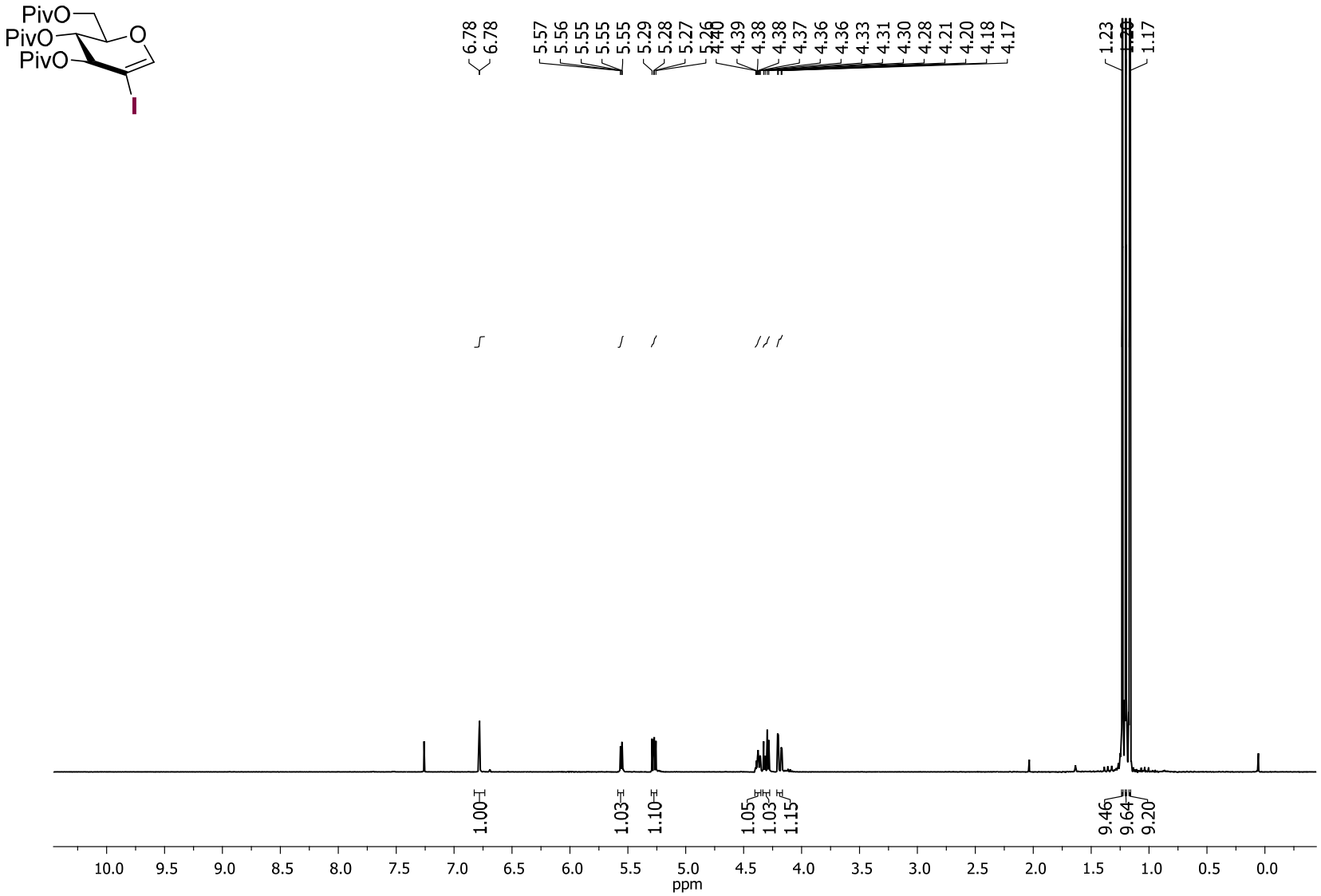

Figure S3. ^{1}H NMR ($CDCl_3$, 400 MHz) of **1d**

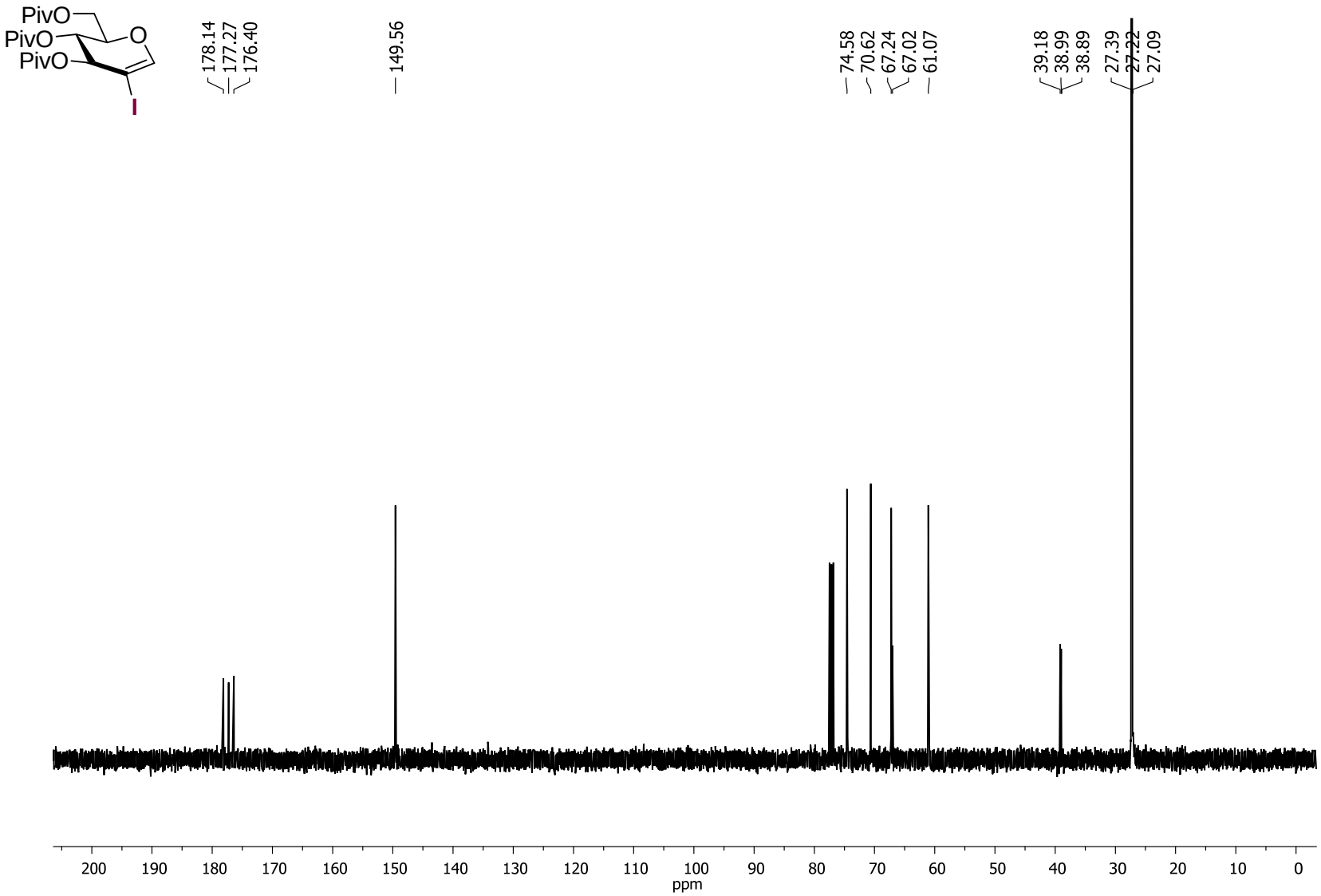

Figure S4. ^{13}C NMR ($CDCl_3$, 100.6 MHz) of **1d**

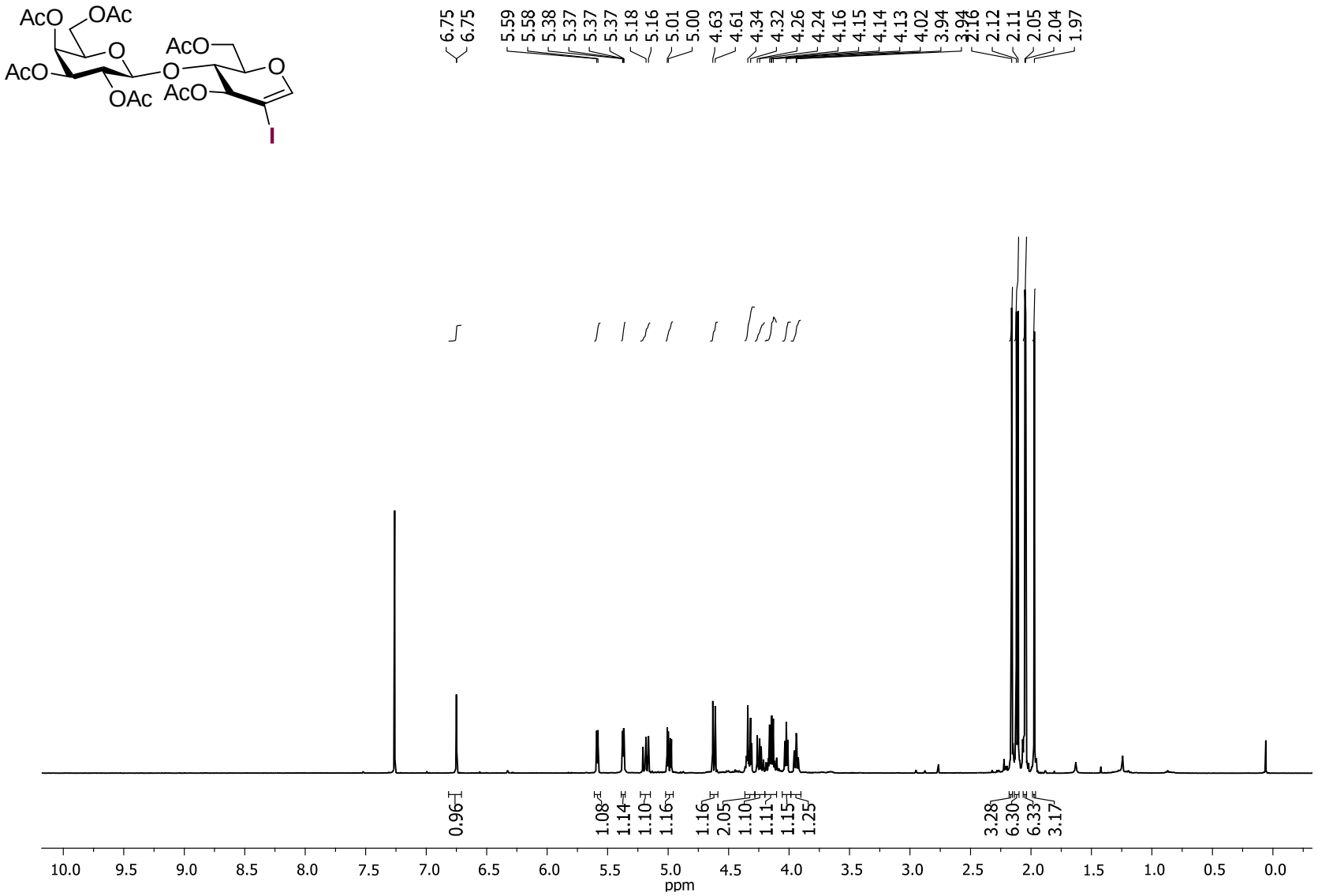

Figure S5. ^{1}H NMR ($CDCl_3$, 400 MHz) of **1h**

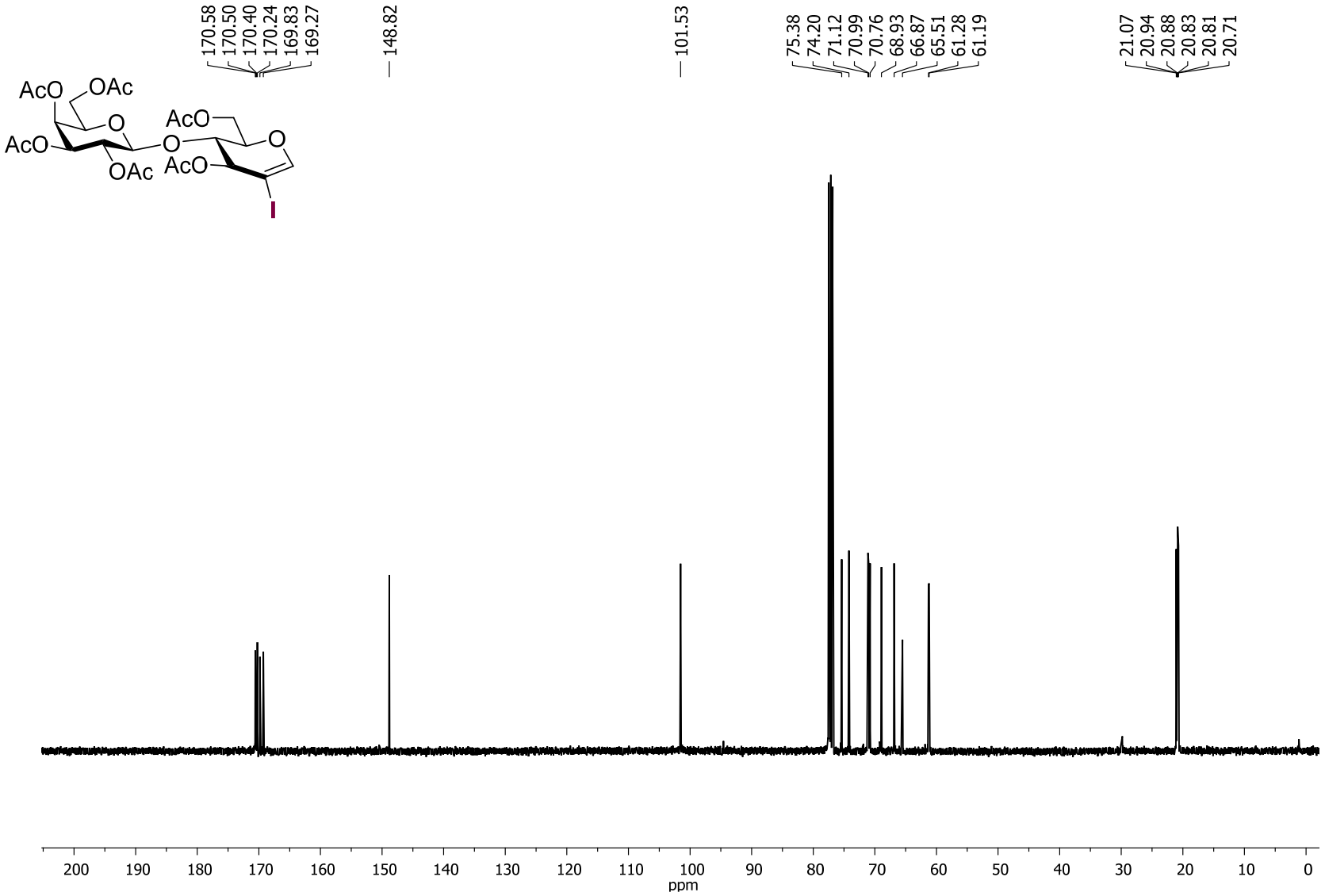

Figure S6. ^{13}C NMR ($CDCl_3$, 100.6 MHz) of **1h**

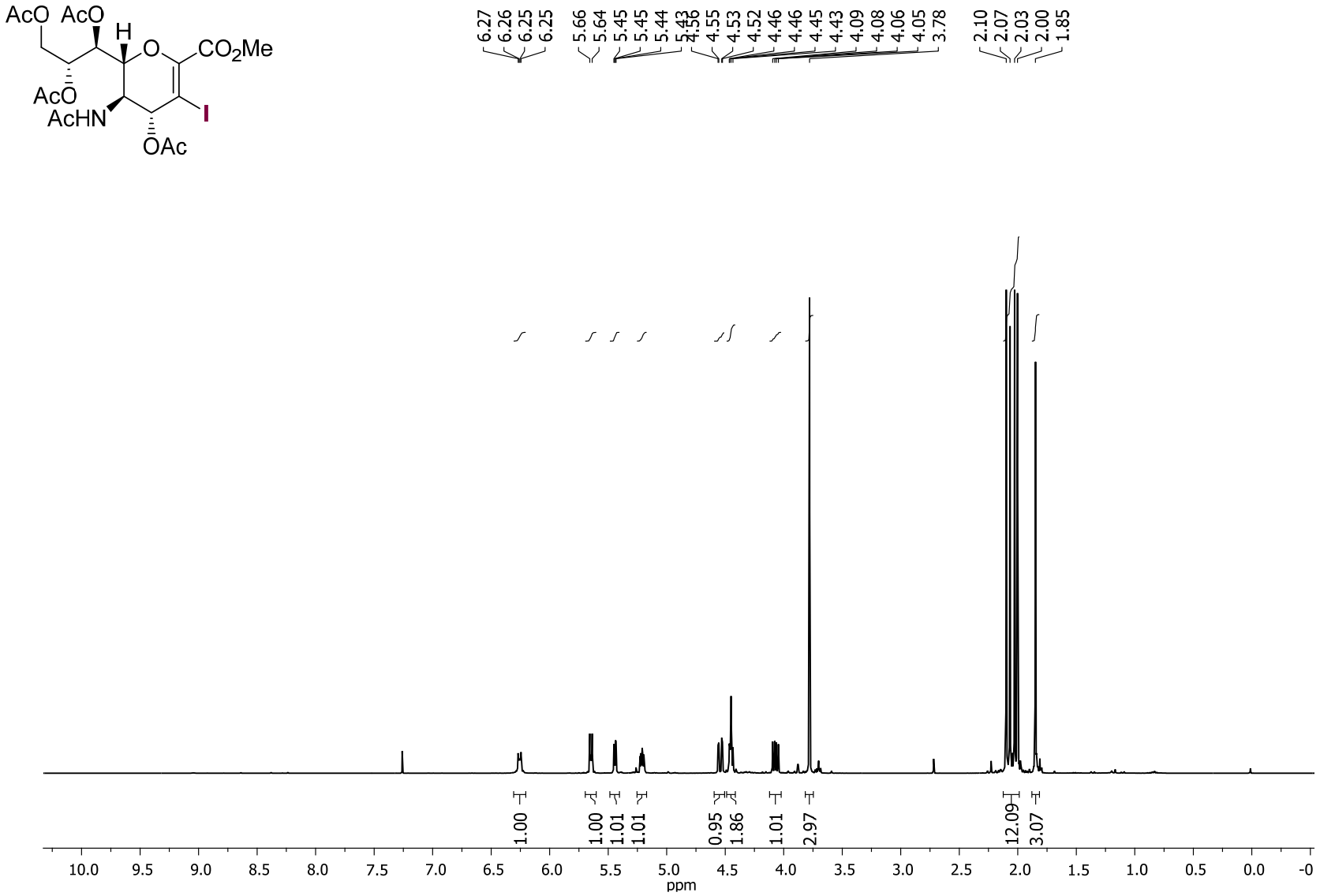

Figure S7. ^{1}H NMR ($CDCl_3$, 400 MHz) of **1i**

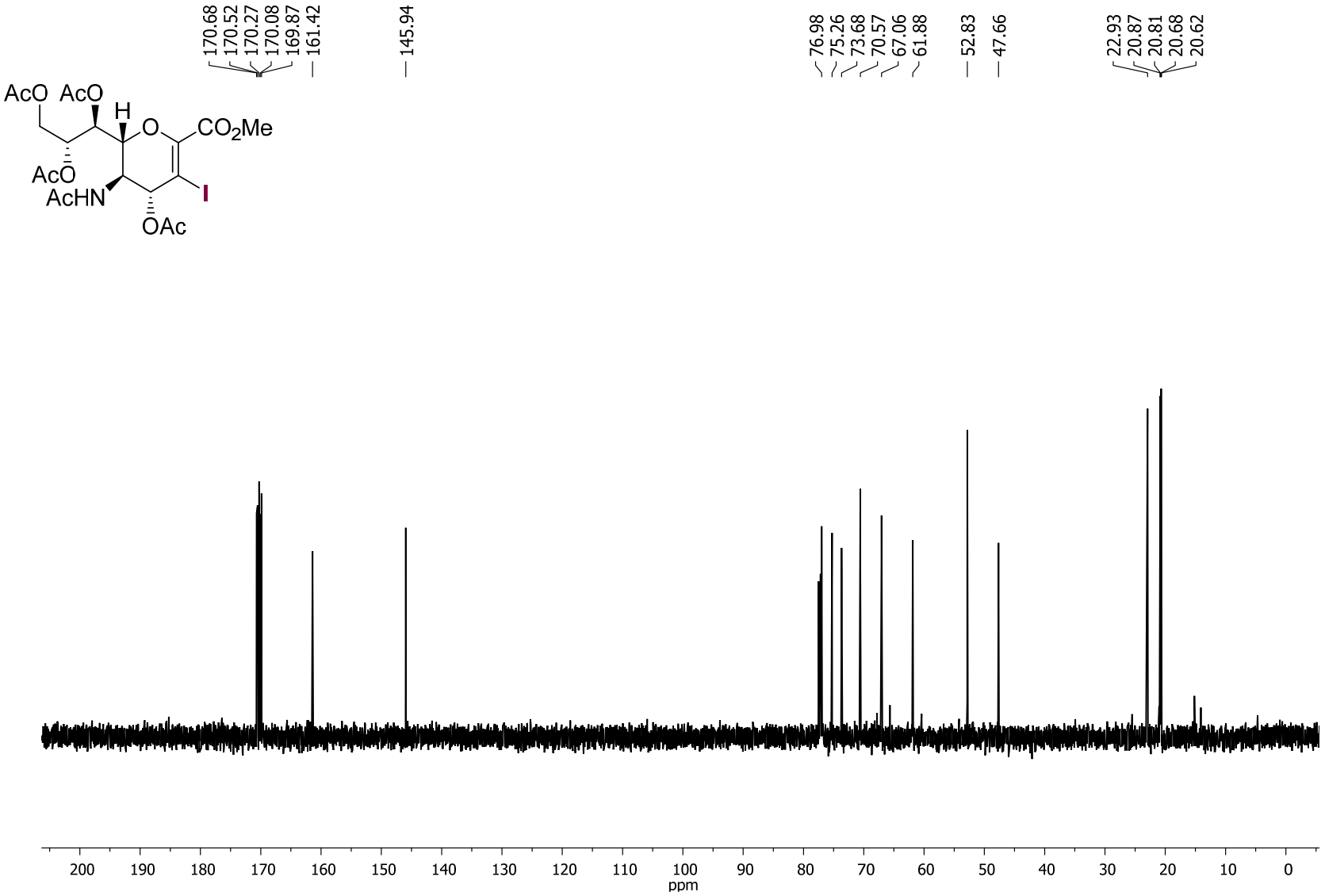

Figure S8. ^{13}C NMR ($CDCl_3$, 100.6 MHz) of **1i**

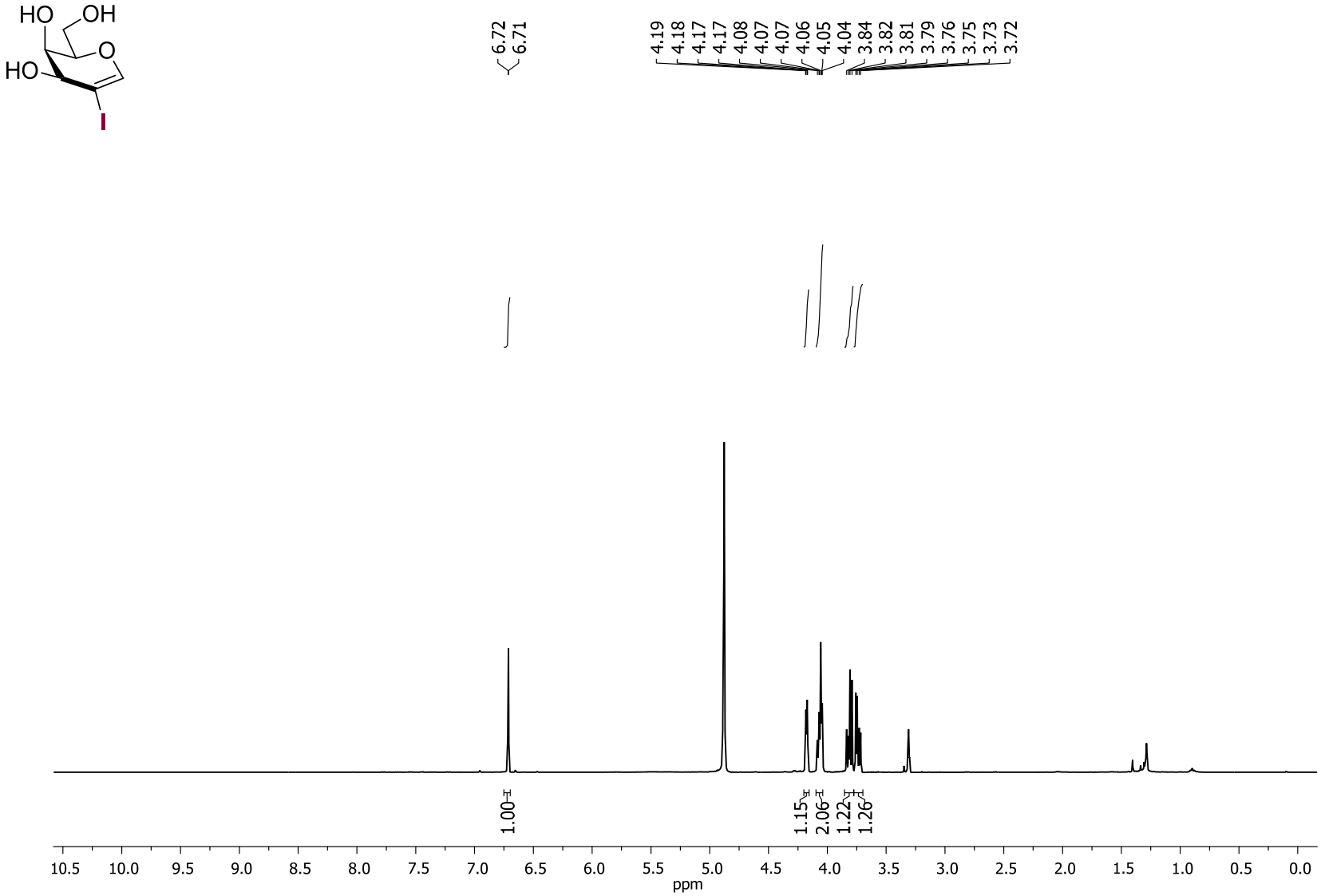

Figure S9. ^{1}H NMR (CD_3OD, 400 MHz) of **1j**

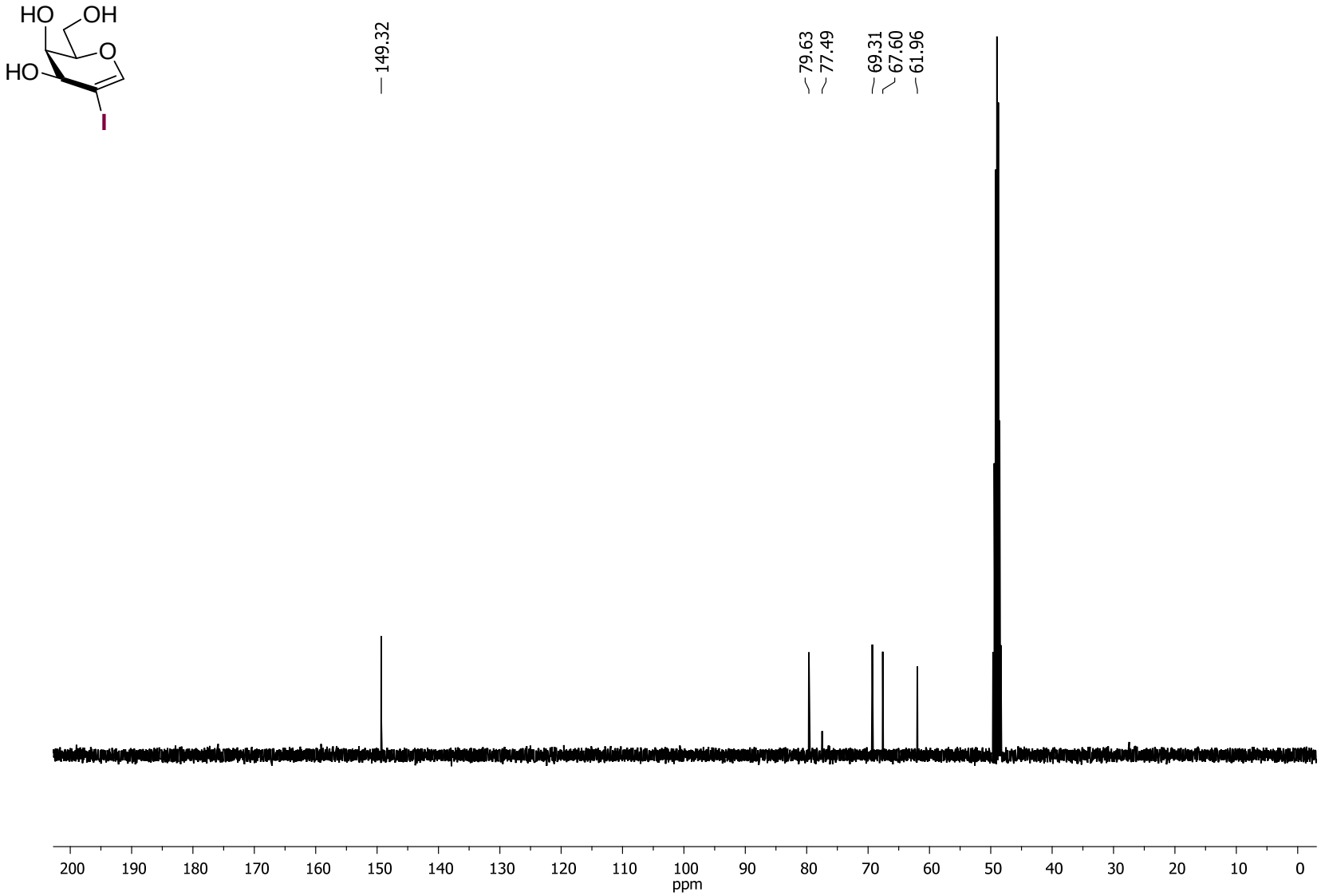

Figure S10. ^{13}C NMR (CD_3OD, 100.6 MHz) of **1j**

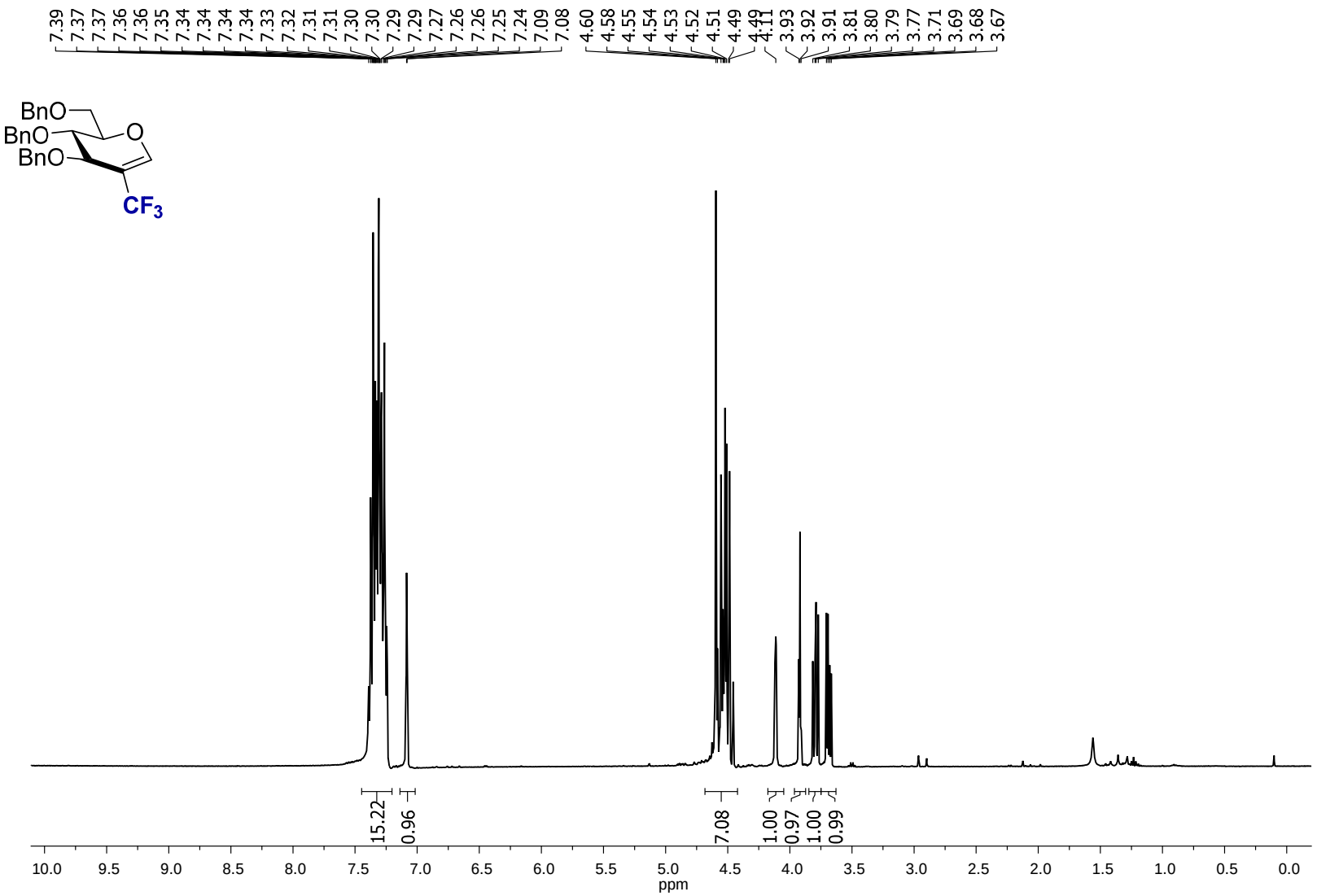

Figure S11. ^{1}H NMR ($CDCl_3$, 400 MHz) of **2a** *from the crude reaction mixture*

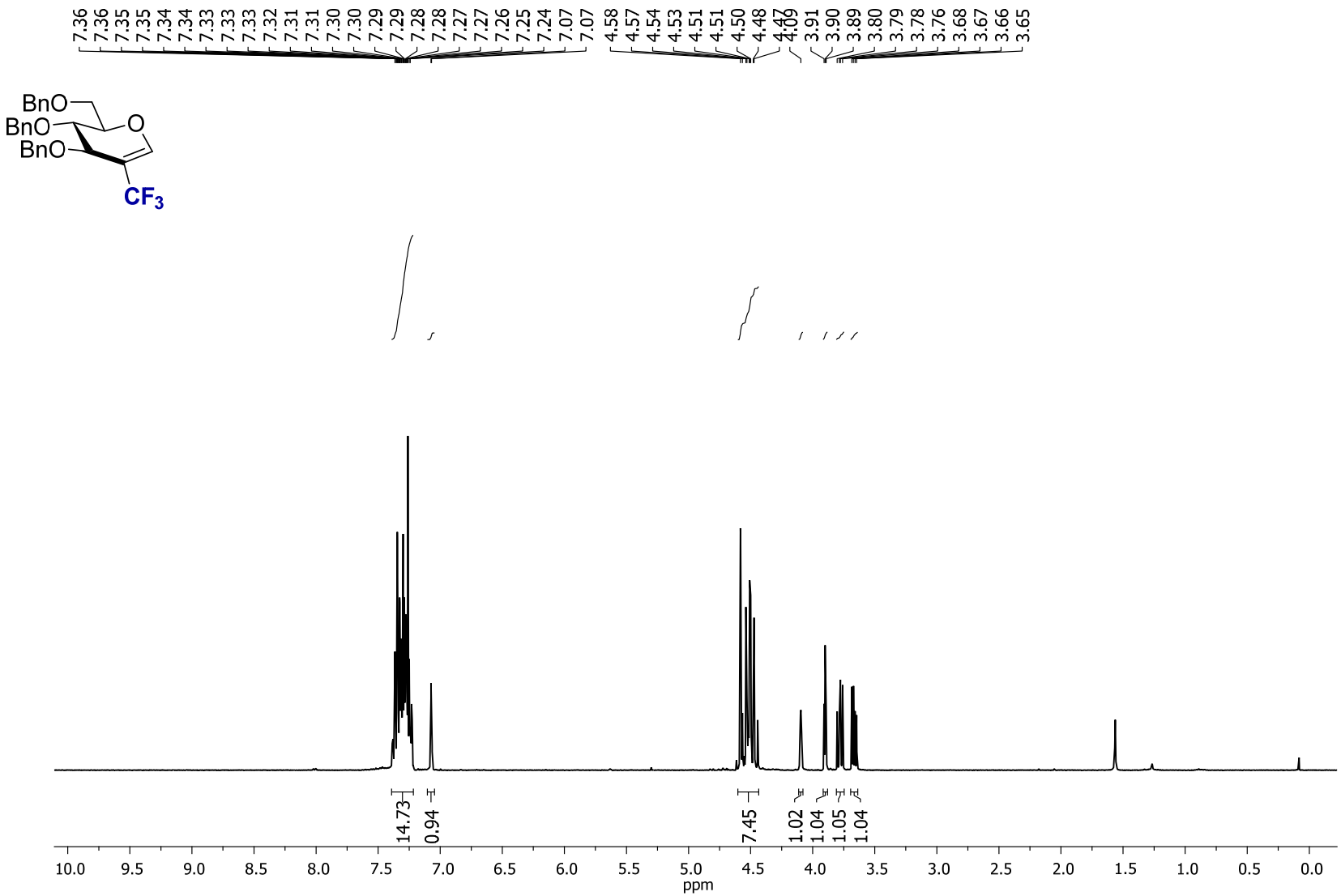

Figure S12. ^{1}H NMR ($CDCl_3$, 400 MHz) of *purified* **2a**

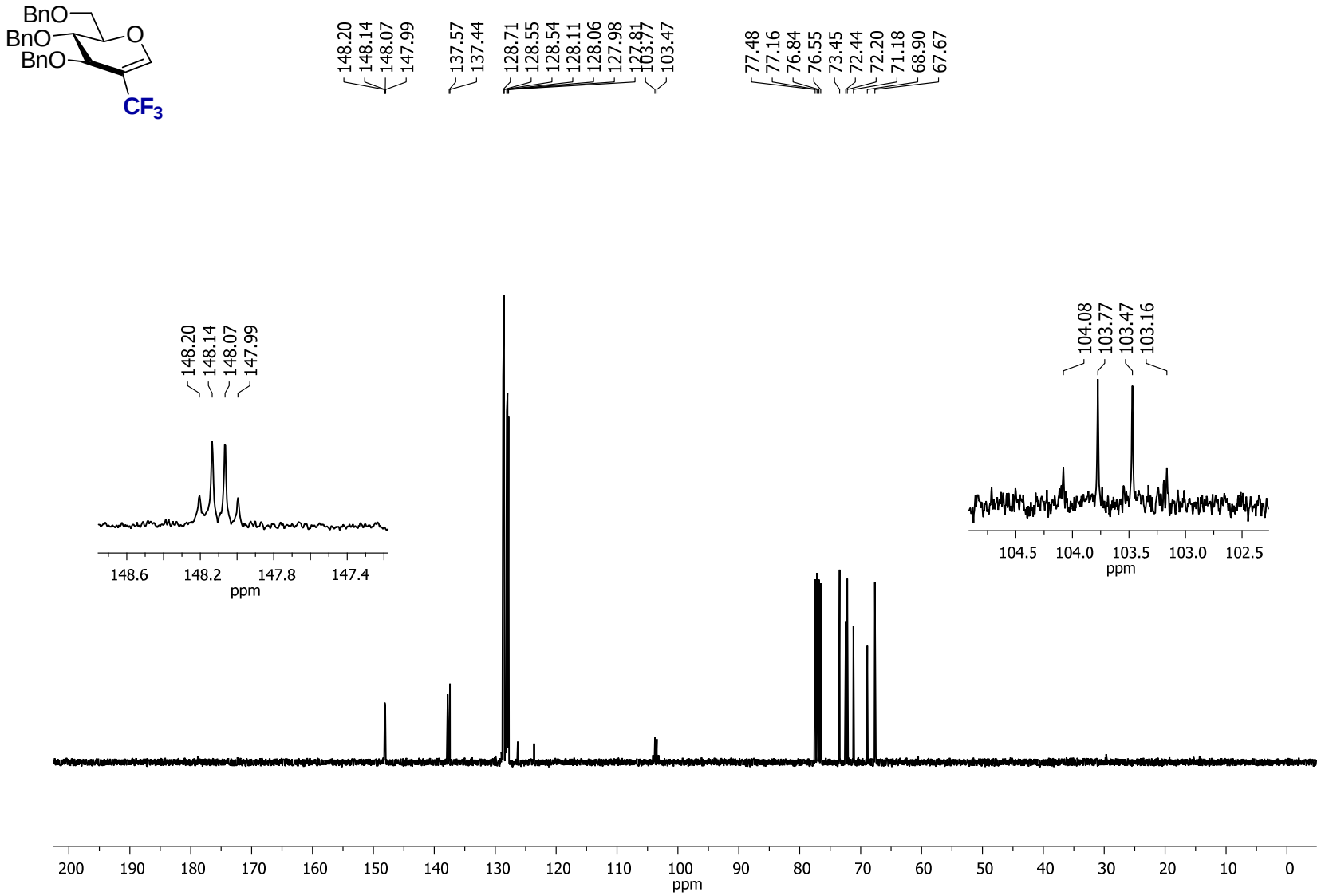

Figure S13. ^{13}C NMR ($CDCl_3$, 100.6 MHz) of **2a**

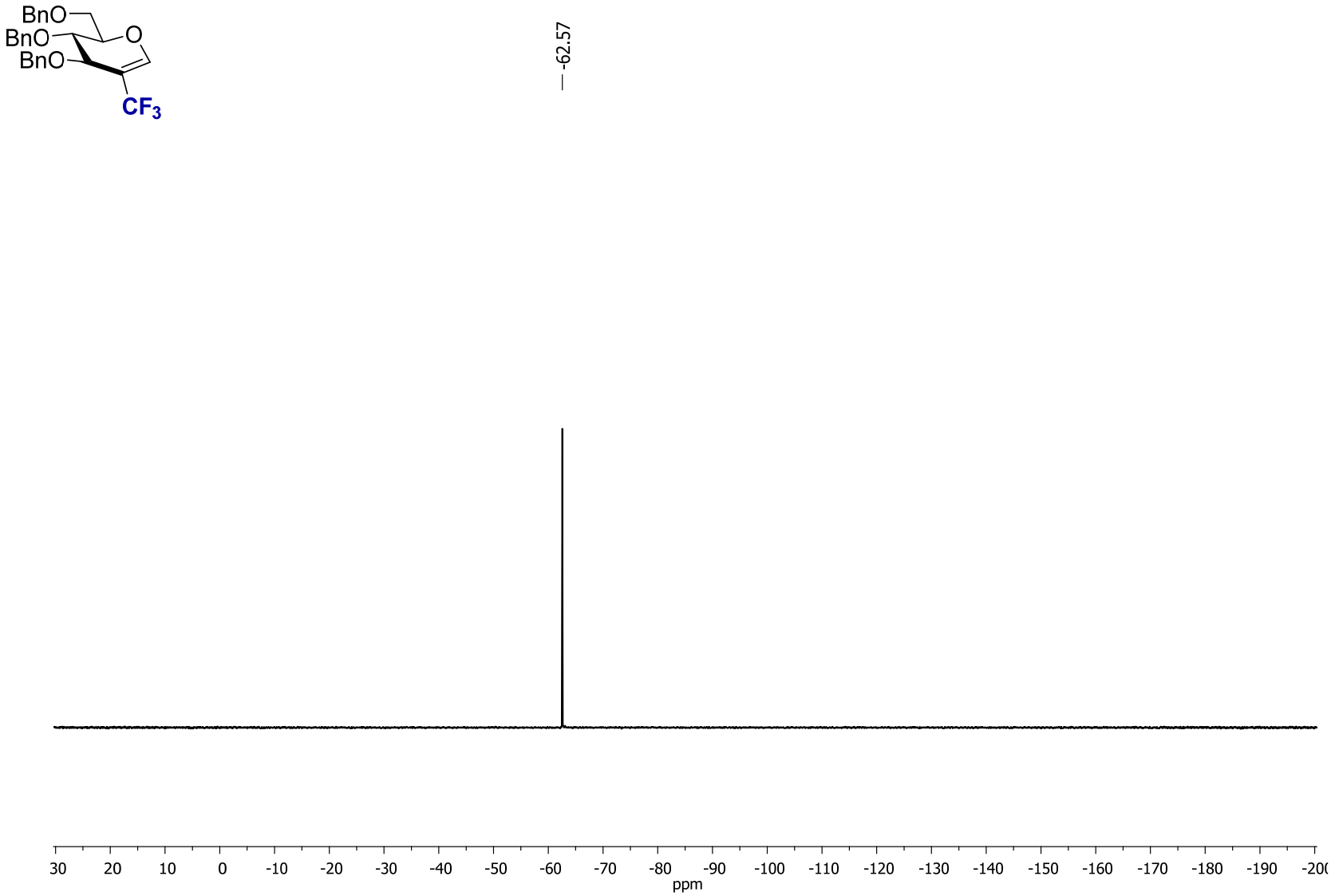

Figure S14. ^{19}F NMR ($CDCl_3$, 376.5 MHz) of **2a**

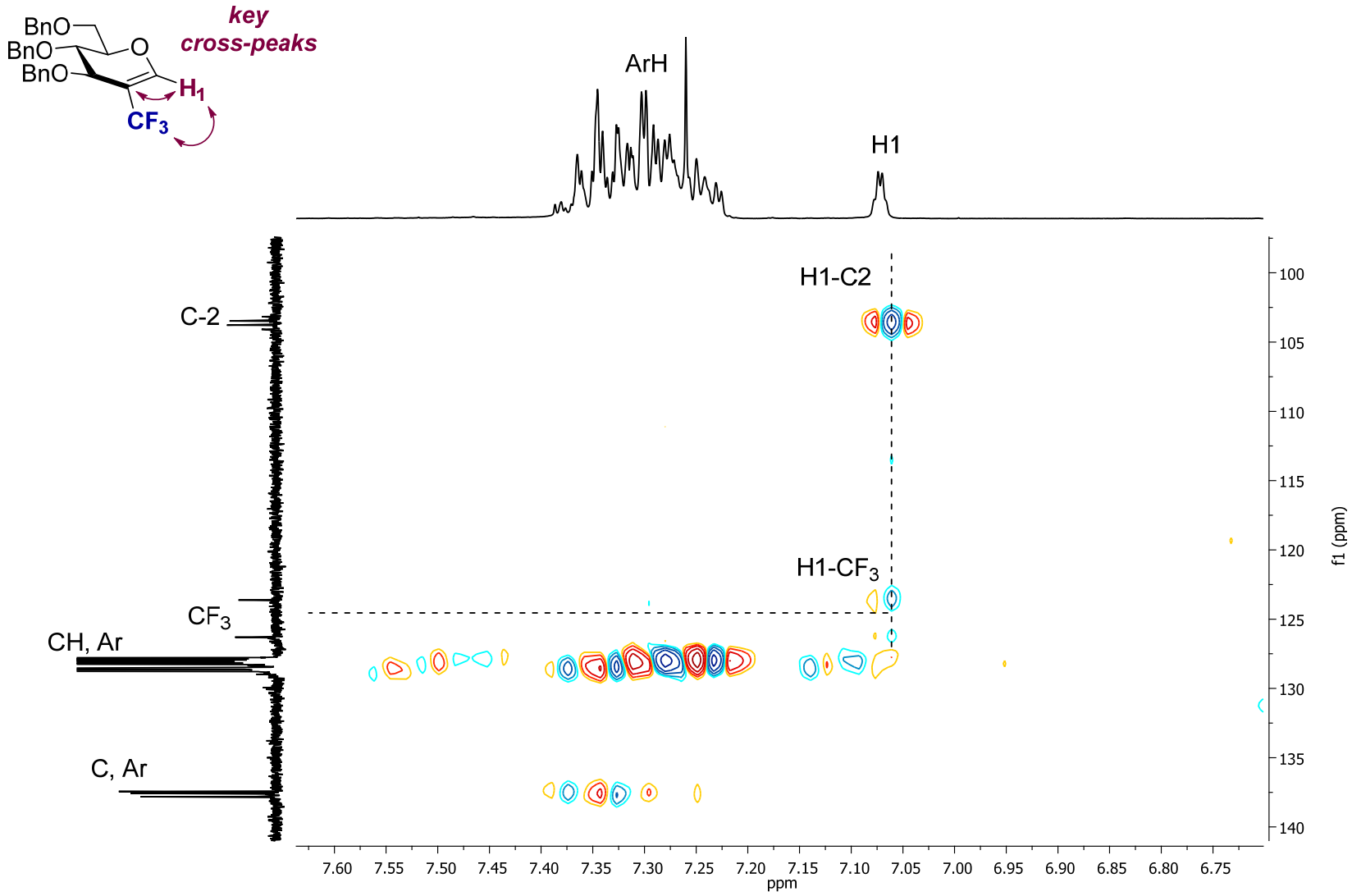

Figure S15. Selected region of the 2D HMBC of **2a** in $CDCl_3$

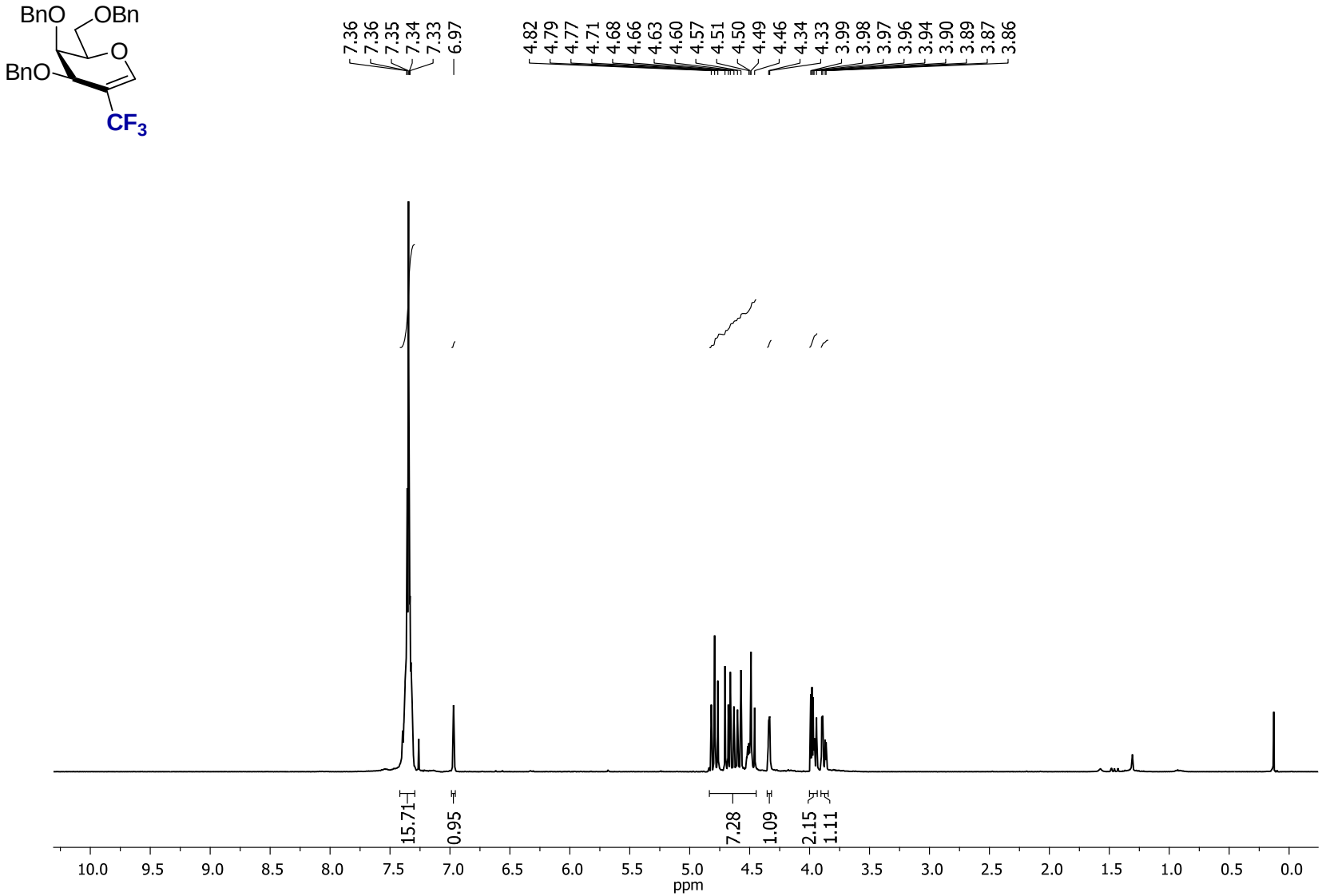

Figure S16. ^{1}H NMR ($CDCl_3$, 400 MHz) of **2b**

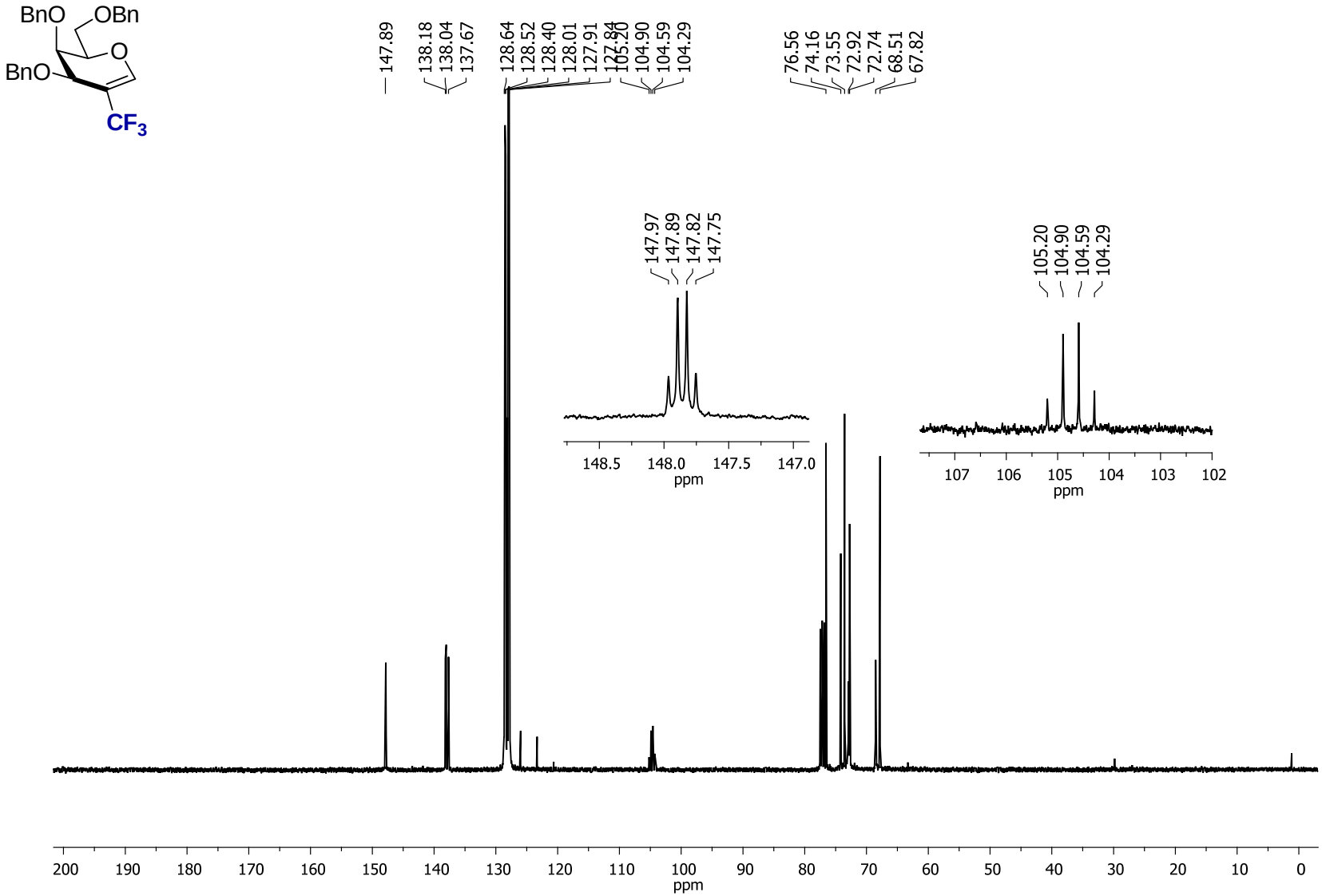

Figure S17. ^{13}C NMR ($CDCl_3$, 100.6 MHz) of **2b**

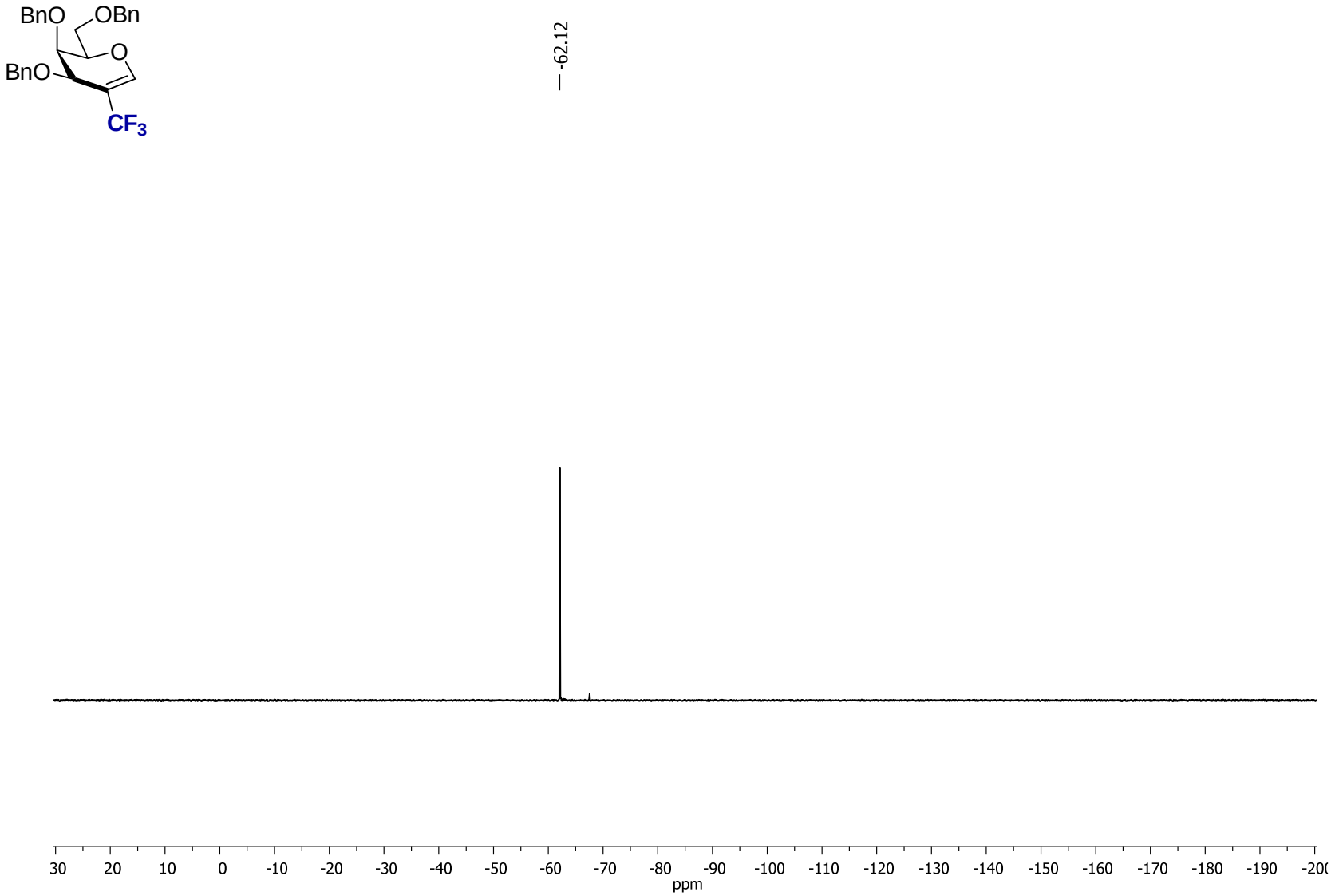

Figure S18. ^{19}F NMR ($CDCl_3$, 376.5 MHz) of **2b**

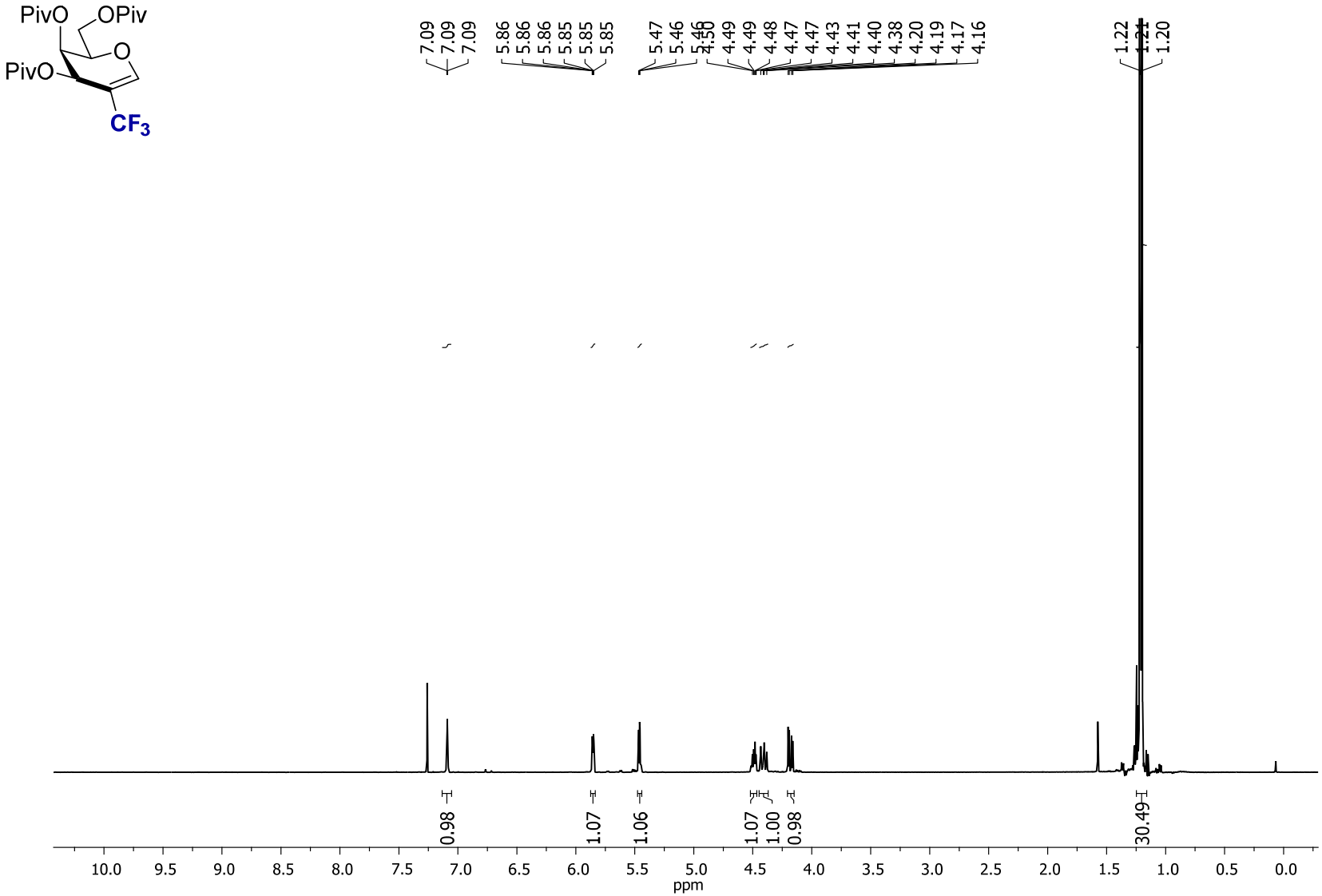

Figure S19. ^{1}H NMR ($CDCl_3$, 400 MHz) of **2c**

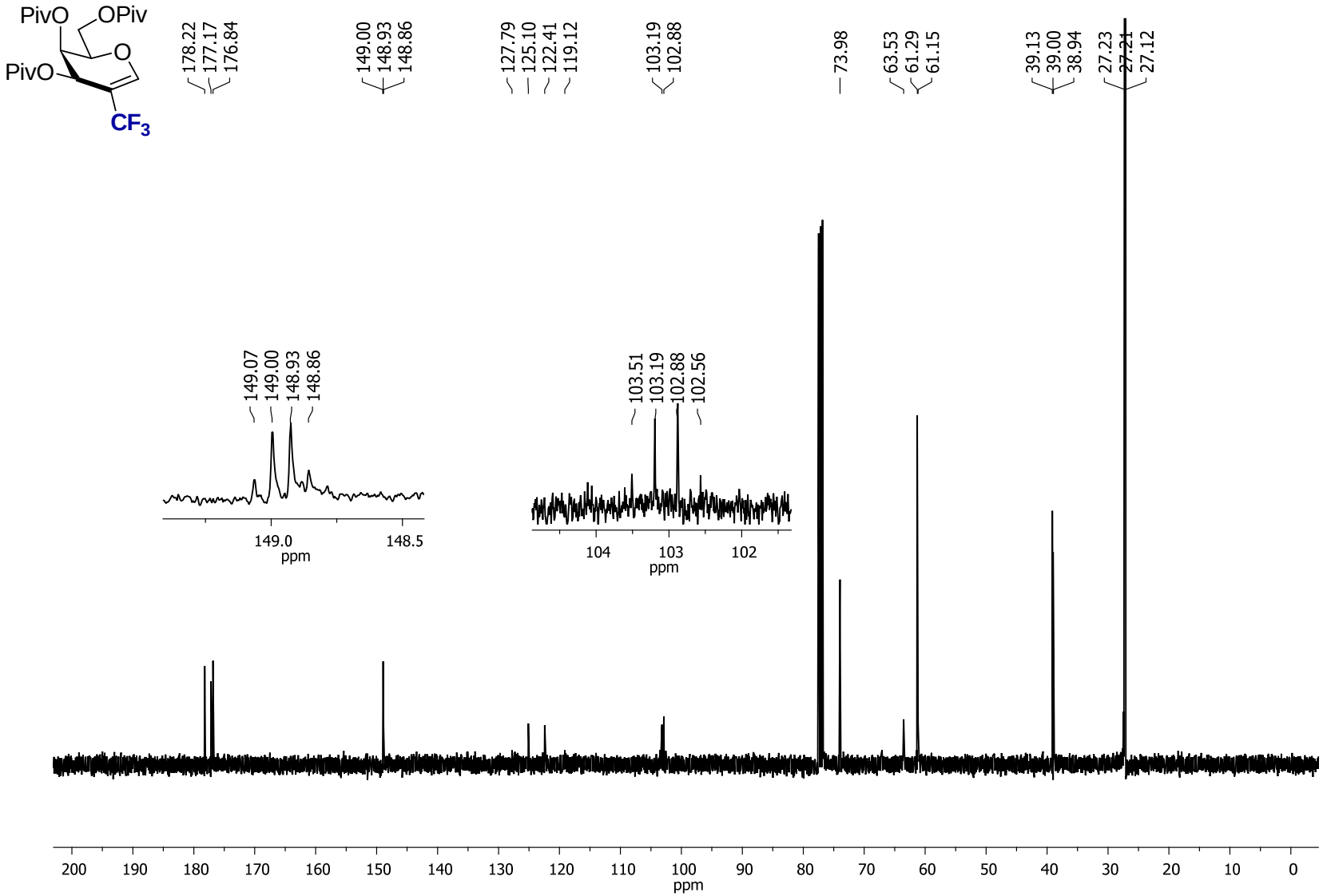

Figure S20. ^{13}C NMR ($CDCl_3$, 100.6 MHz) of **2c**

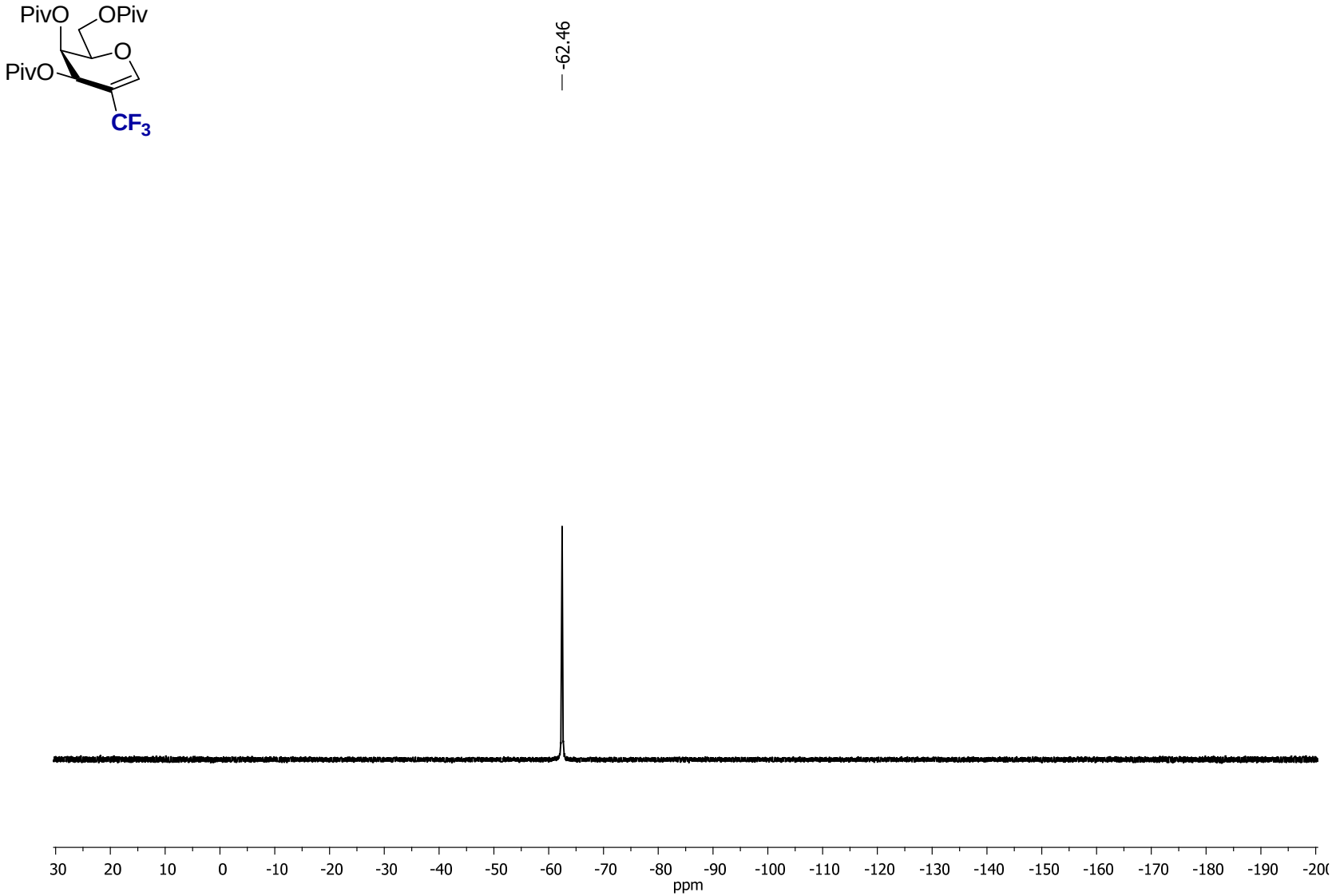

Figure S21. ^{19}F NMR ($CDCl_3$, 376.5 MHz) of **2c**

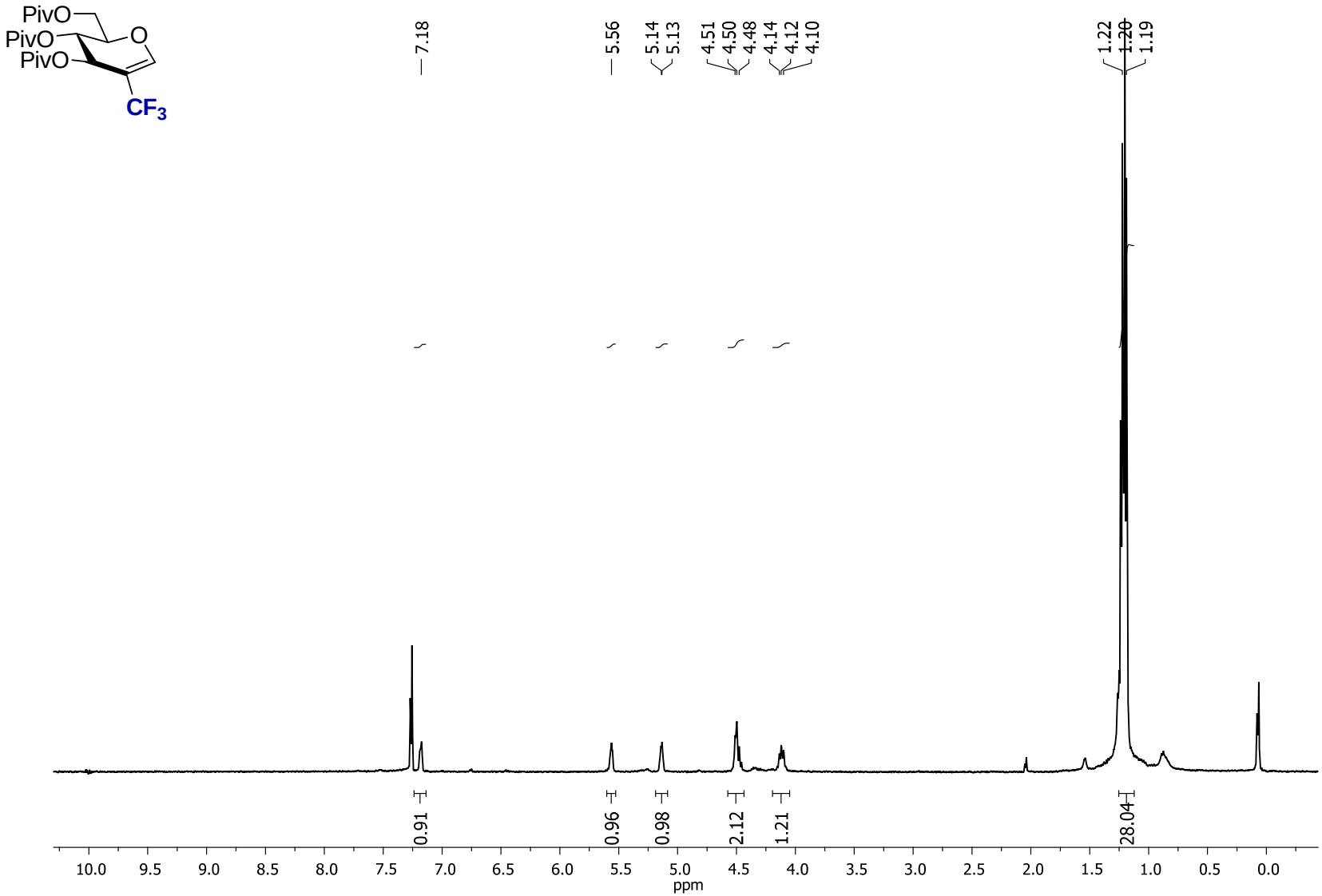

Figure S22. ^{1}H NMR ($CDCl_3$, 400 MHz) of **2d**

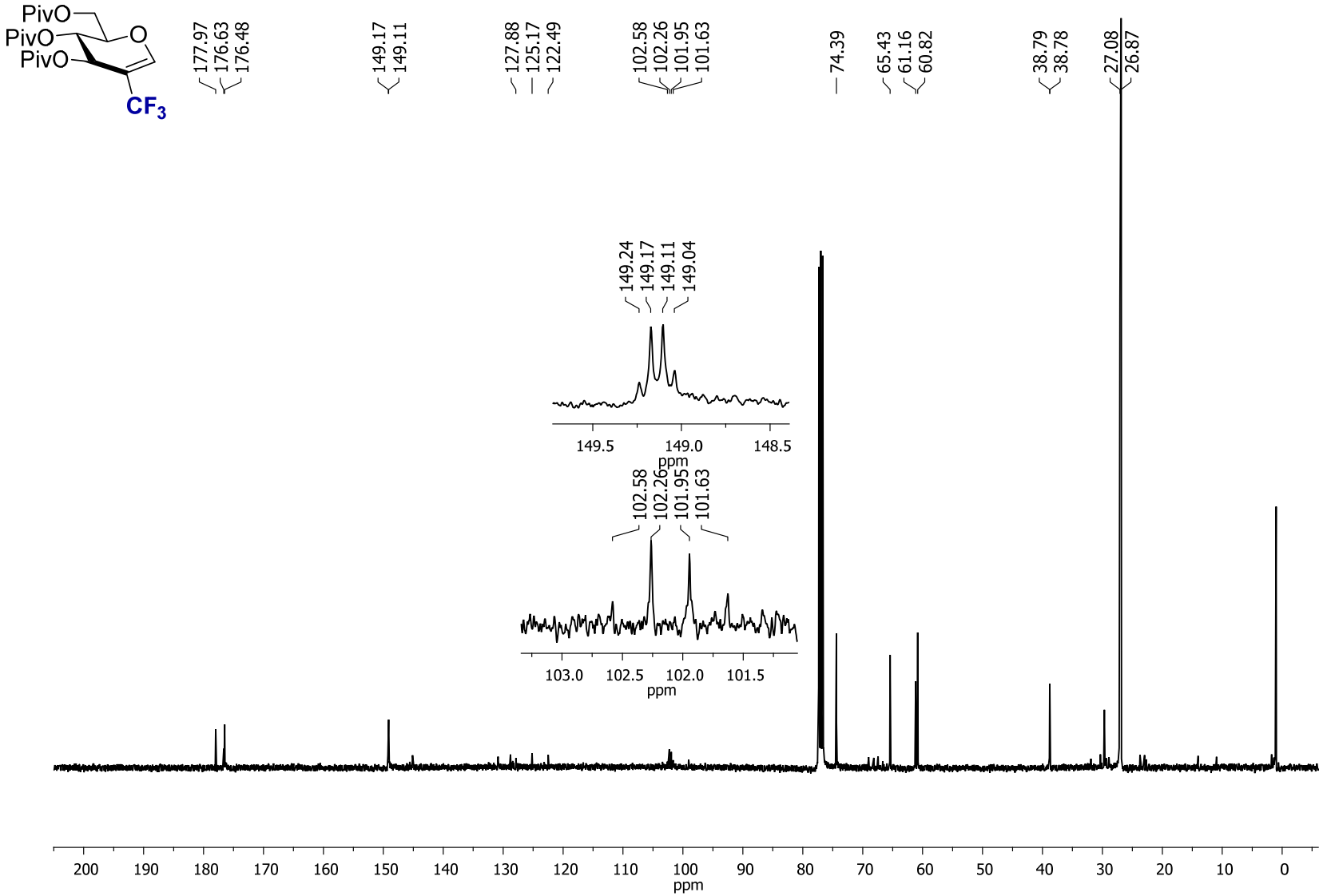

Figure S23. ^{13}C NMR ($CDCl_3$, 100.6 MHz) of **2d**

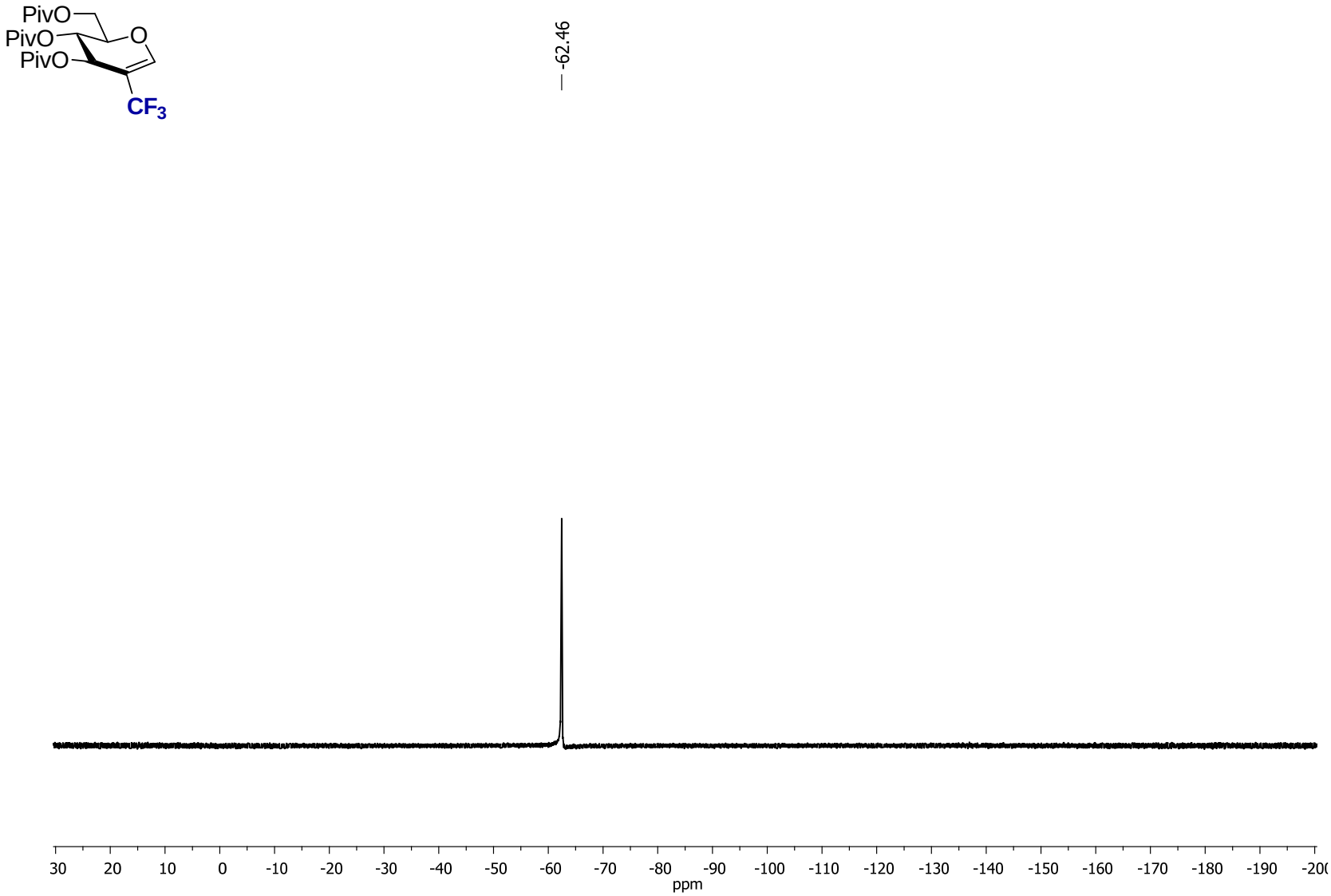

Figure S24. ^{19}F NMR ($CDCl_3$, 376.5 MHz) of **2d**

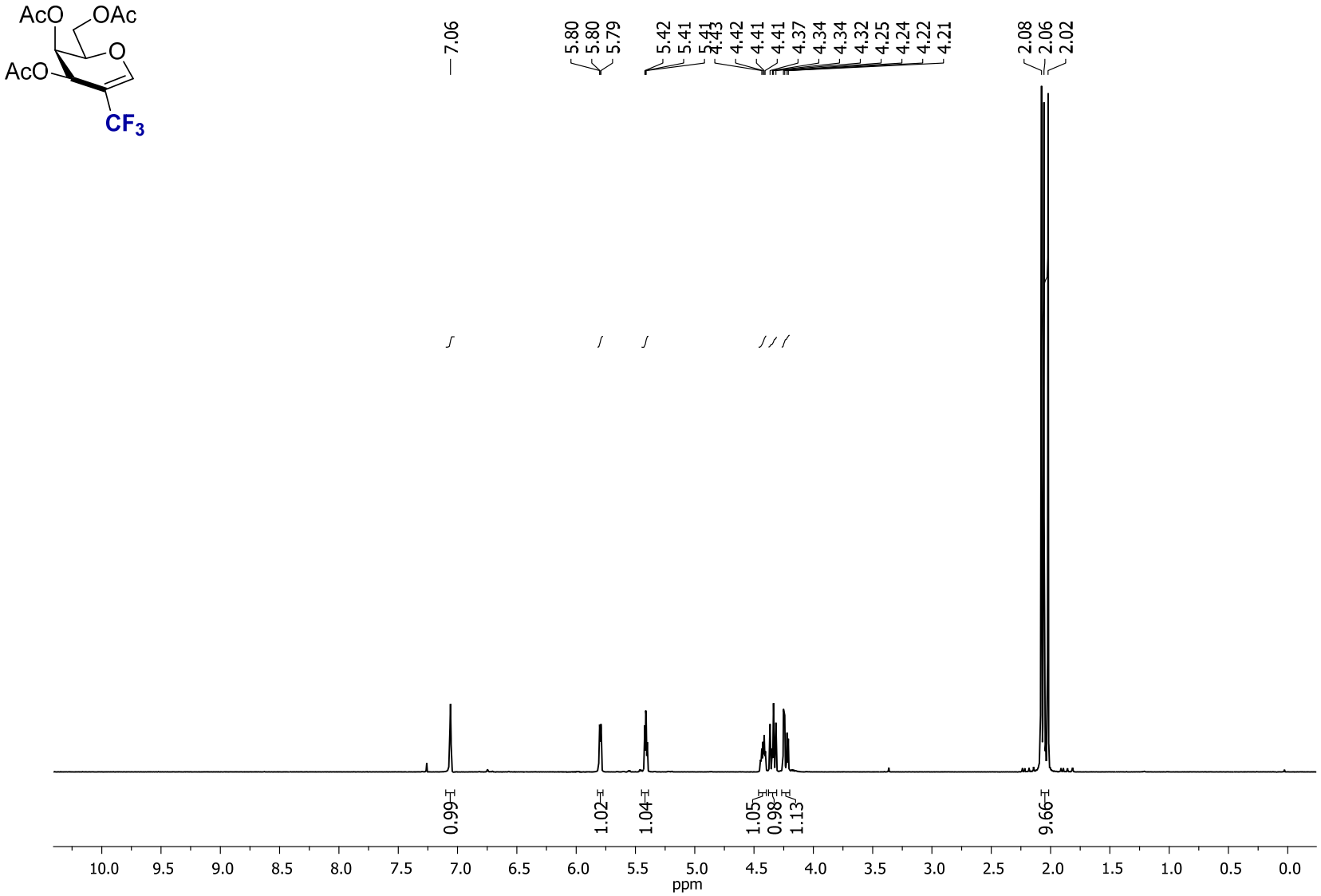

Figure S25. ^{1}H NMR ($CDCl_3$, 400 MHz) of **2e**

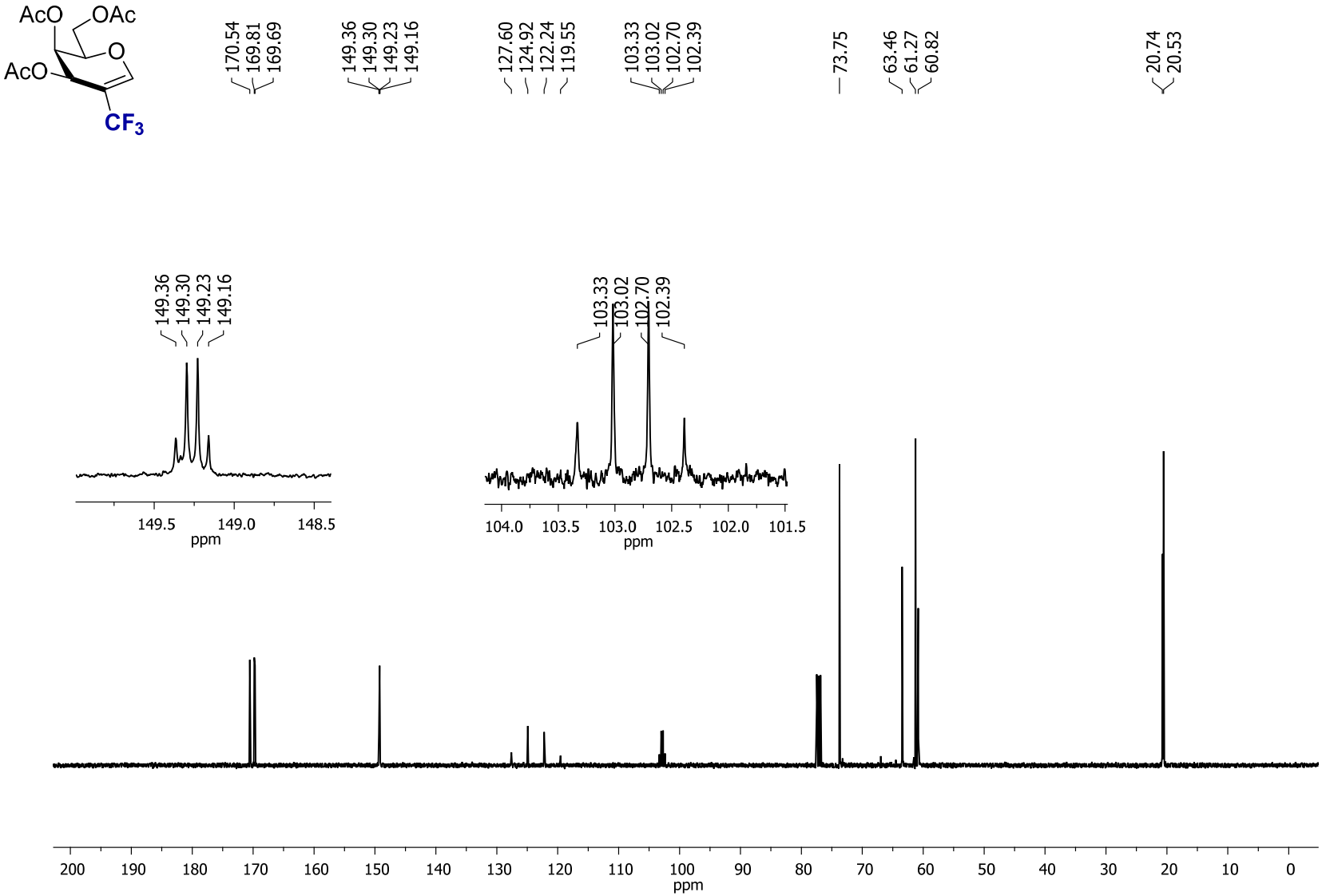

Figure S26. ^{13}C NMR ($CDCl_3$, 100.6 MHz) of **2e**

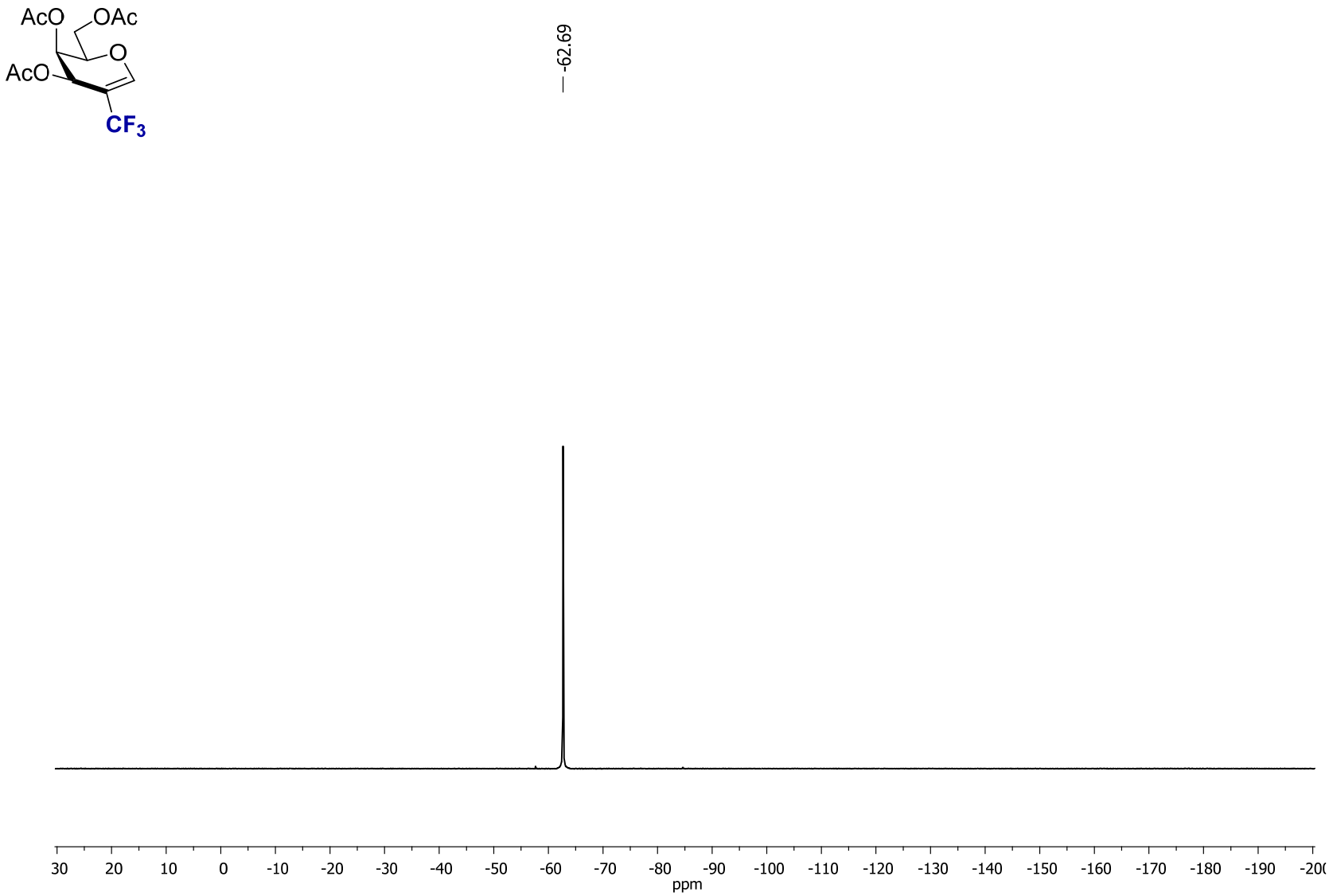

Figure S27. ^{19}F NMR ($CDCl_3$, 376.5 MHz) of **2e**

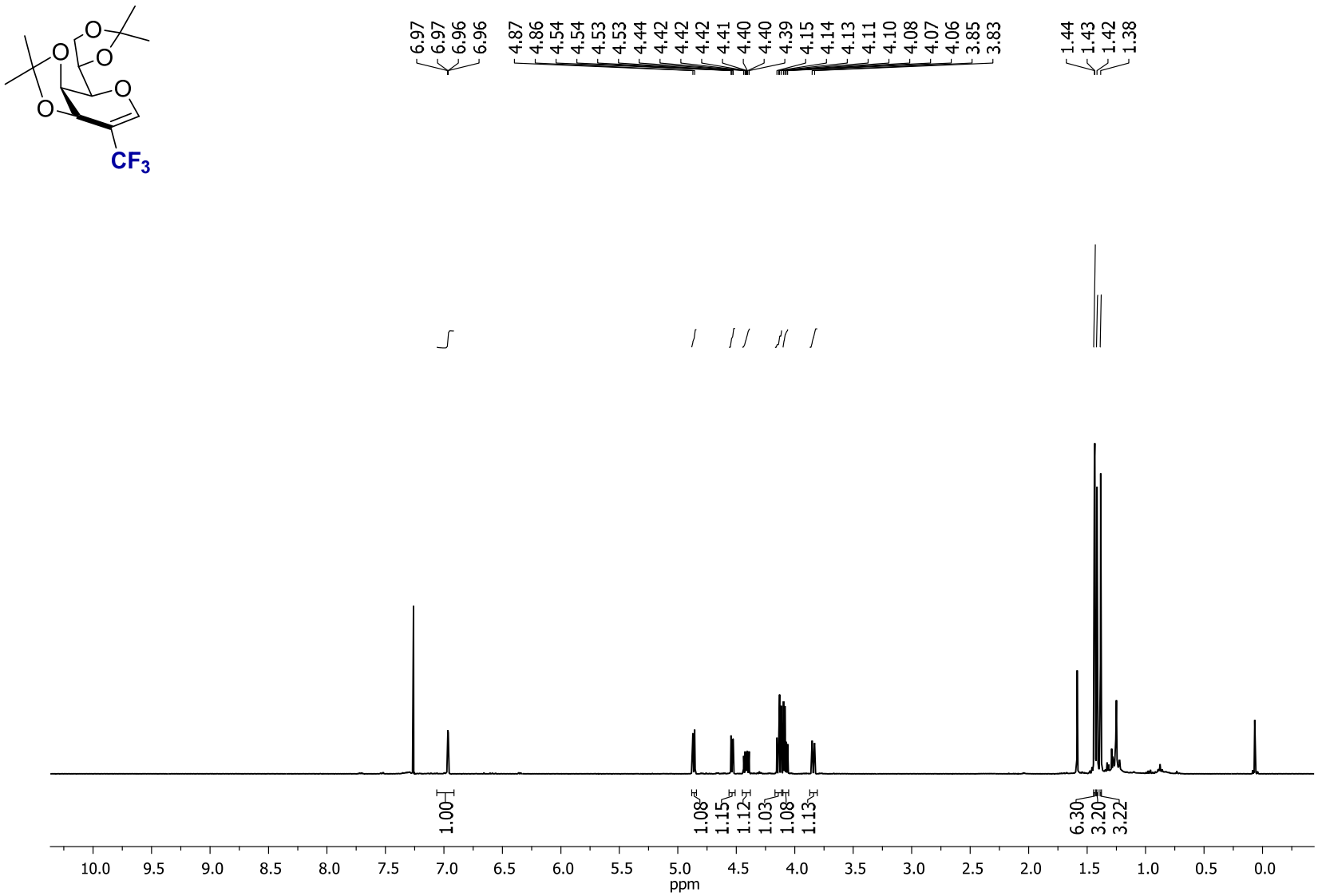

Figure S28. ^{1}H NMR ($CDCl_3$, 400 MHz) of **2f**

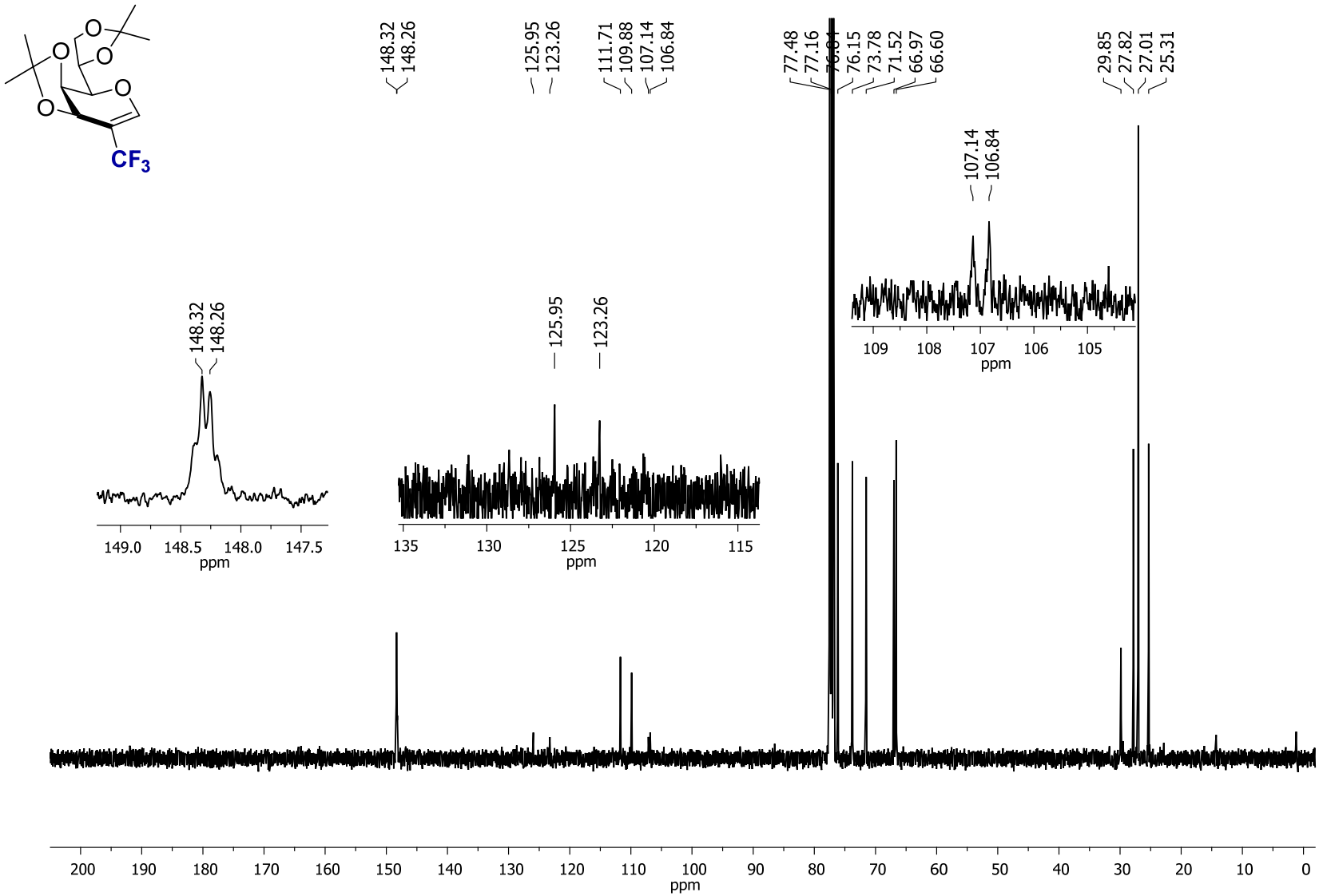

Figure S29. ^{13}C NMR ($CDCl_3$, 100.6 MHz) of **2f**

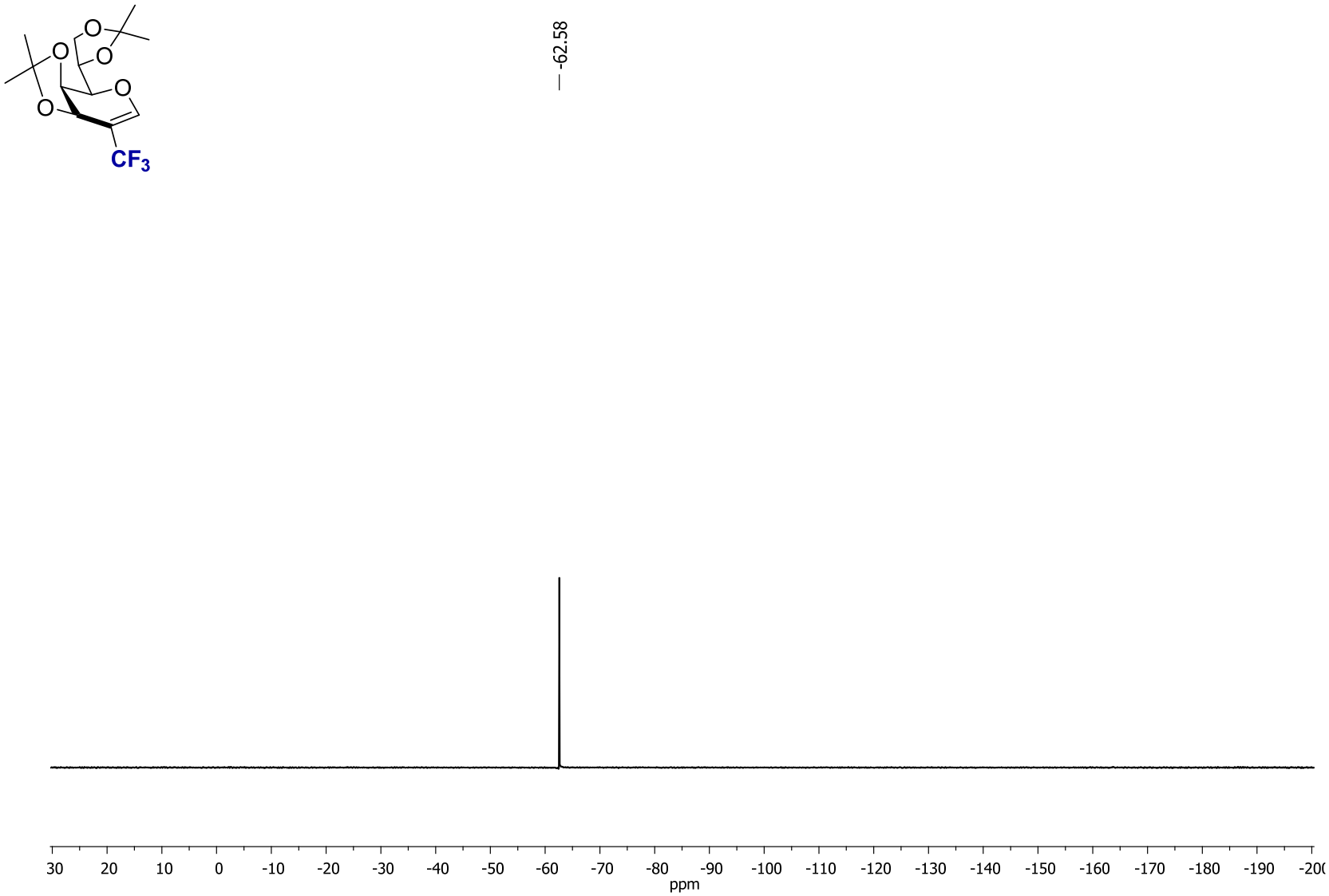

Figure S30. ^{19}F NMR ($CDCl_3$, 376.5 MHz) of **2f**

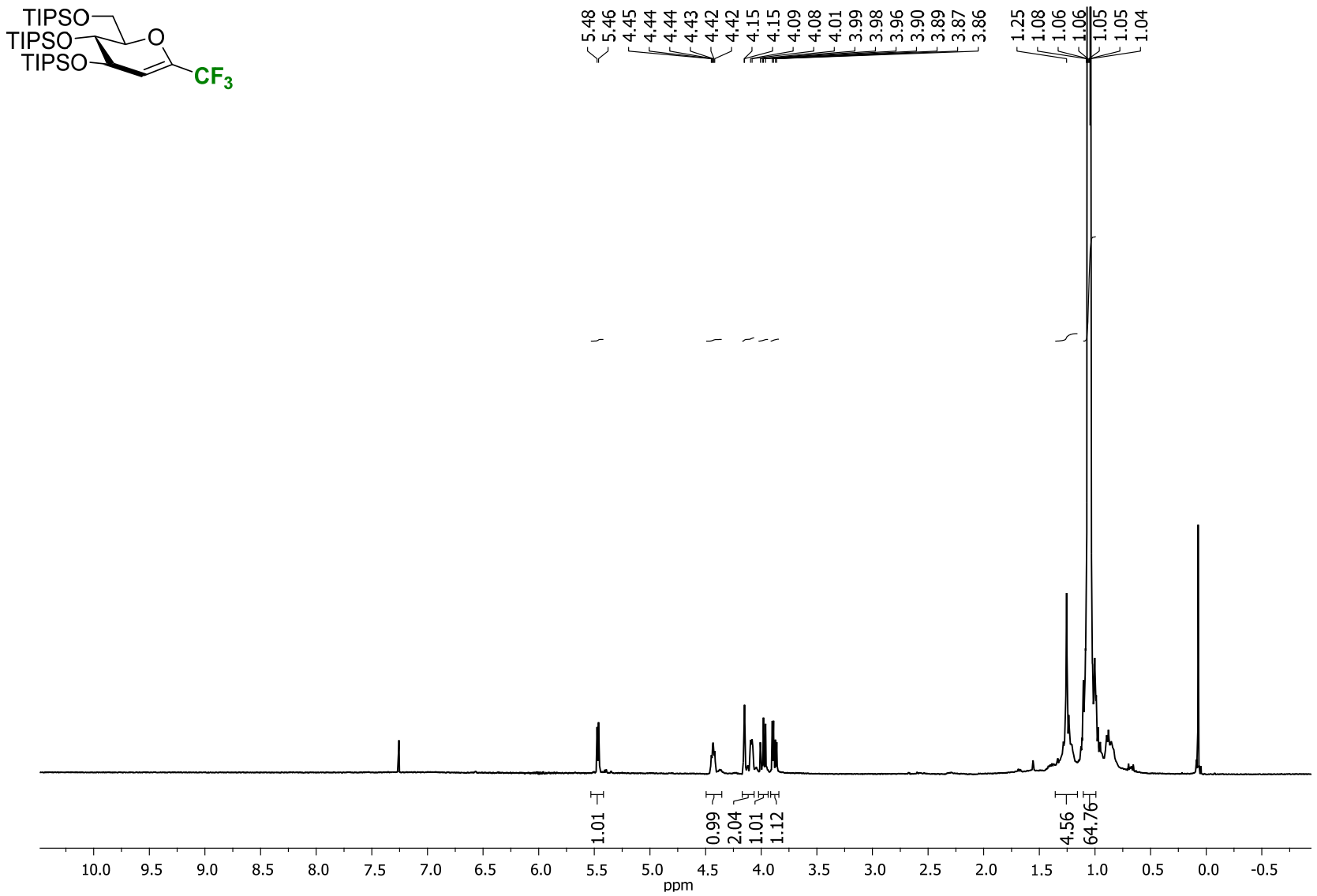

Figure S31. ^{1}H NMR ($CDCl_3$, 400 MHz) of **2g**

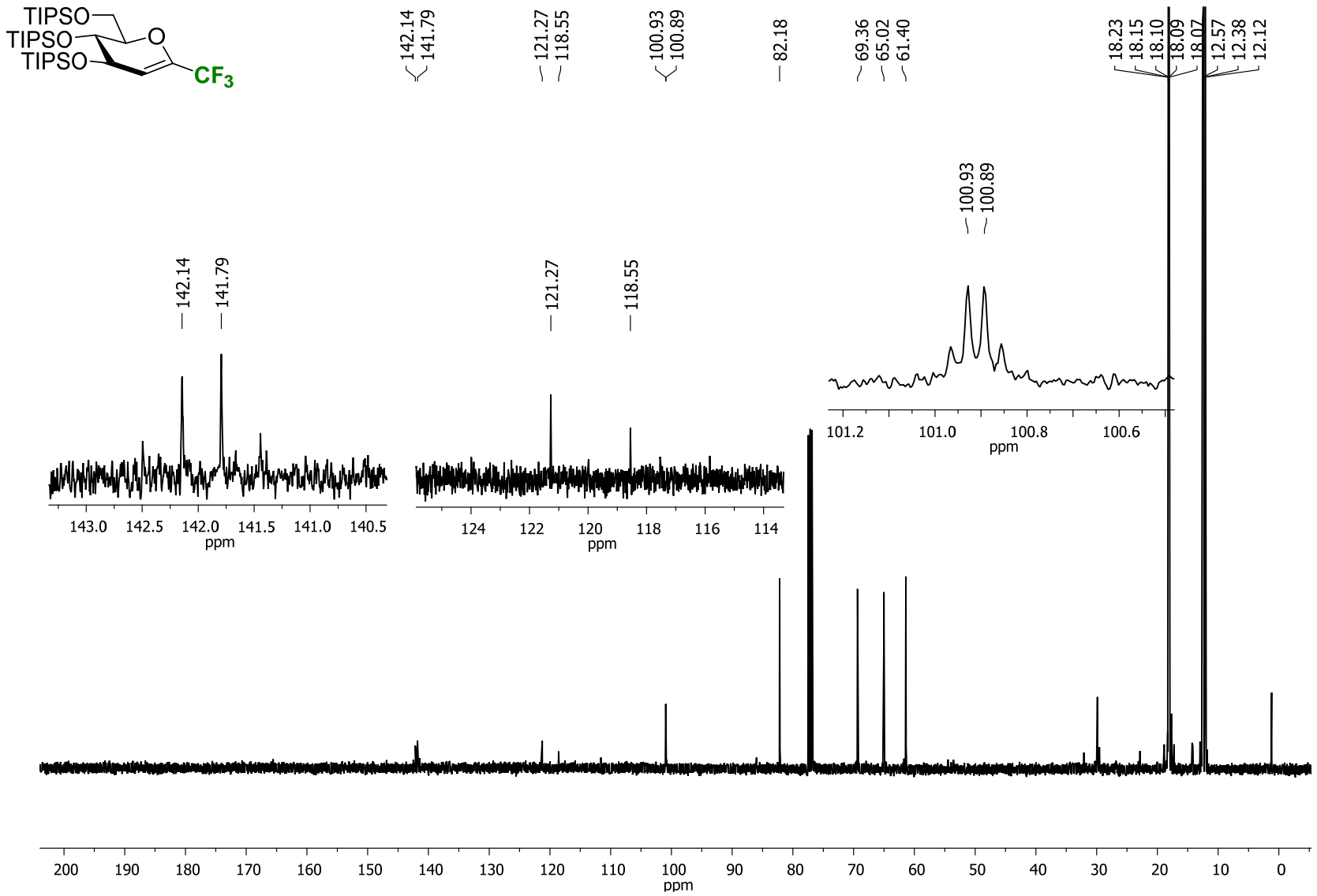

Figure S32. ^{13}C NMR ($CDCl_3$, 100.6 MHz) of **2g**

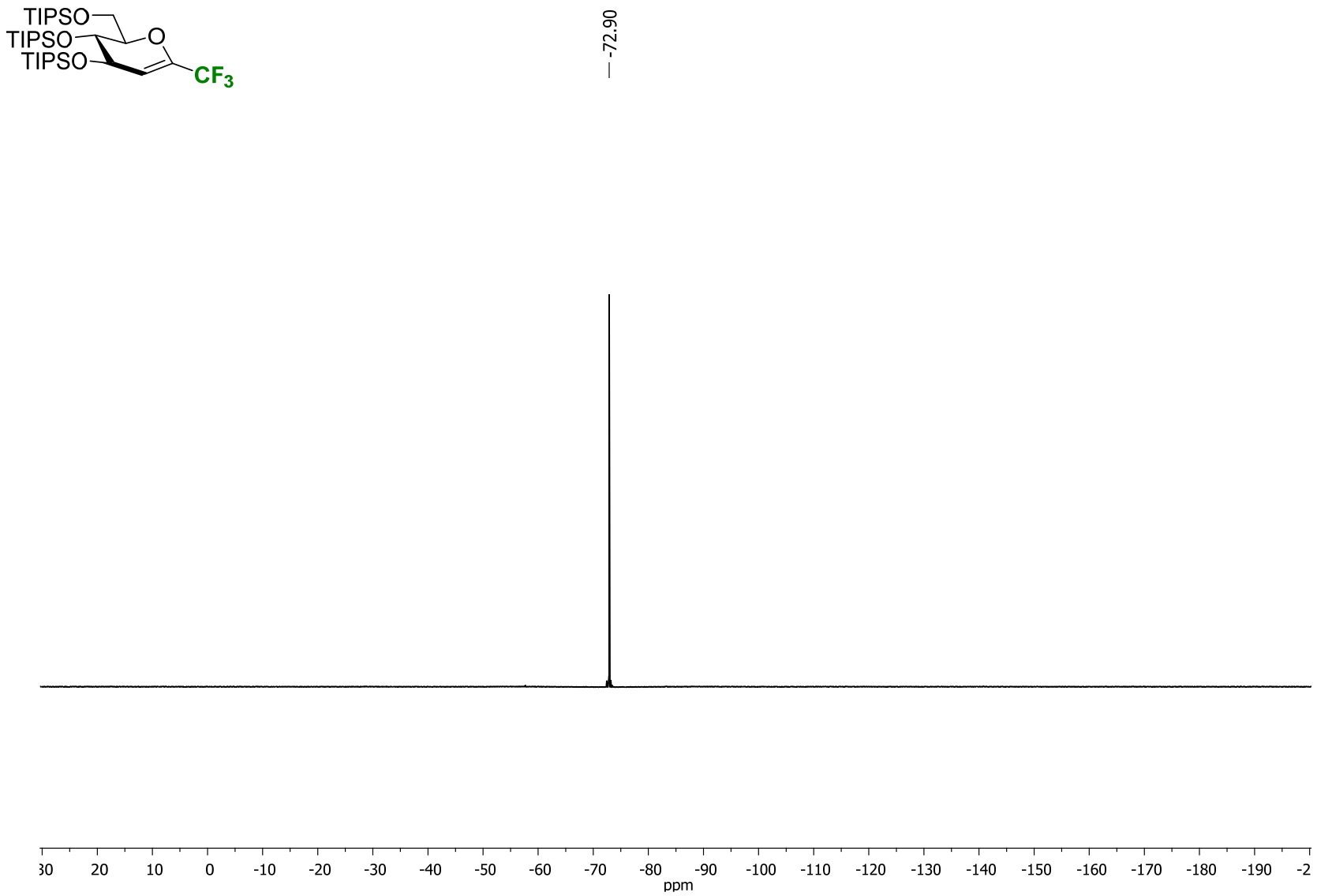

Figure S33. ^{19}F NMR ($CDCl_3$, 376.5 MHz) of **2g**

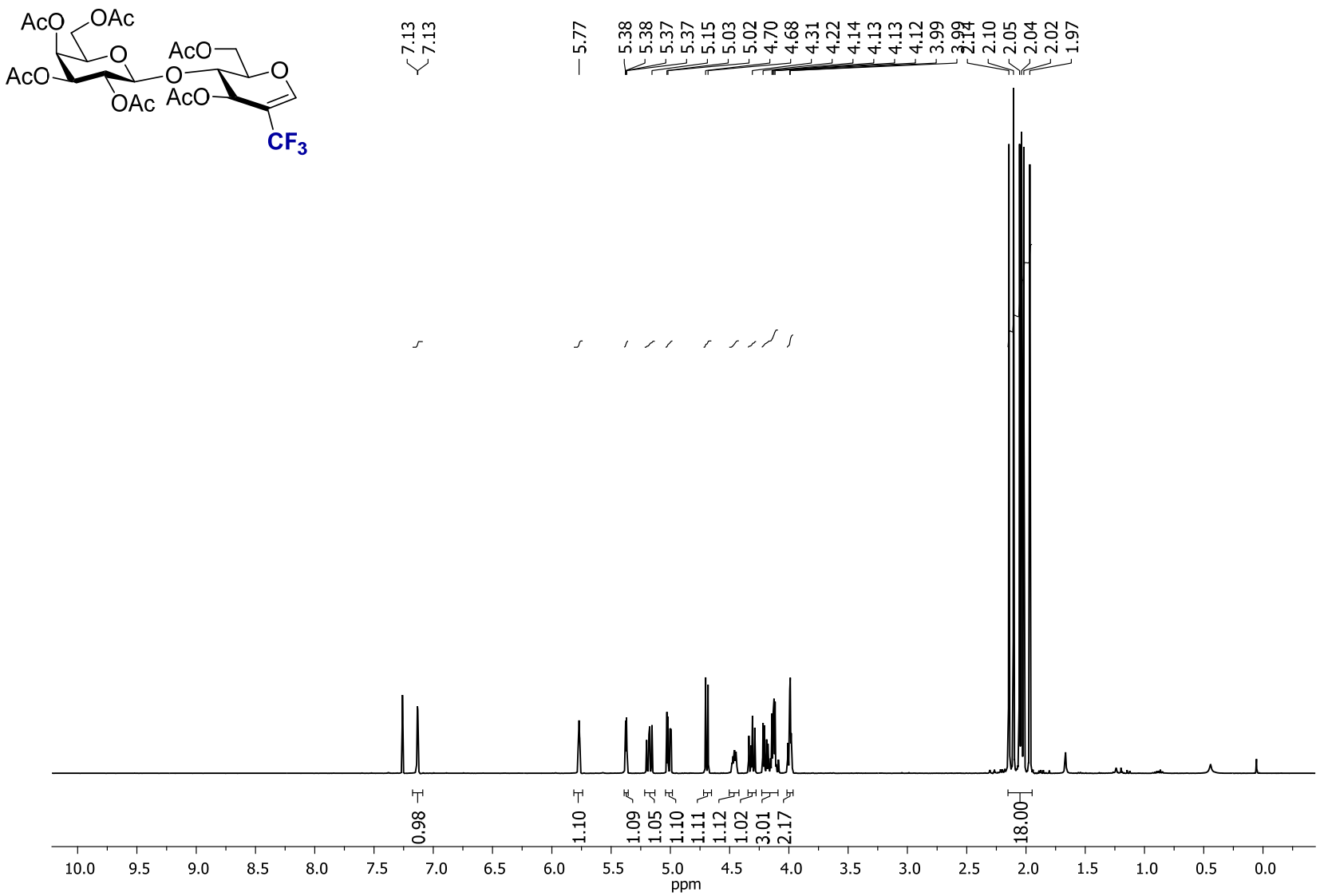

Figure S34. ^{1}H NMR ($CDCl_3$, 400 MHz) of **2h**

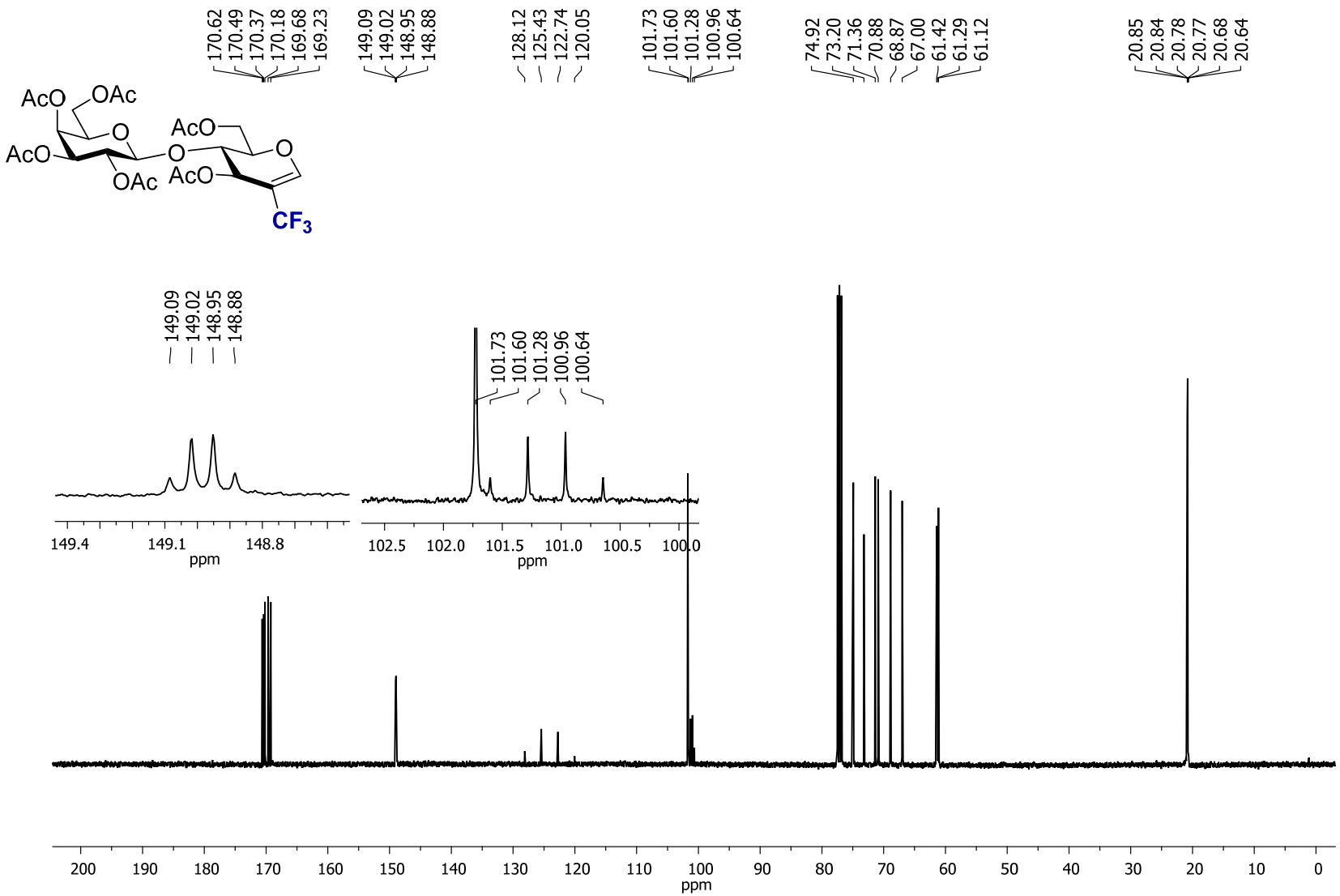

Figure S35. ^{13}C NMR ($CDCl_3$, 100.6 MHz) of **2h**

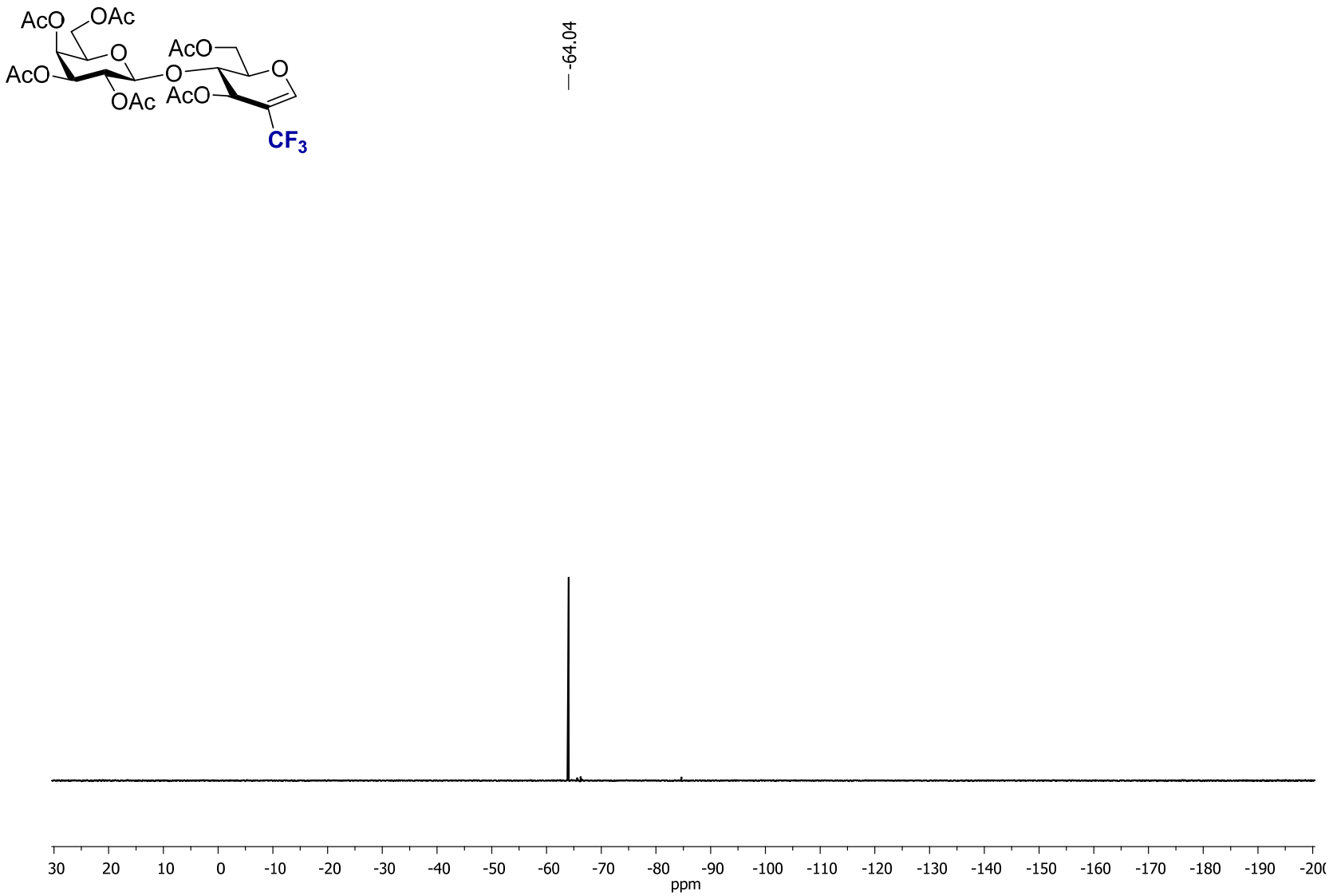

Figure S36. ^{19}F NMR ($CDCl_3$, 376.5 MHz) of **2h**

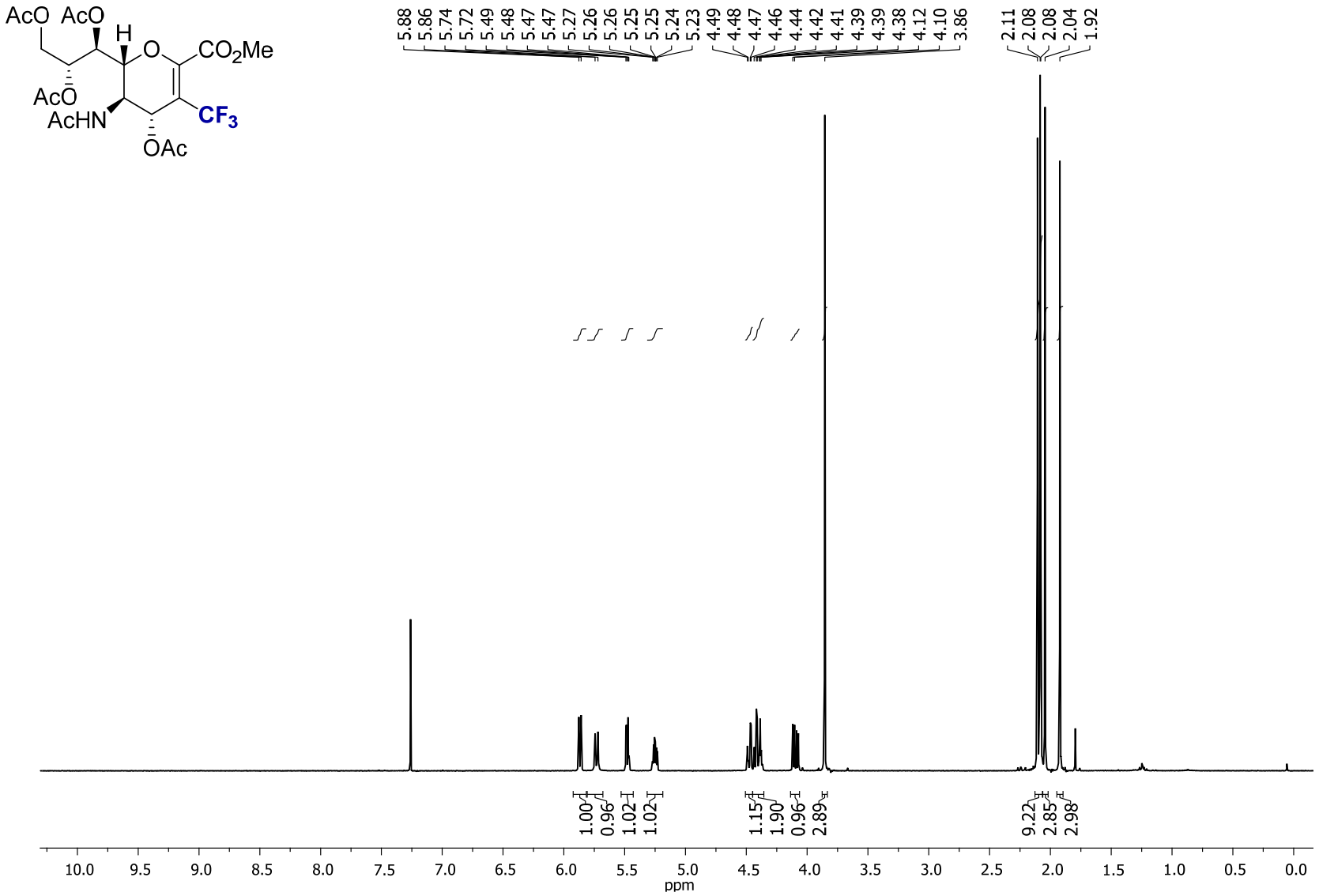

Figure S37. ^{1}H NMR ($CDCl_3$, 400 MHz) of **2i**

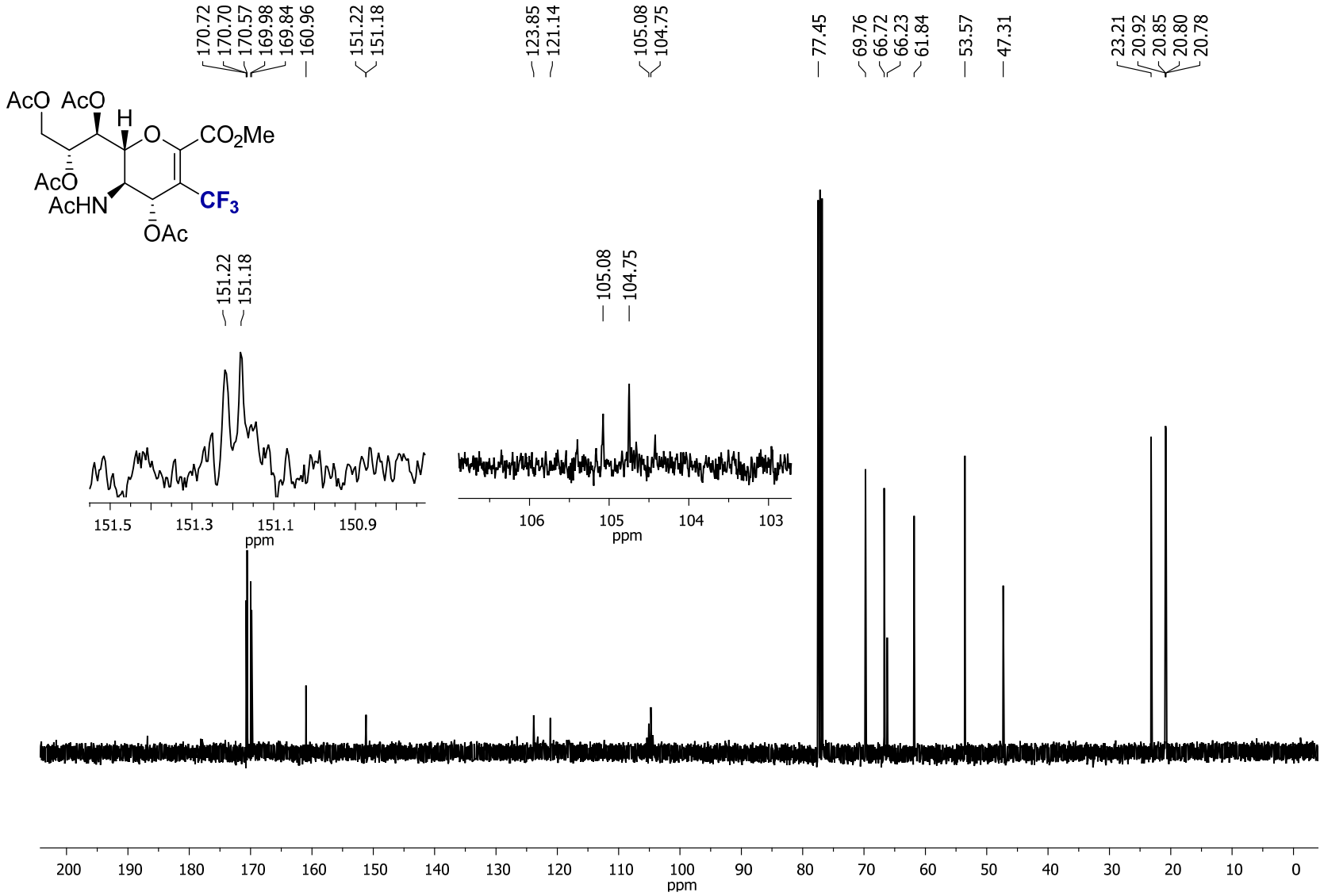

Figure S38. ^{13}C NMR ($CDCl_3$, 100.6 MHz) of **2i**

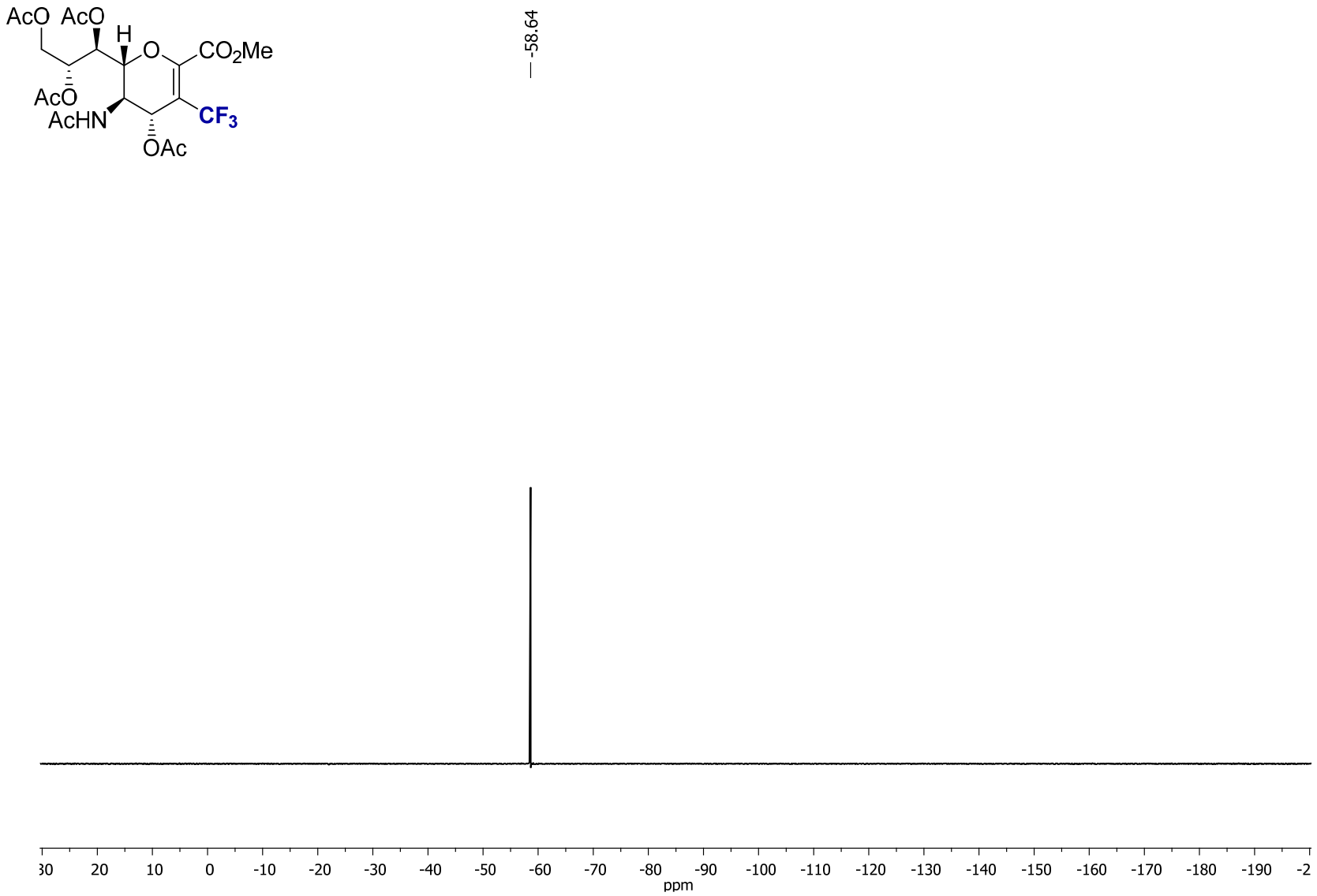

Figure S39. ^{19}F NMR ($CDCl_3$, 376.5 MHz) of **2i**

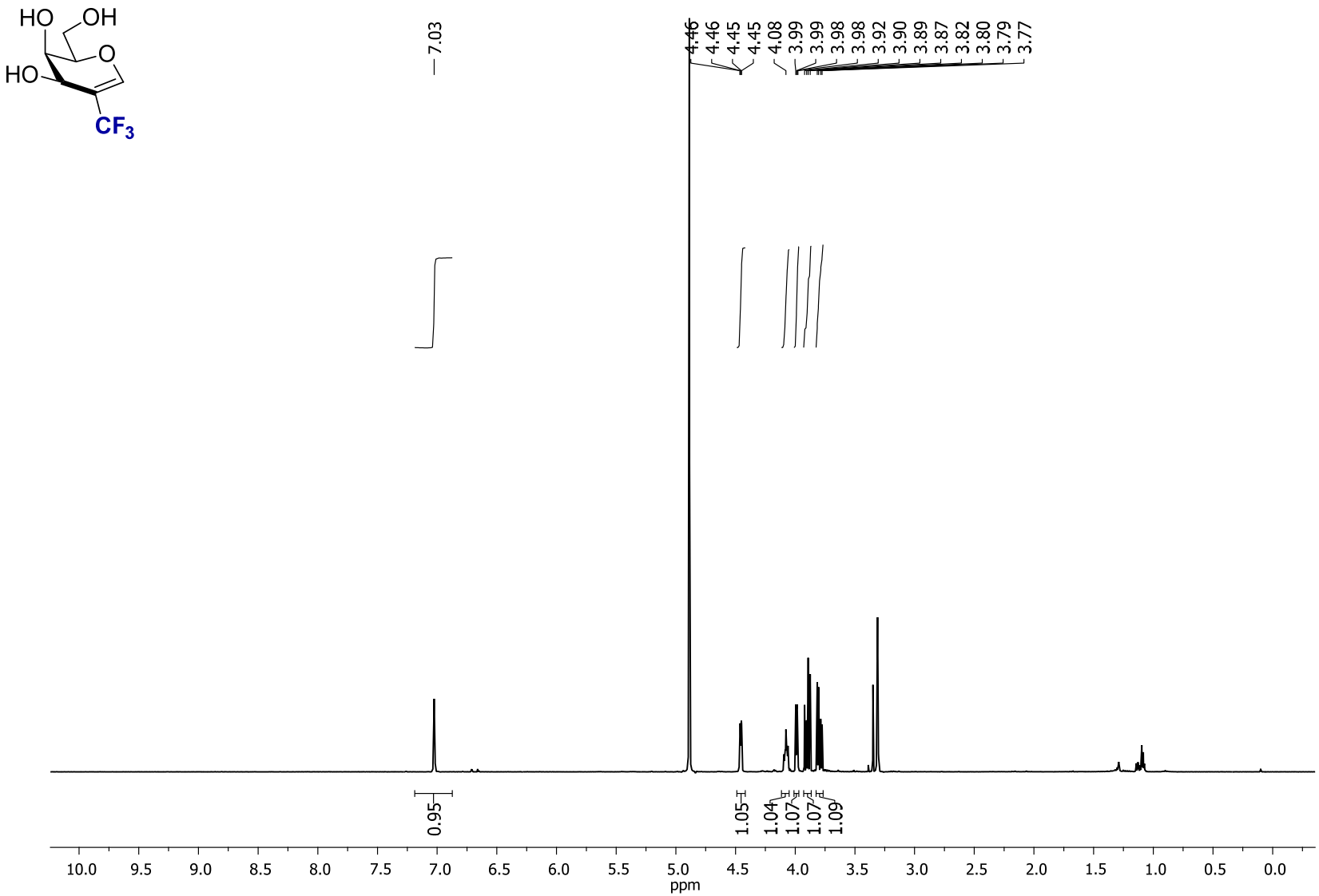

Figure S40. ^{1}H NMR (CD_3OD, 400 MHz) of **2j**

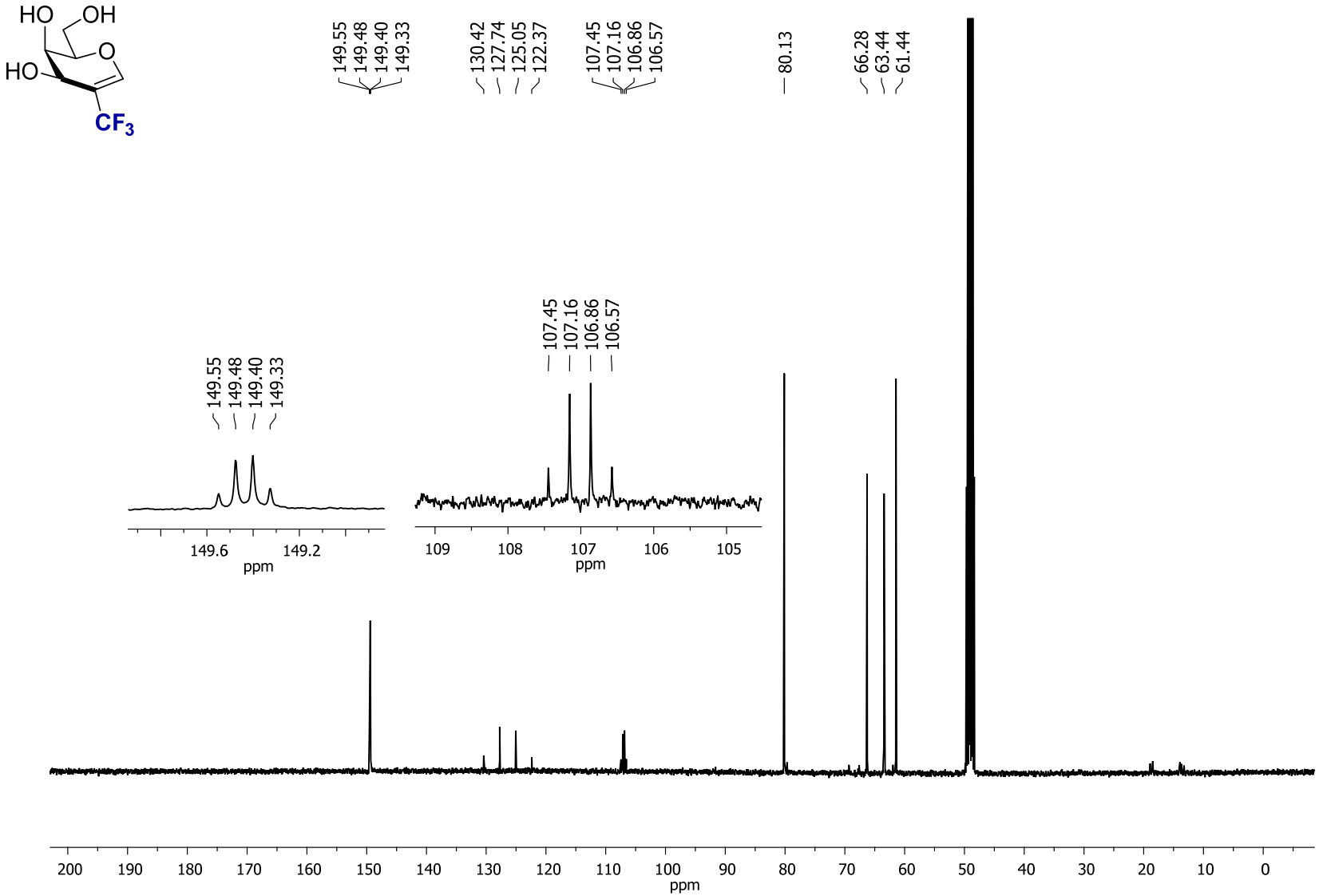

Figure S41. ^{13}C NMR (CD_3OD, 100.6 MHz) of **2j**

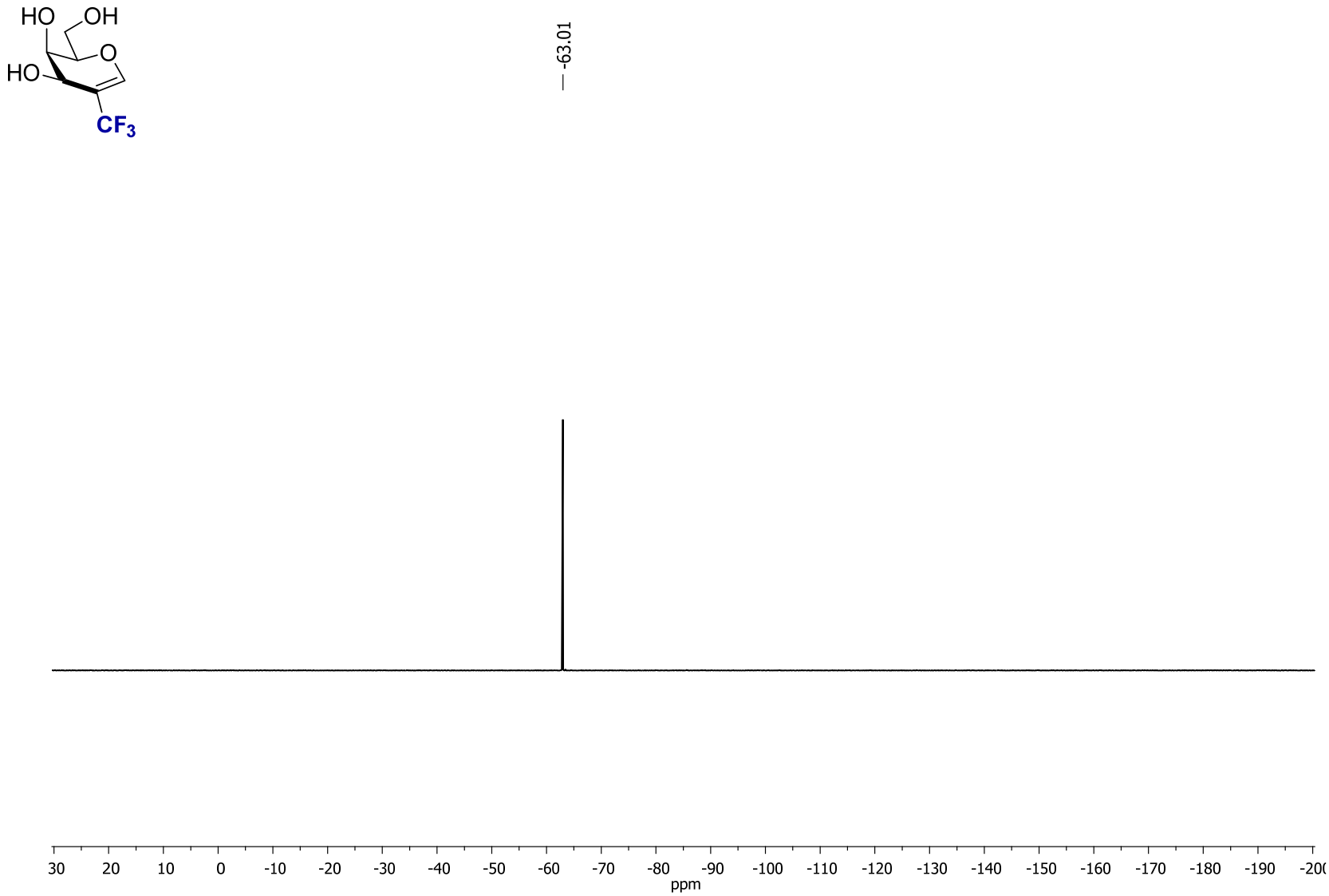

Figure S42. ^{19}F NMR (CD_3OD, 376.5 MHz) of **2j**

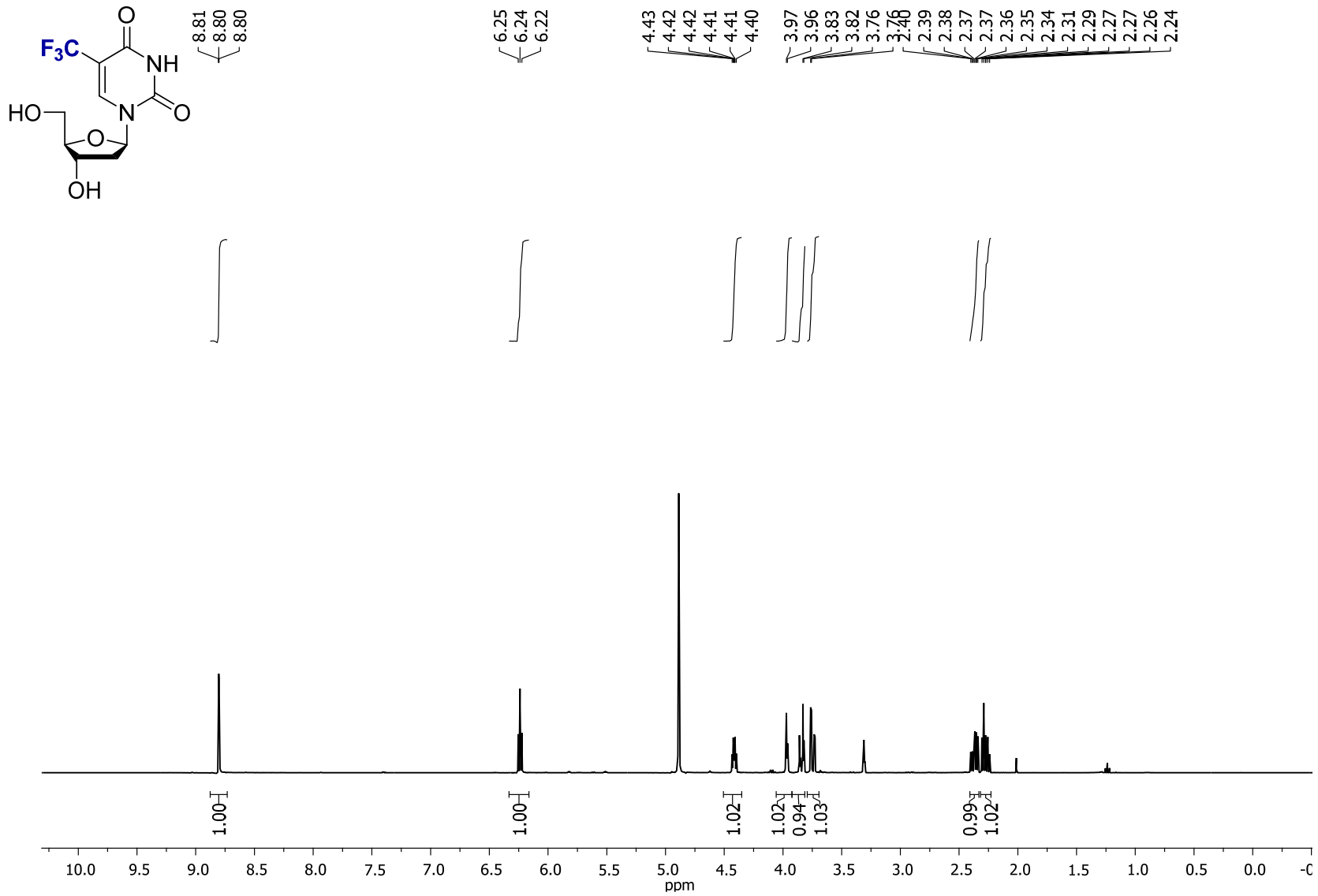

Figure S43. ^{1}H NMR (CD_3OD, 400 MHz) of **2k**

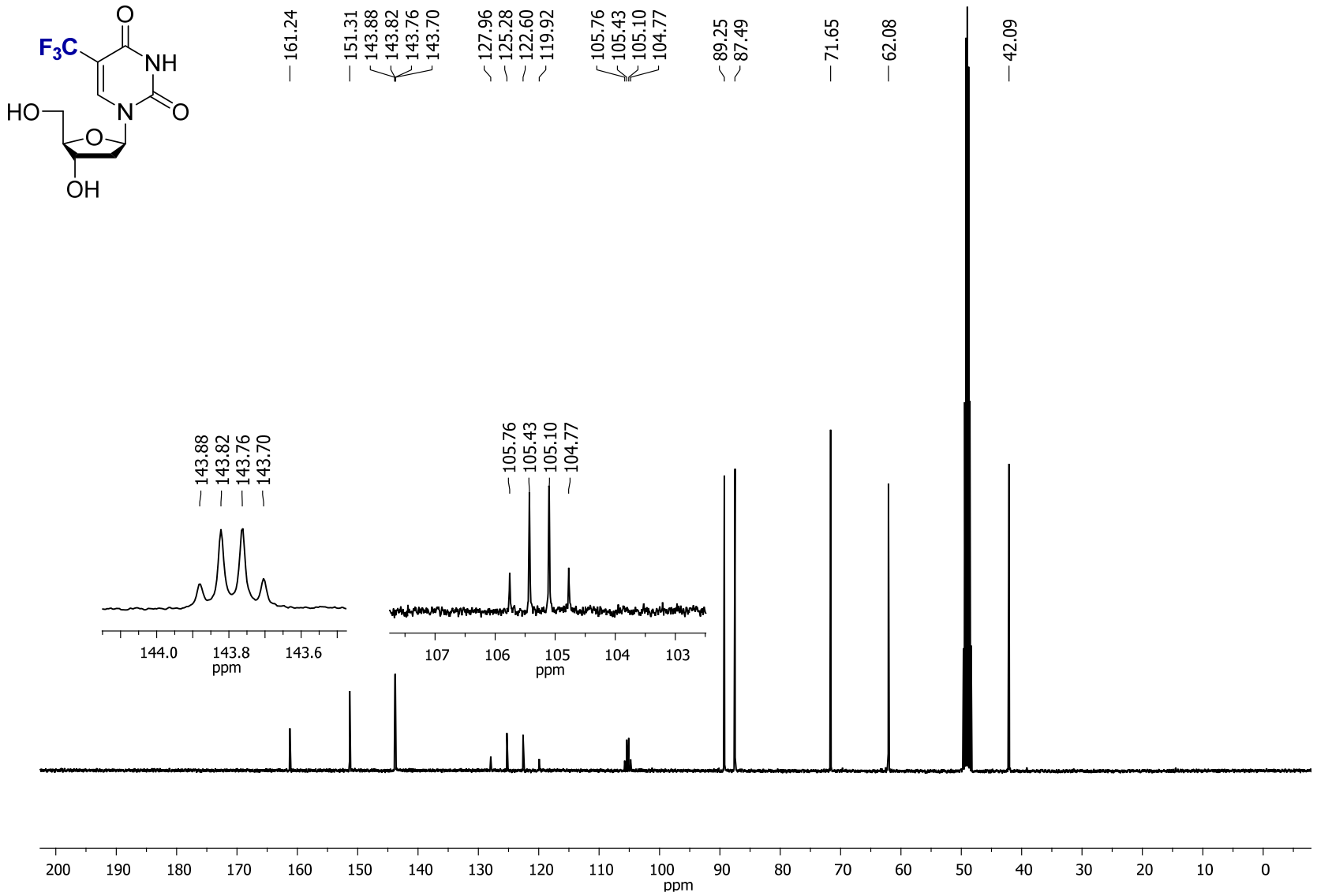

Figure S44. ^{13}C NMR (CD_3OD, 100.6 MHz) of **2k**

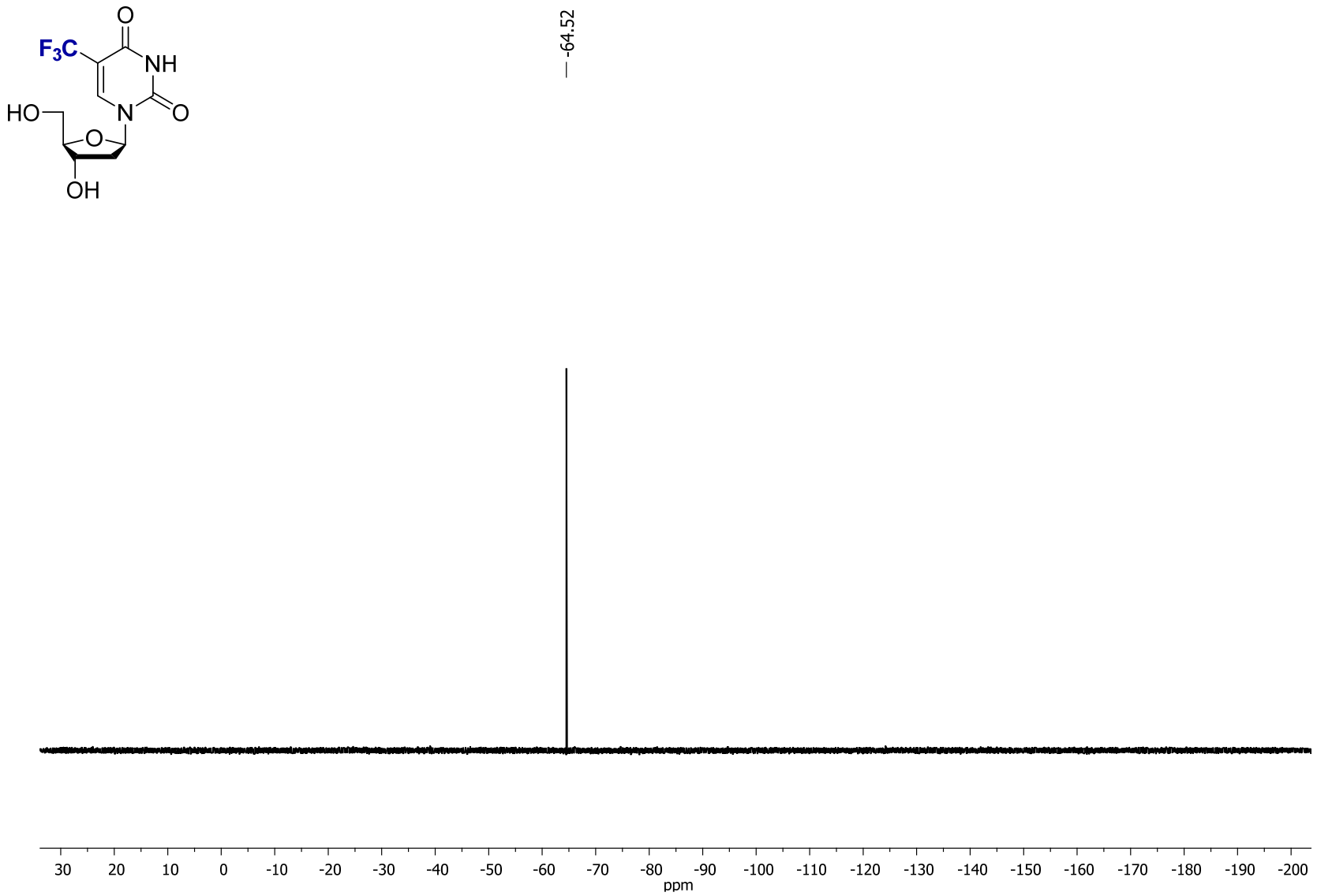

Figure S45. ^{19}F NMR (CD_3OD, 376.5 MHz) of **2k**

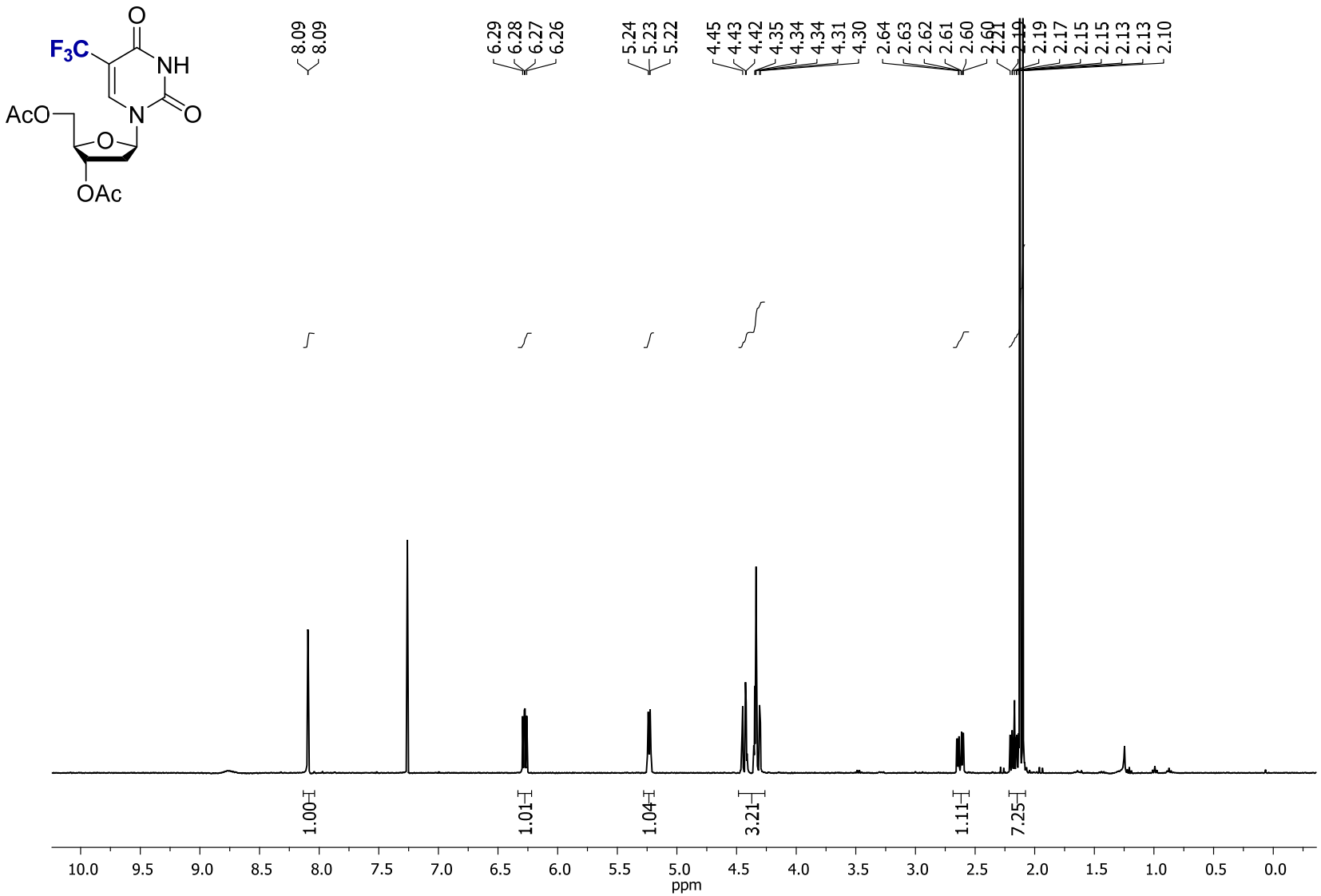

Figure S46. ^{1}H NMR ($CDCl_3$, 400 MHz) of **2l**

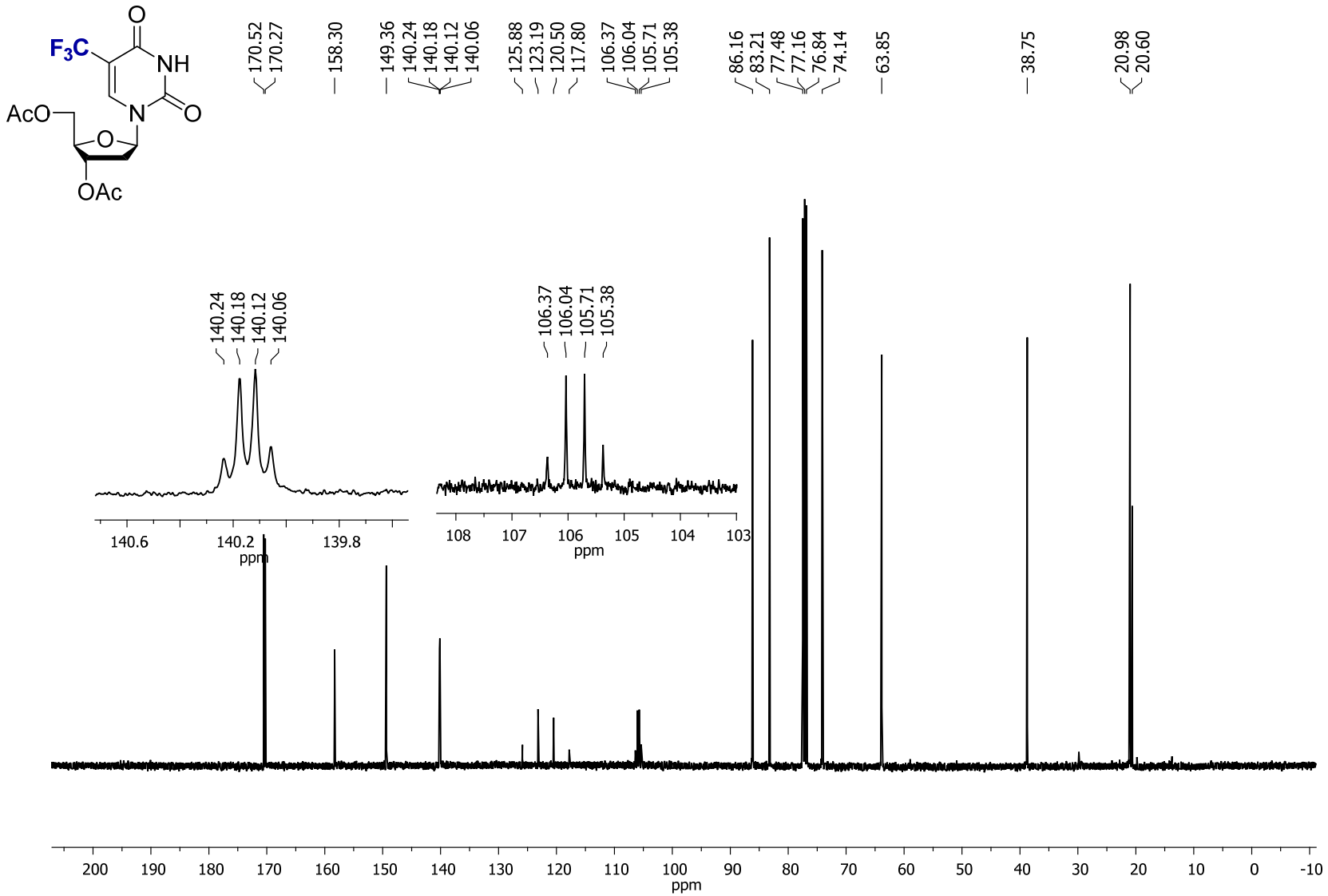

Figure S47. ^{13}C NMR ($CDCl_3$, 100.6 MHz) of **2l**

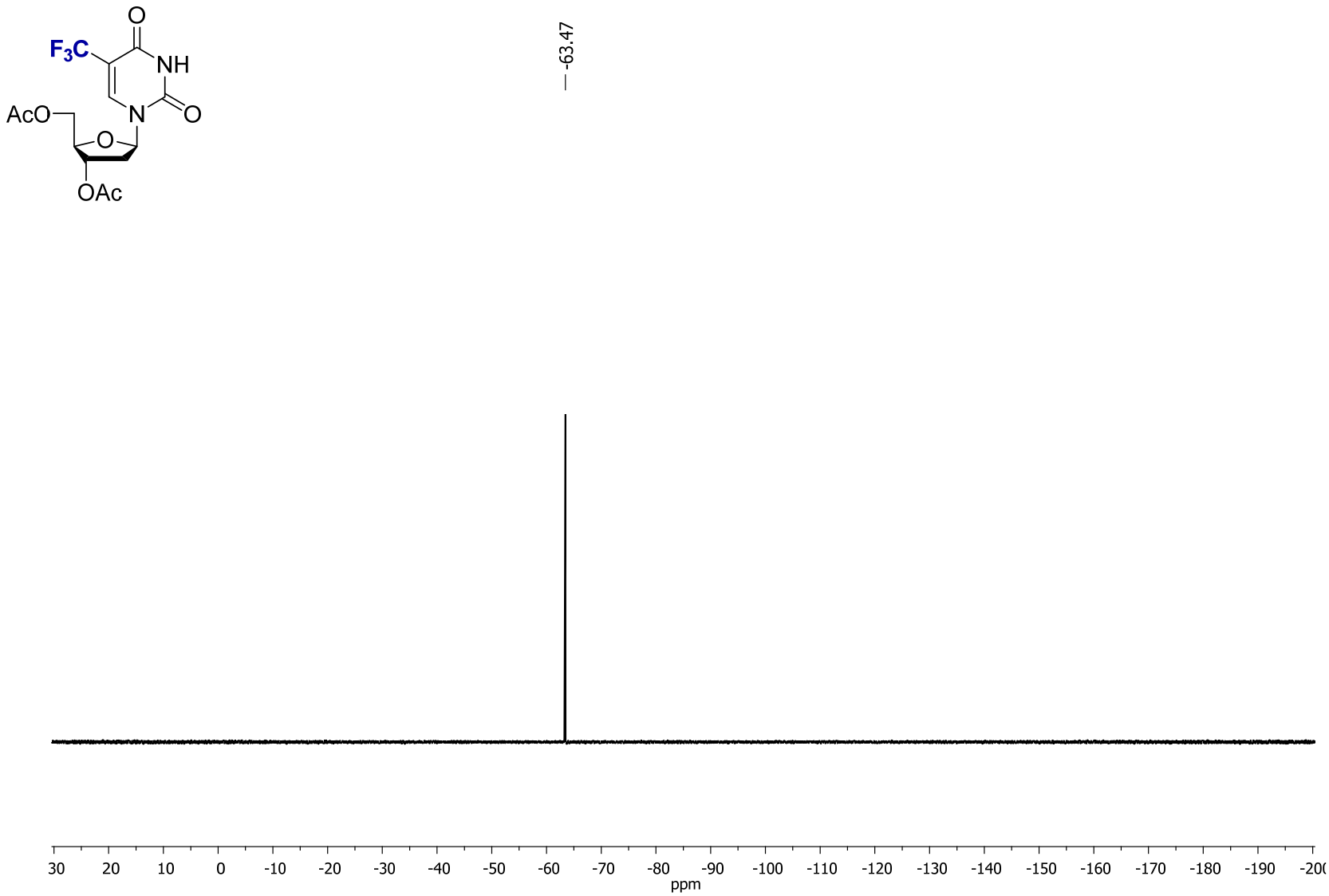

Figure S48. ^{19}F NMR ($CDCl_3$, 376.5 MHz) of **2l**

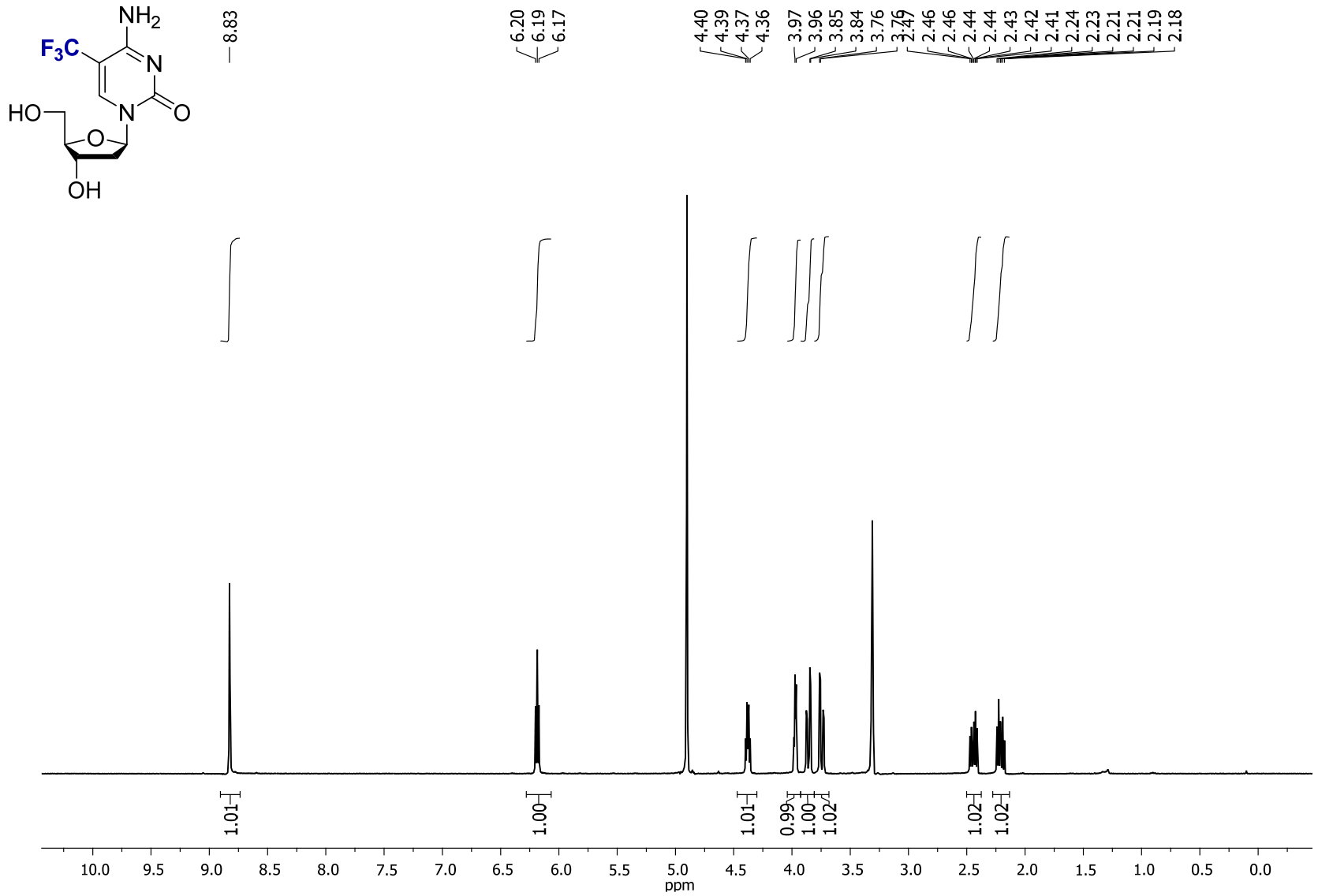

Figure S49. ^{1}H NMR (CD_3OD, 400 MHz) of **2m**

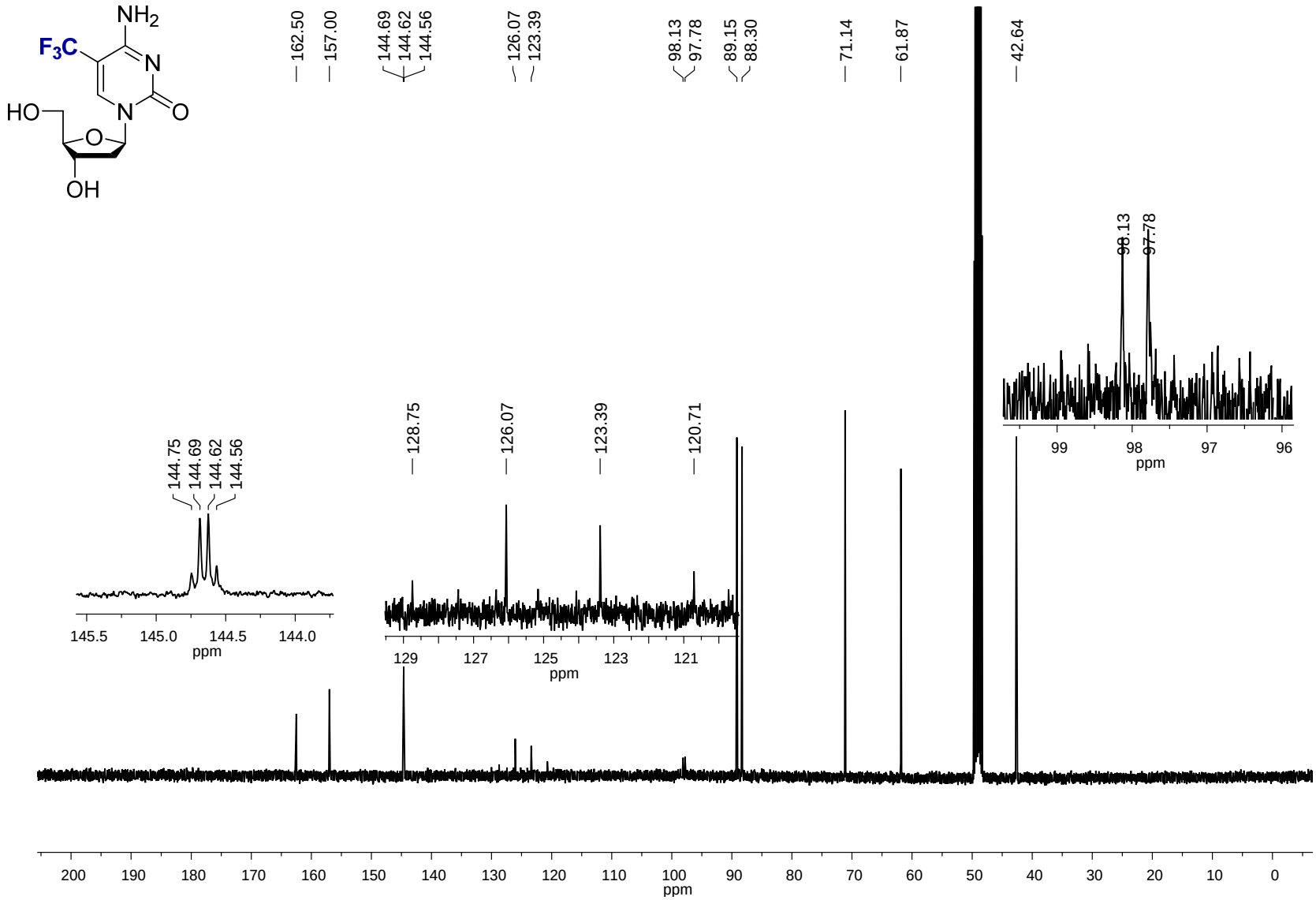

Figure S50. ^{13}C NMR (CD_3OD, 100.6 MHz) of **2m**

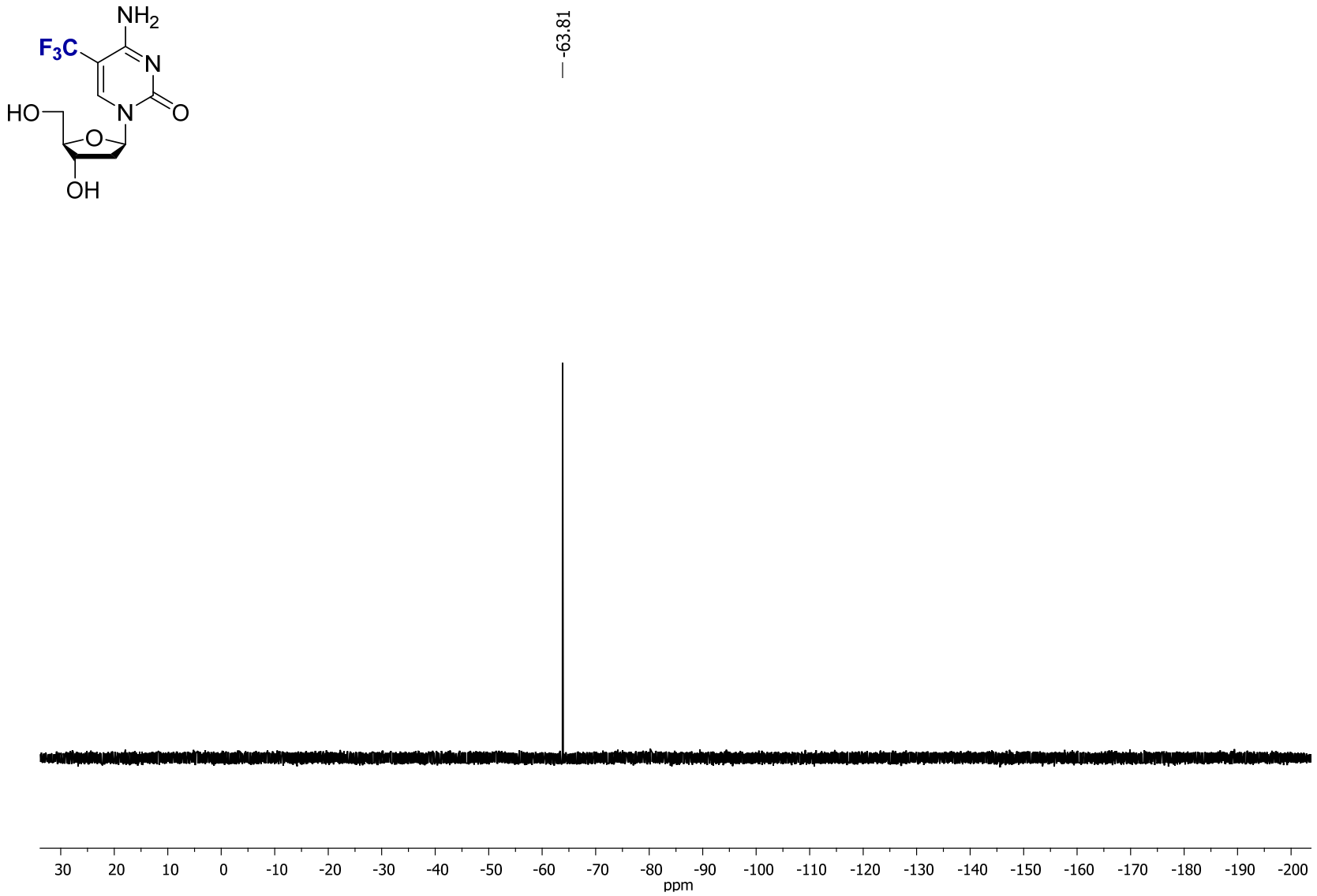

Figure S51. ^{19}F NMR (CD_3OD, 376.5 MHz) of **2m**

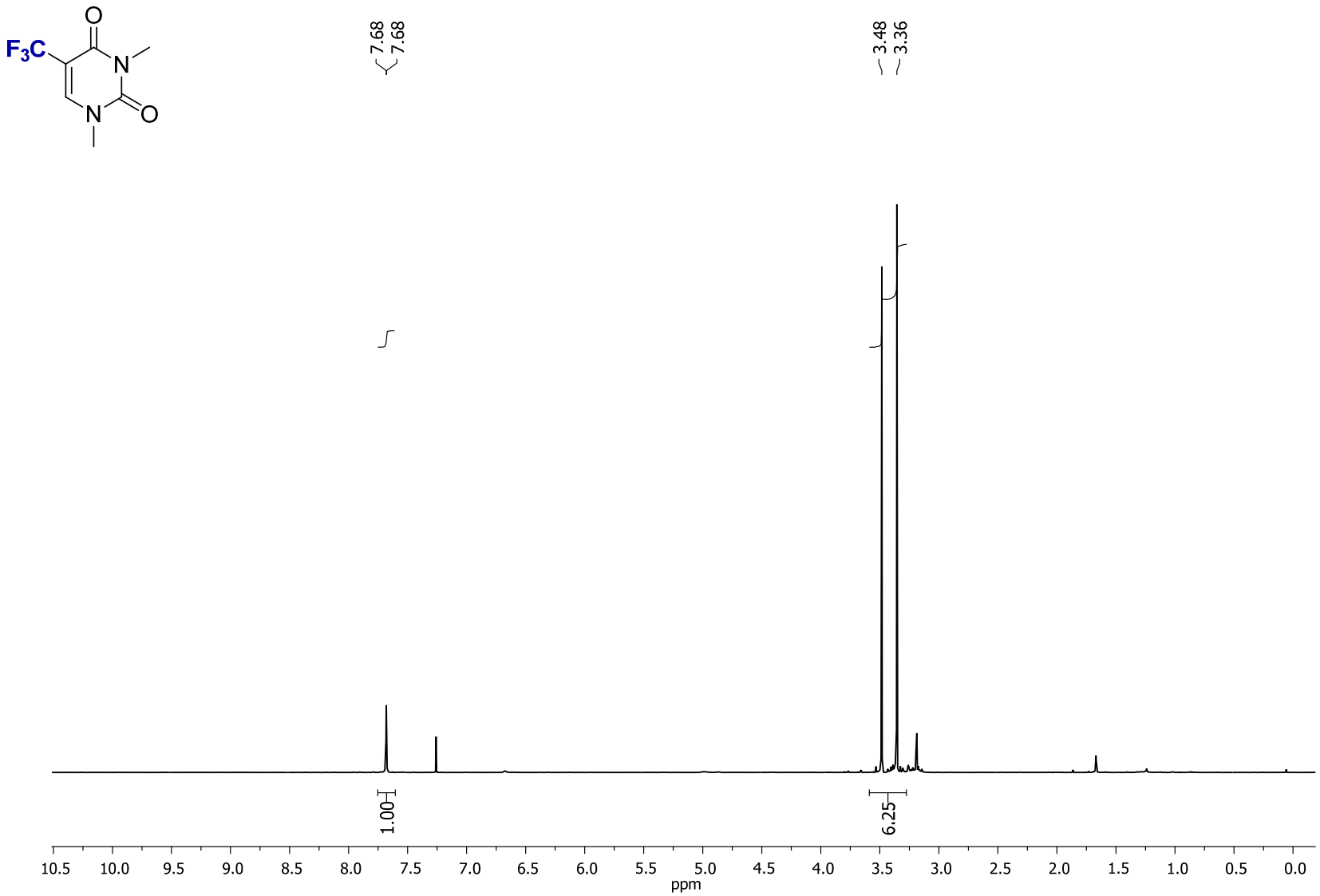

Figure S52. ^{1}H NMR ($CDCl_3$, 400 MHz) of **2n**

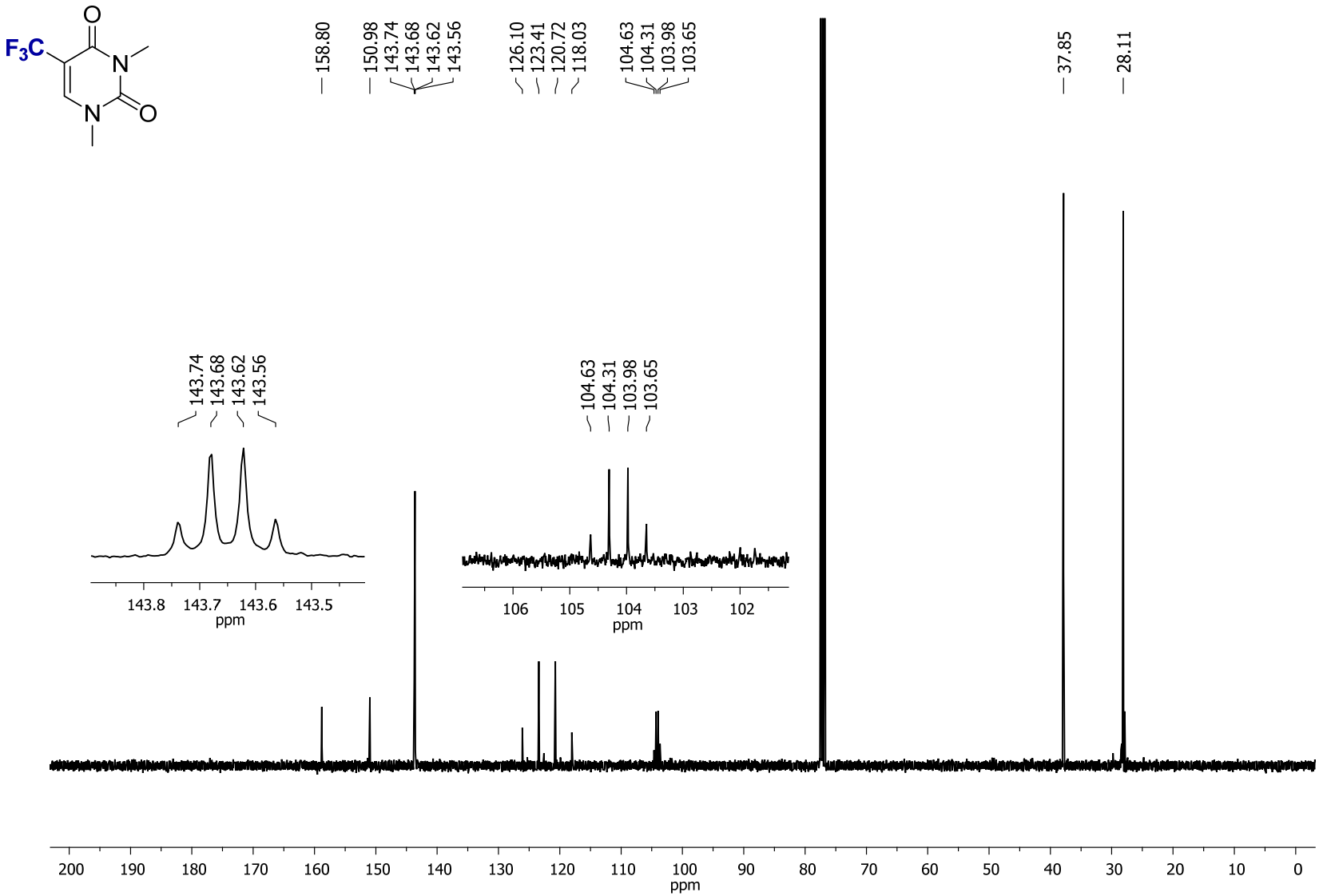

Figure S53. ^{13}C NMR ($CDCl_3$, 100.6 MHz) of **2n**

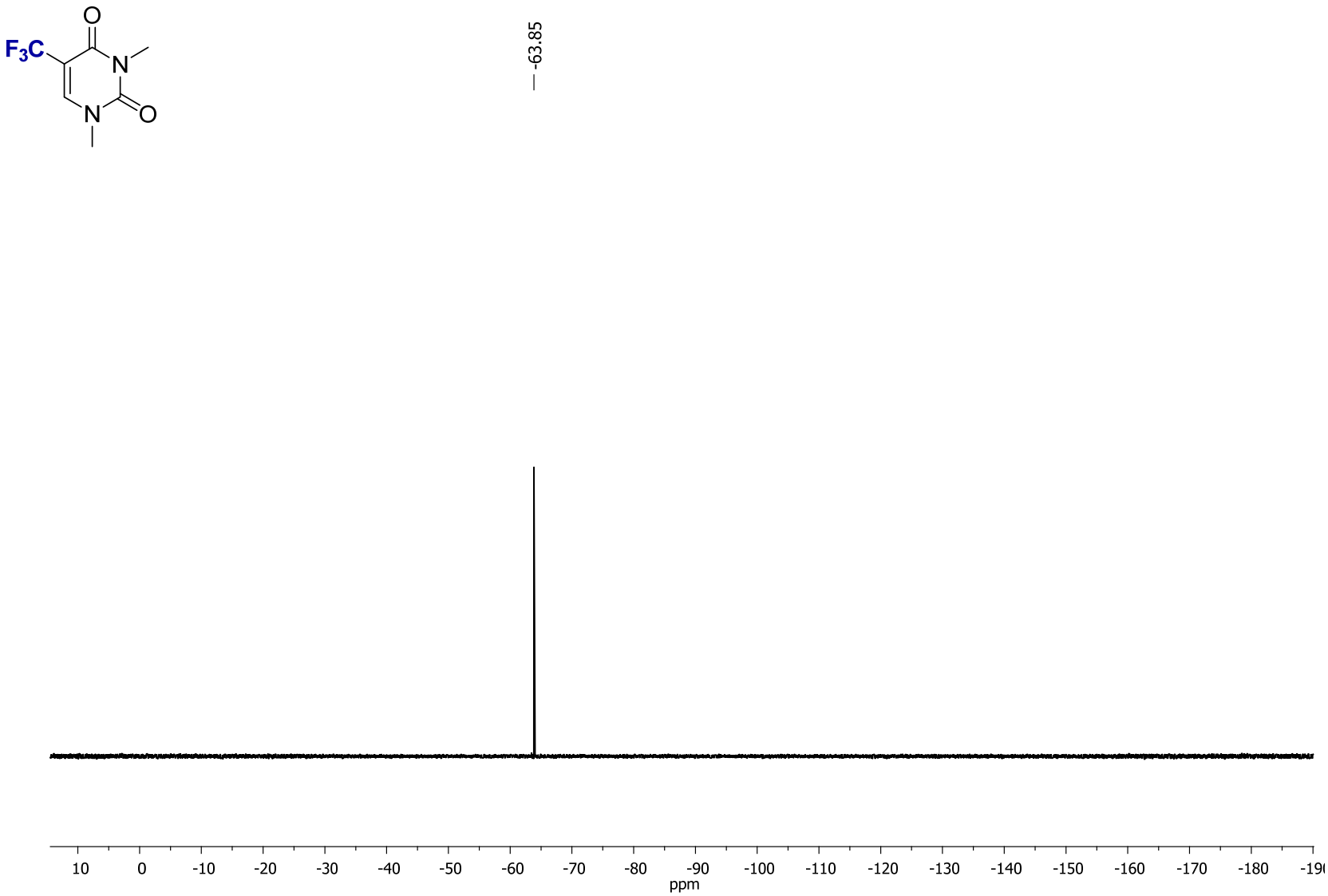

Figure S54. ^{19}F NMR ($CDCl_3$, 376.5 MHz) of **2n**

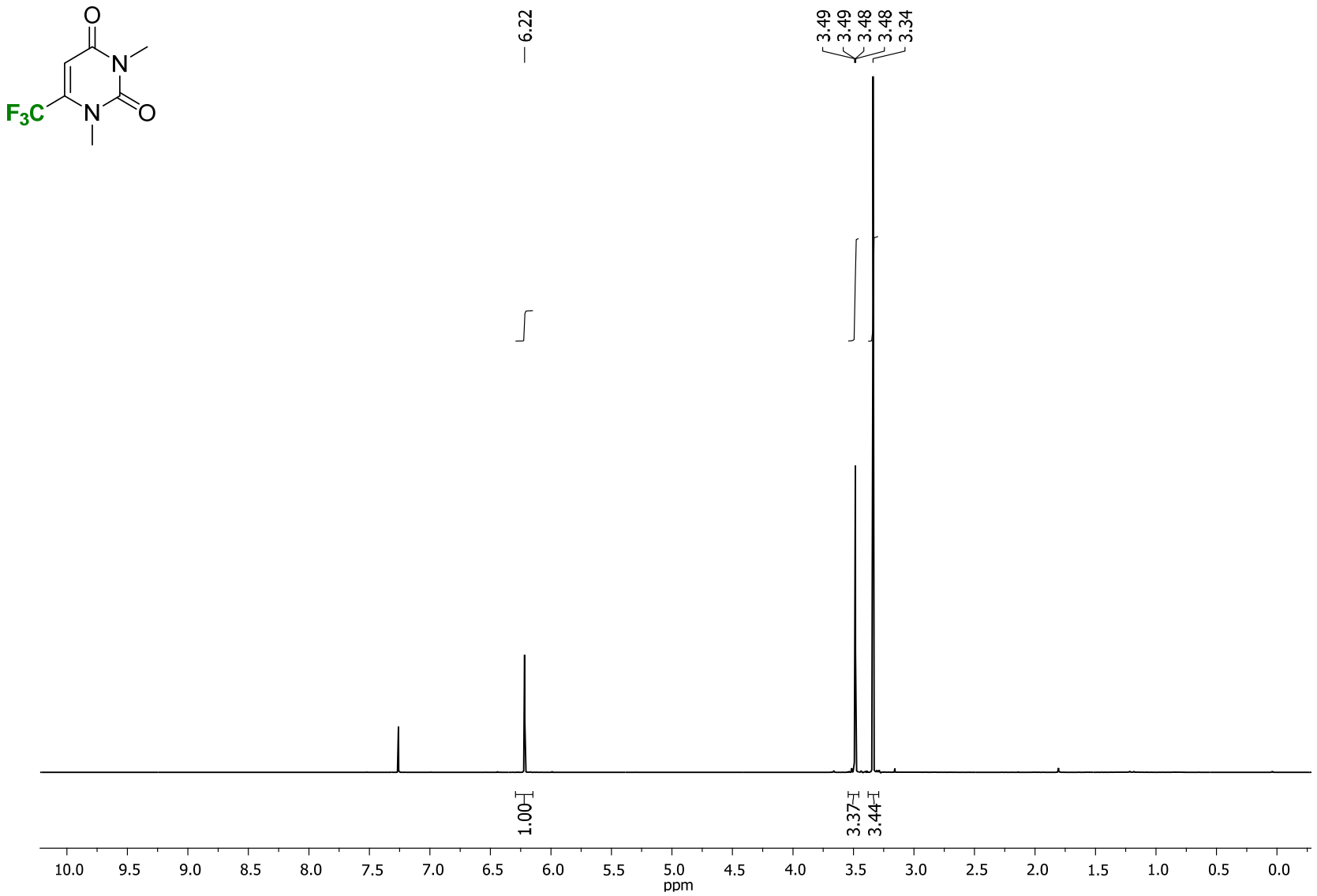

Figure S55. ^{1}H NMR ($CDCl_3$, 400 MHz) of **2o**

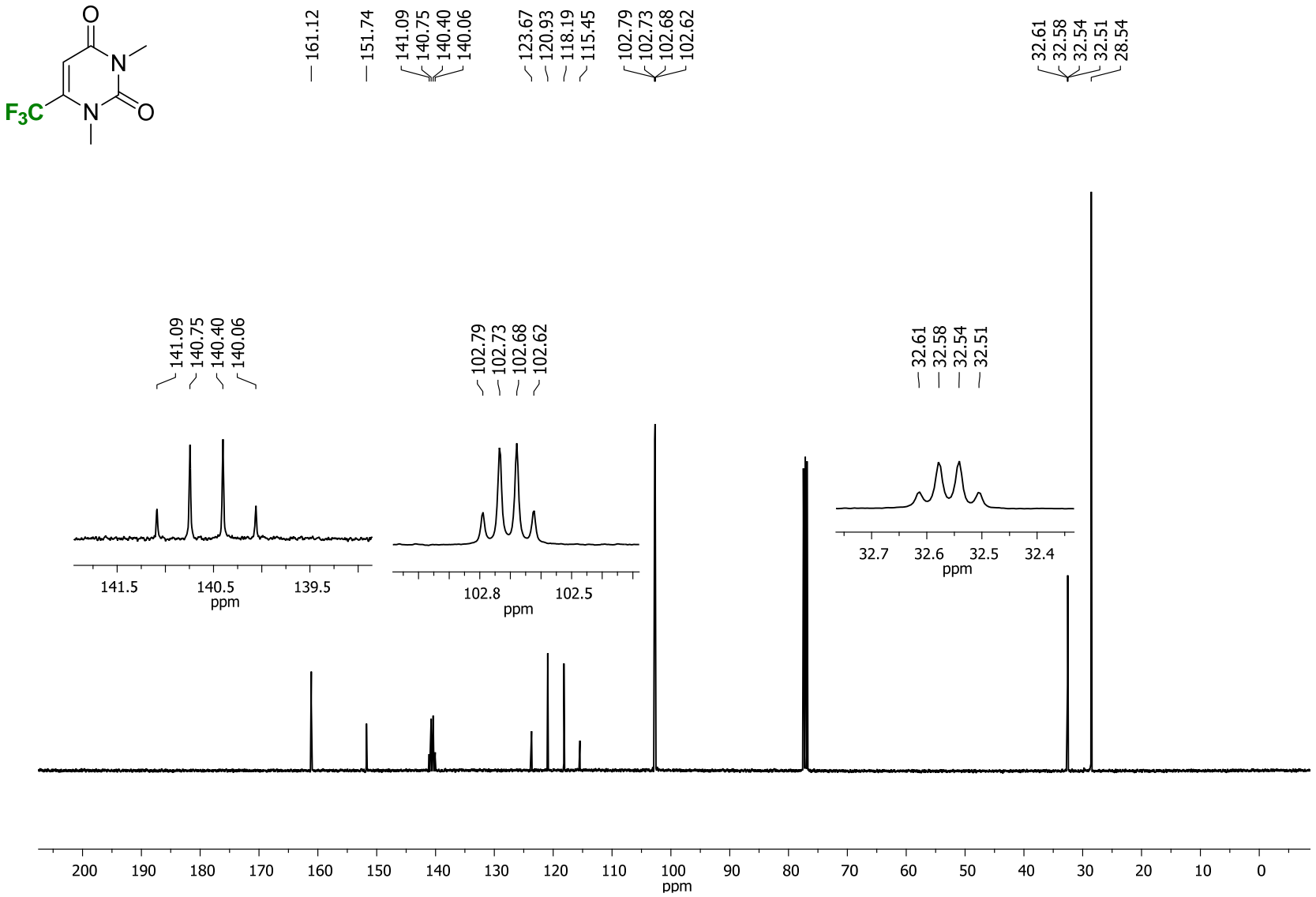

Figure S56. ^{13}C NMR ($CDCl_3$, 100.6 MHz) of **2o**

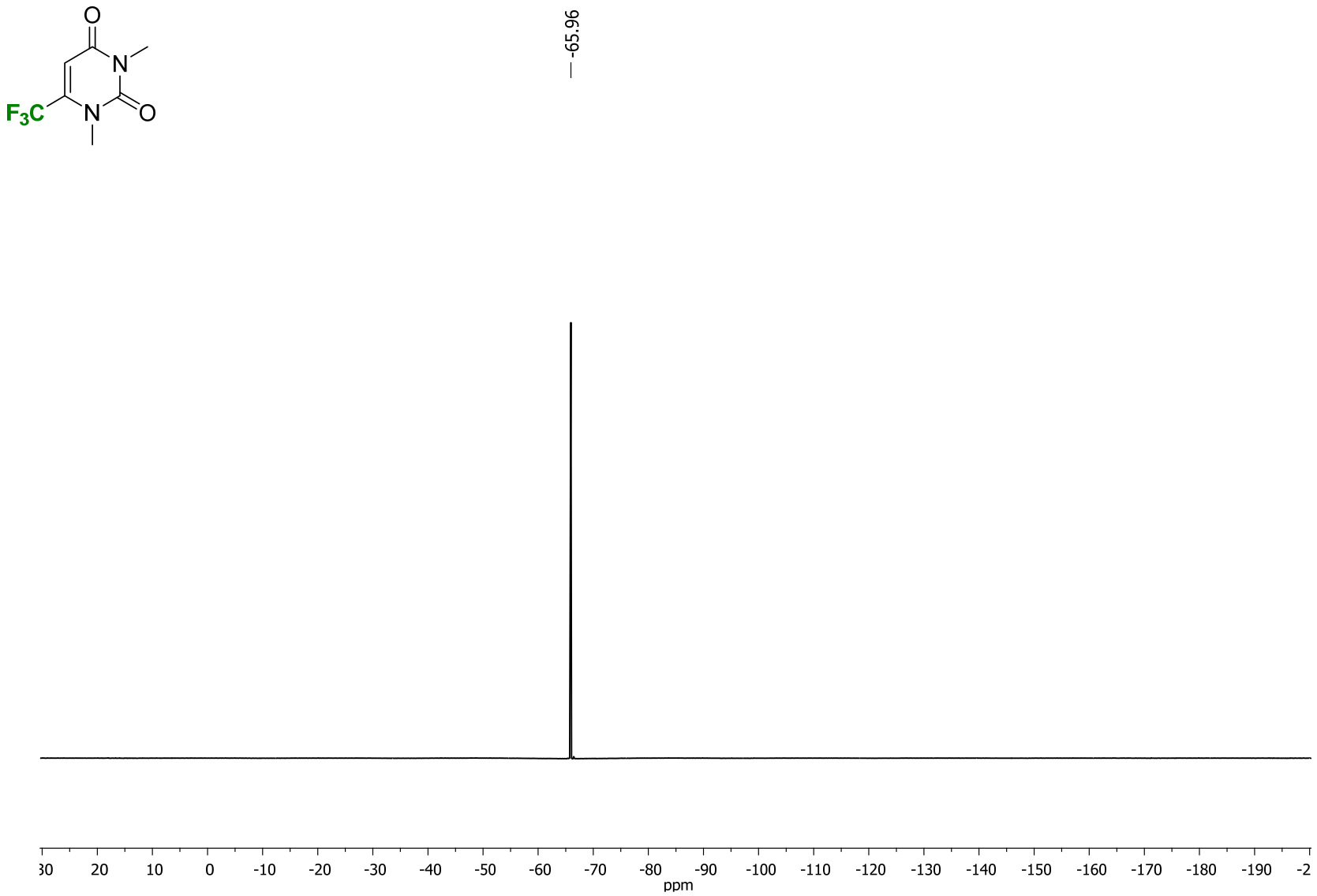

Figure S57. ^{19}F NMR ($CDCl_3$, 376.5 MHz) of **2o**

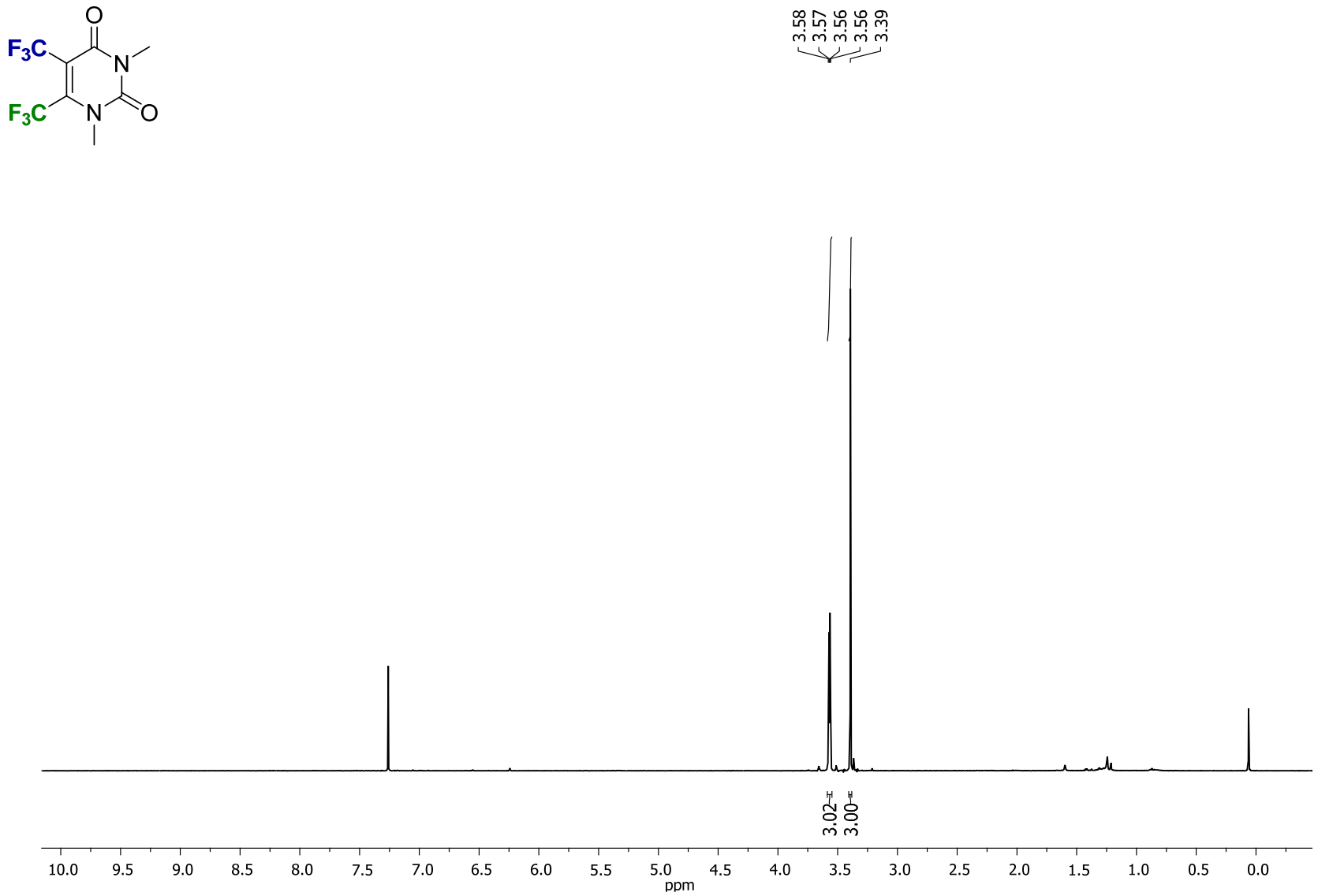

Figure S58. ^{1}H NMR ($CDCl_3$, 400 MHz) of **2p**

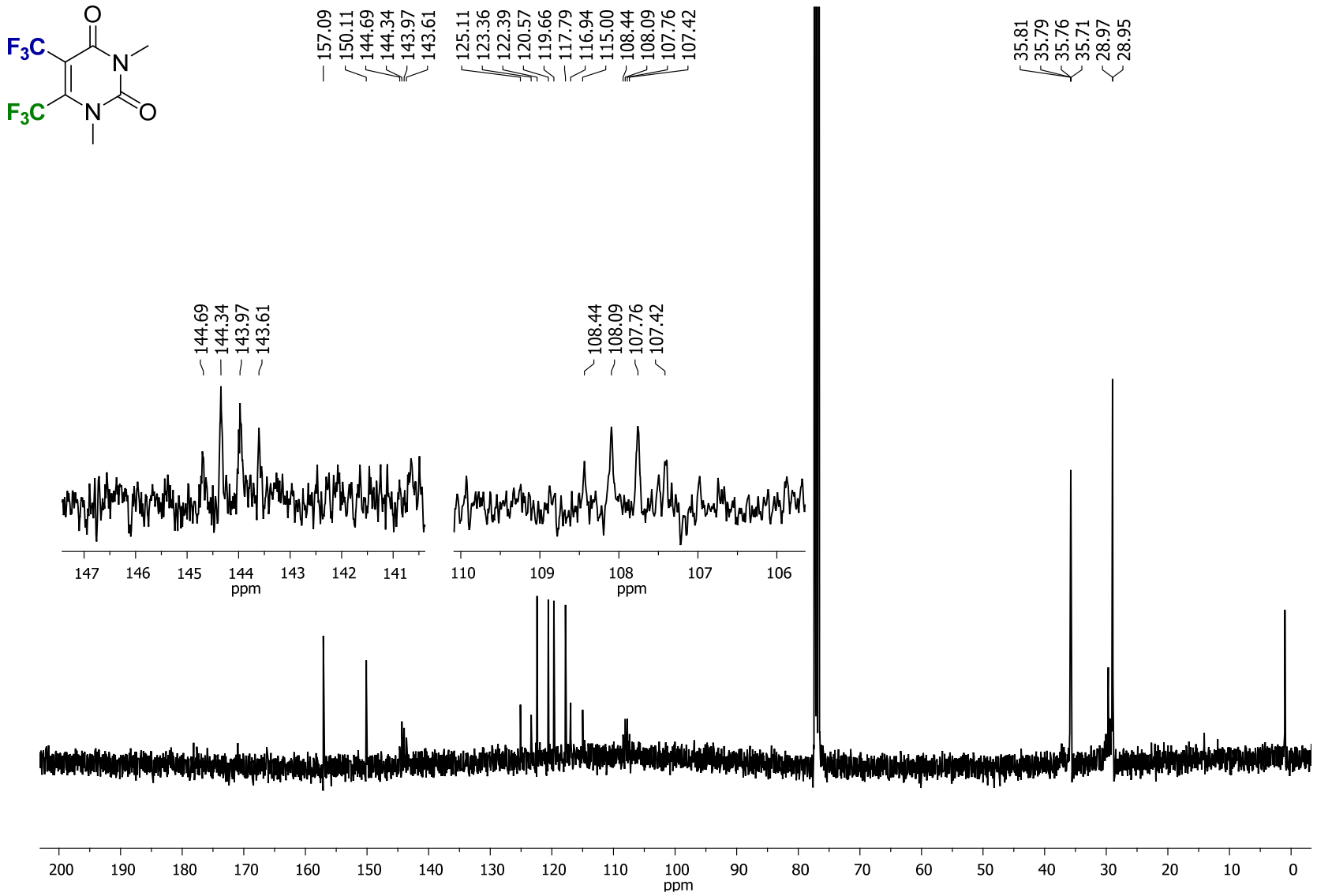

Figure S59. ^{13}C NMR ($CDCl_3$, 100.6 MHz) of **2p**

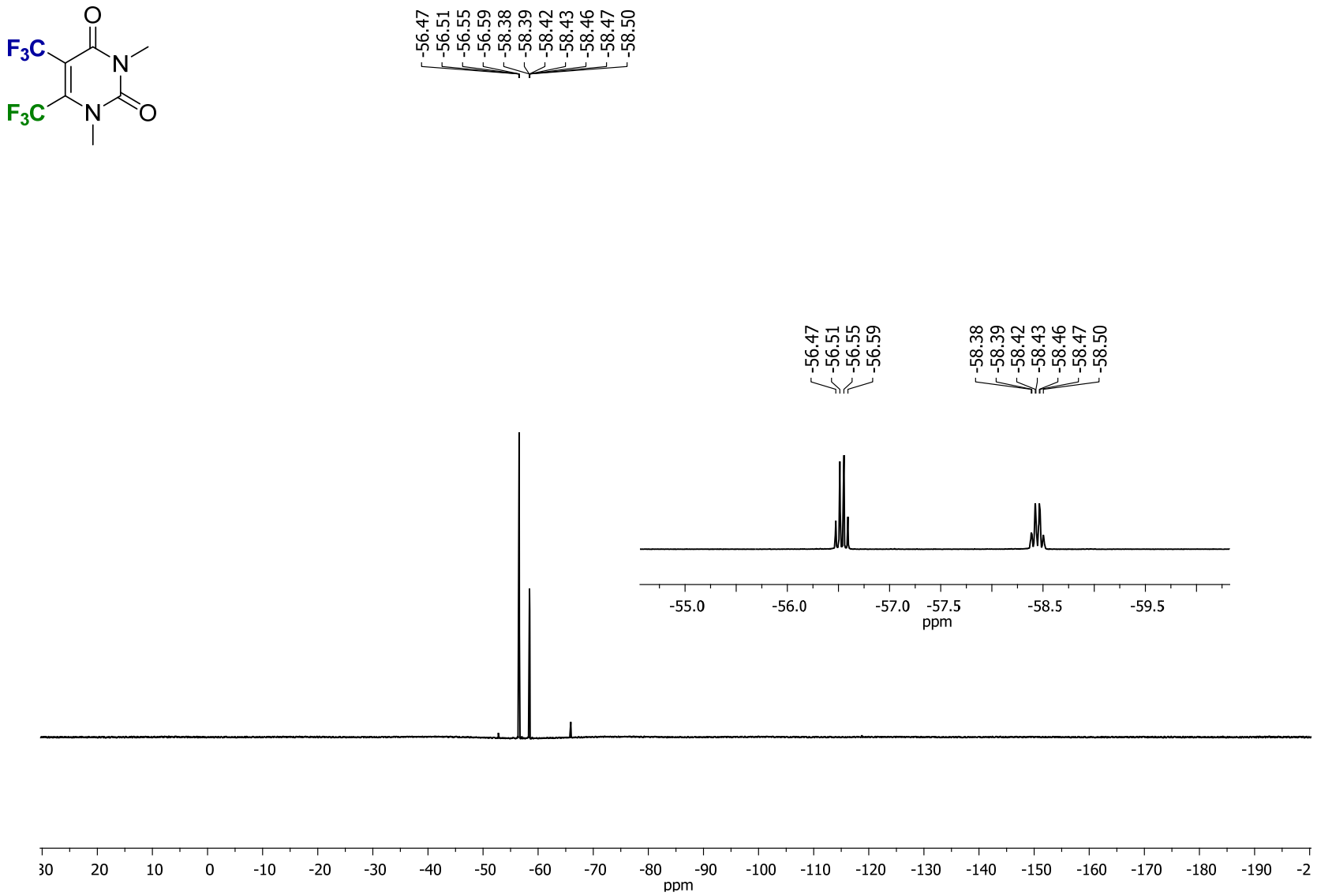

Figure S60. ^{19}F NMR ($CDCl_3$, 376.5 MHz) of **2p**

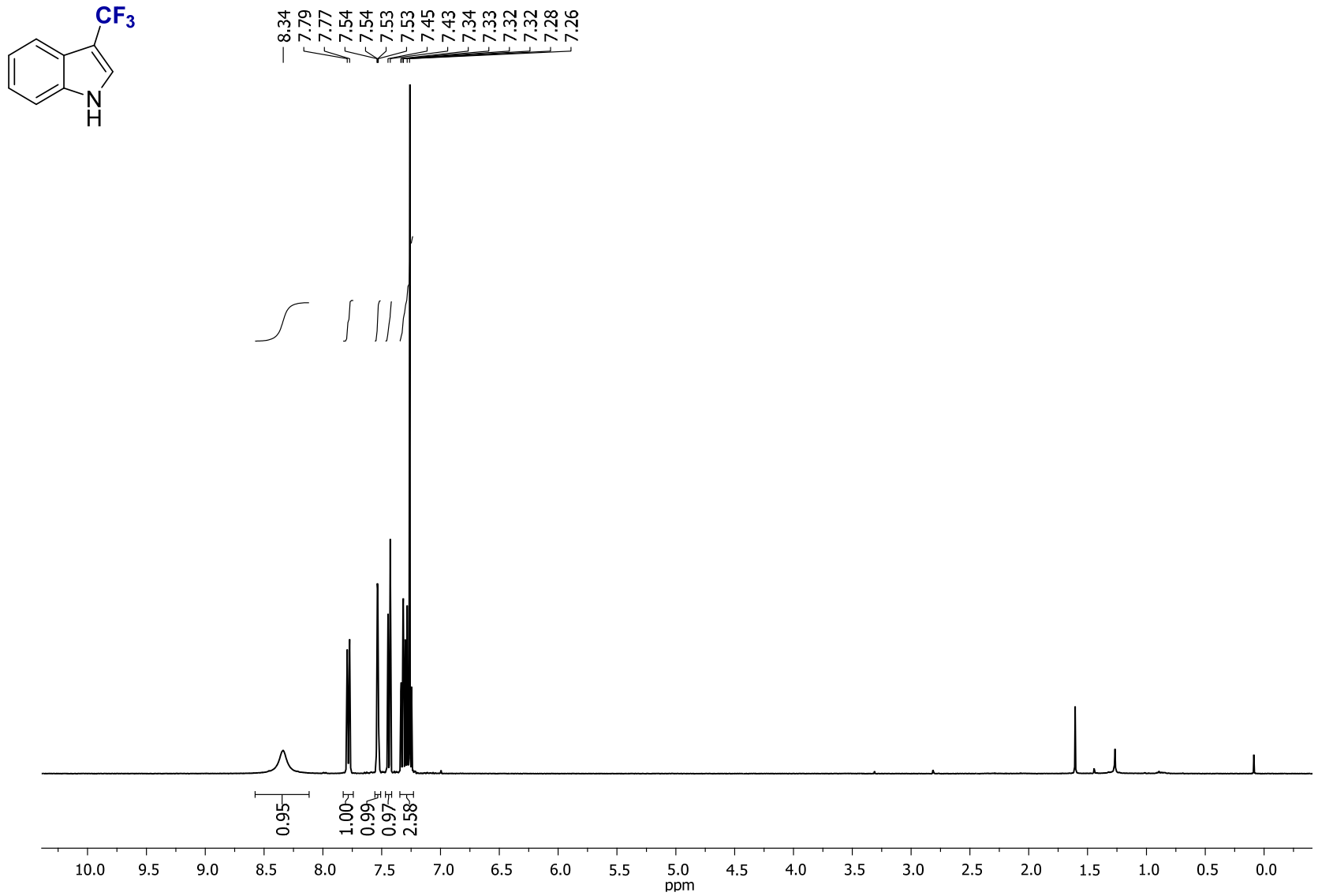

Figure S61. ^{1}H NMR ($CDCl_3$, 400 MHz) of **2q**

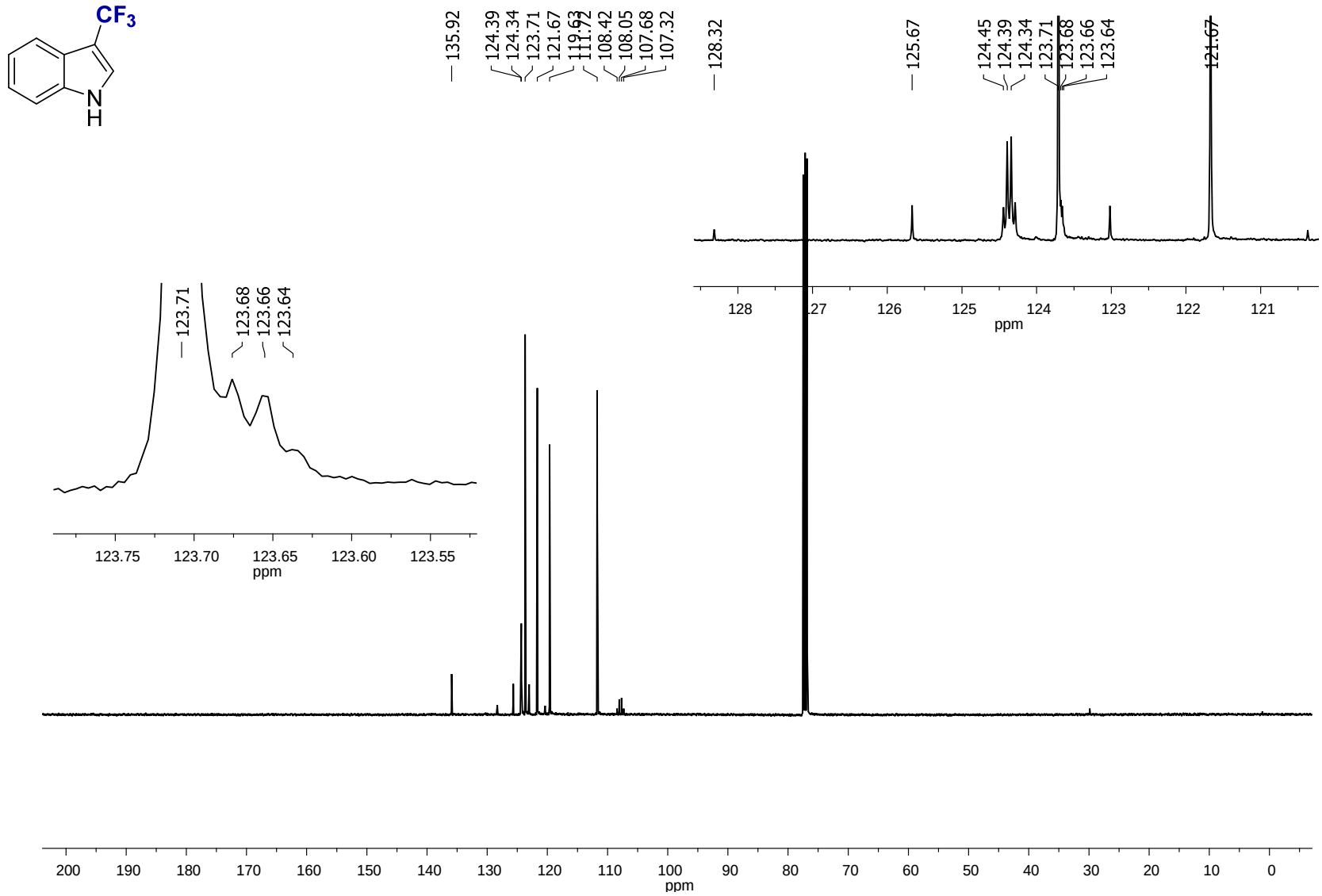

Figure S62. ^{13}C NMR ($CDCl_3$, 100.6 MHz) of **2q**

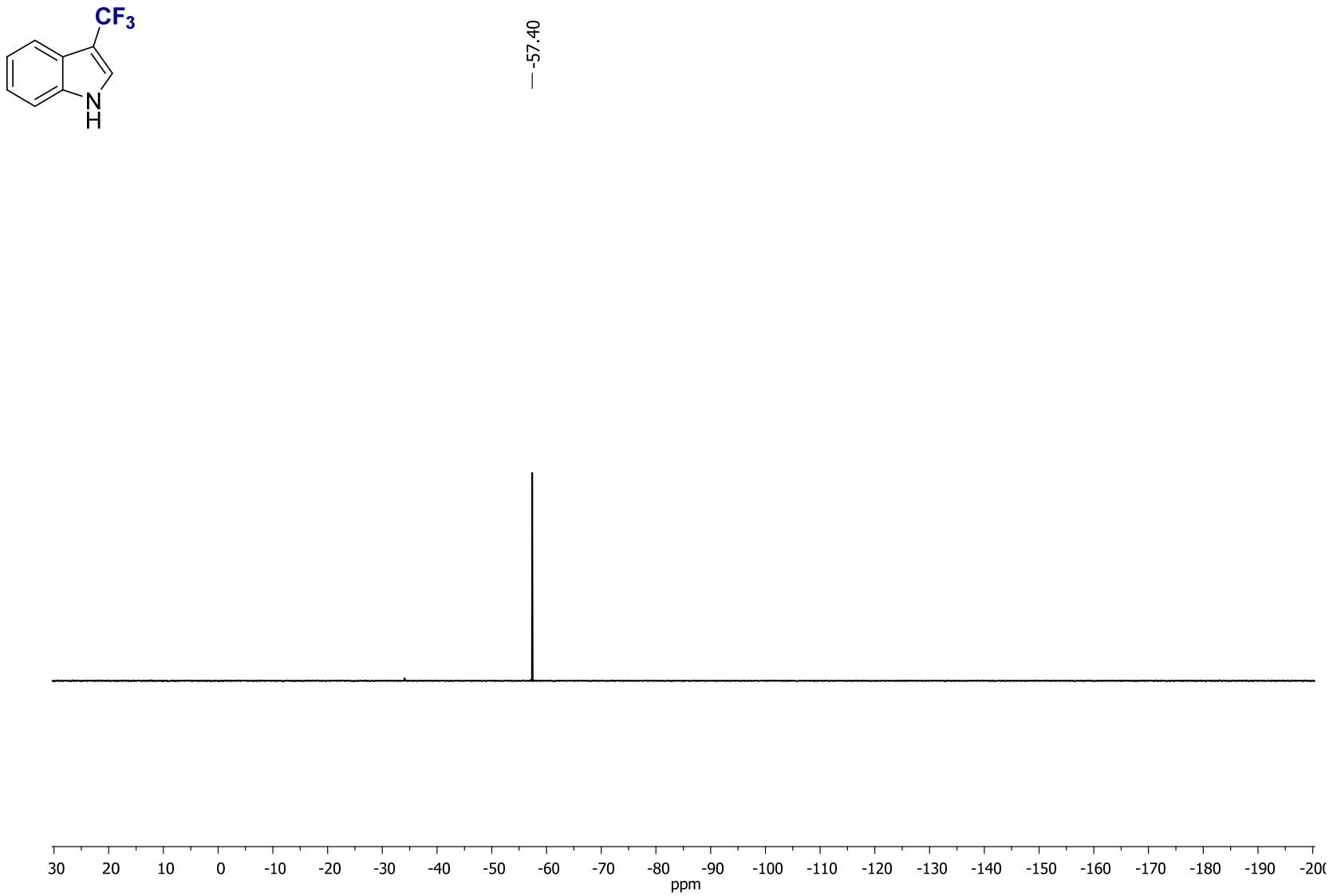

Figure S63. ^{19}F NMR ($CDCl_3$, 376.5 MHz) of **2q**

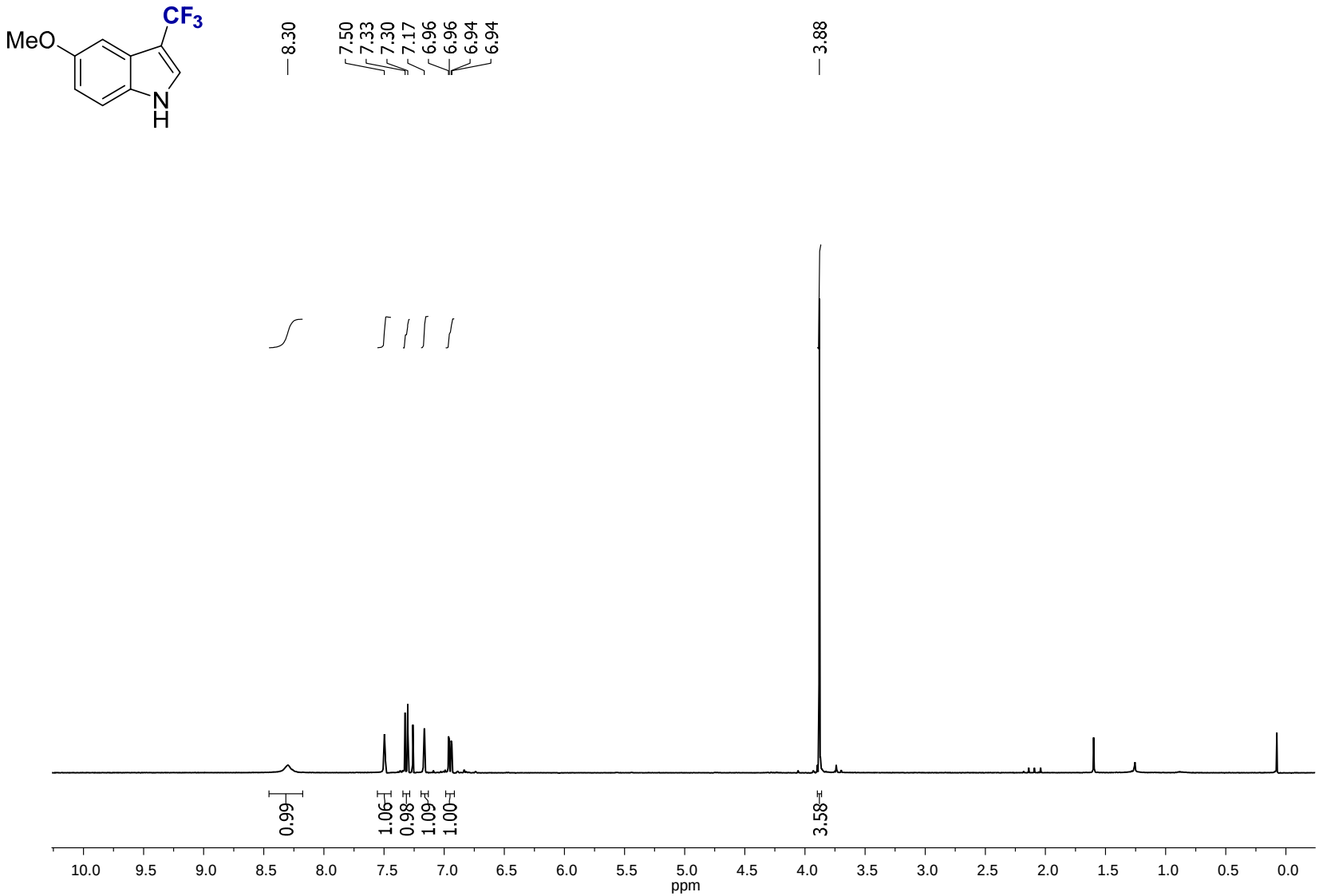

Figure S64. ^{1}H NMR ($CDCl_3$, 400 MHz) of **2r**

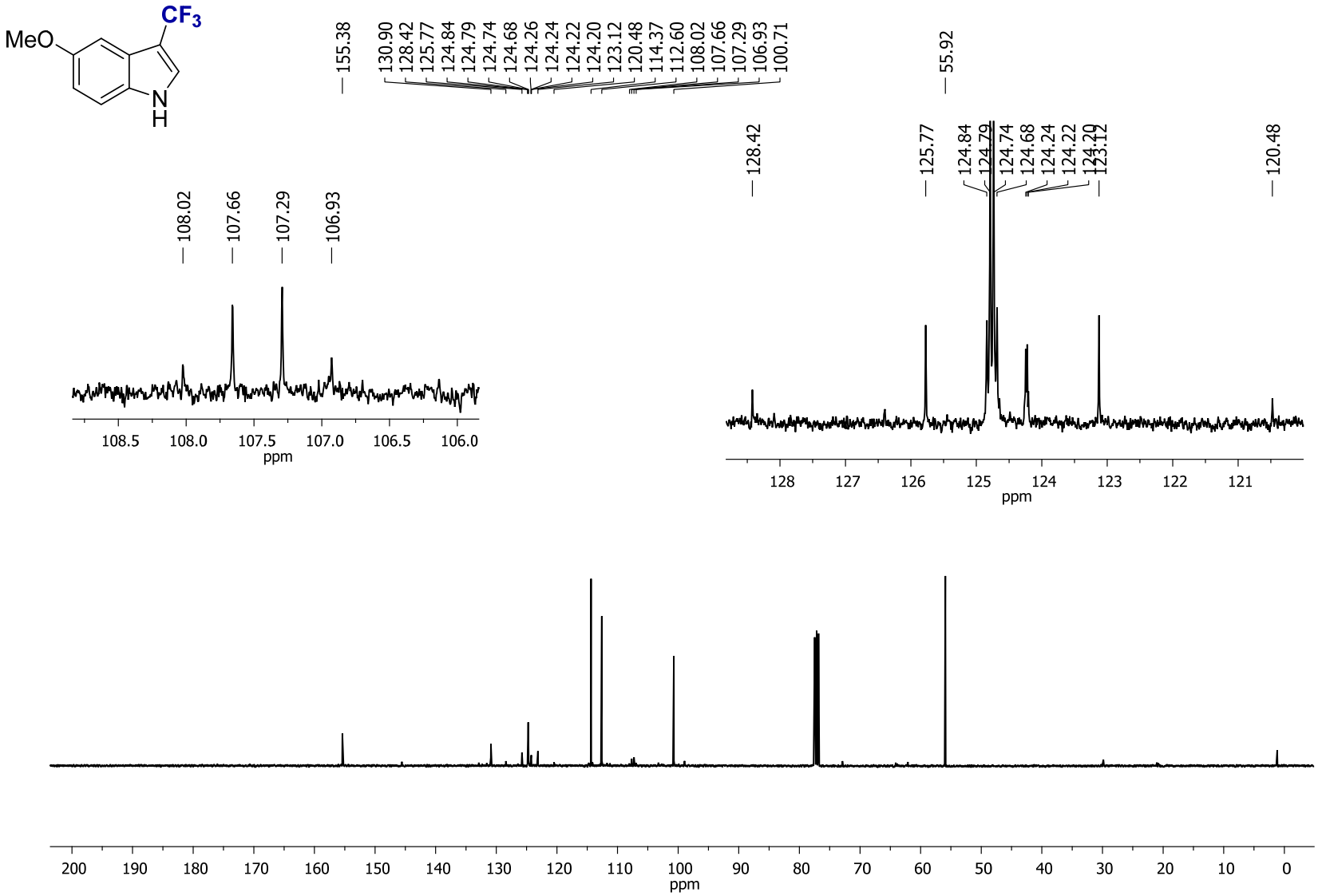

Figure S65. ^{13}C NMR ($CDCl_3$, 100.6 MHz) of **2r**

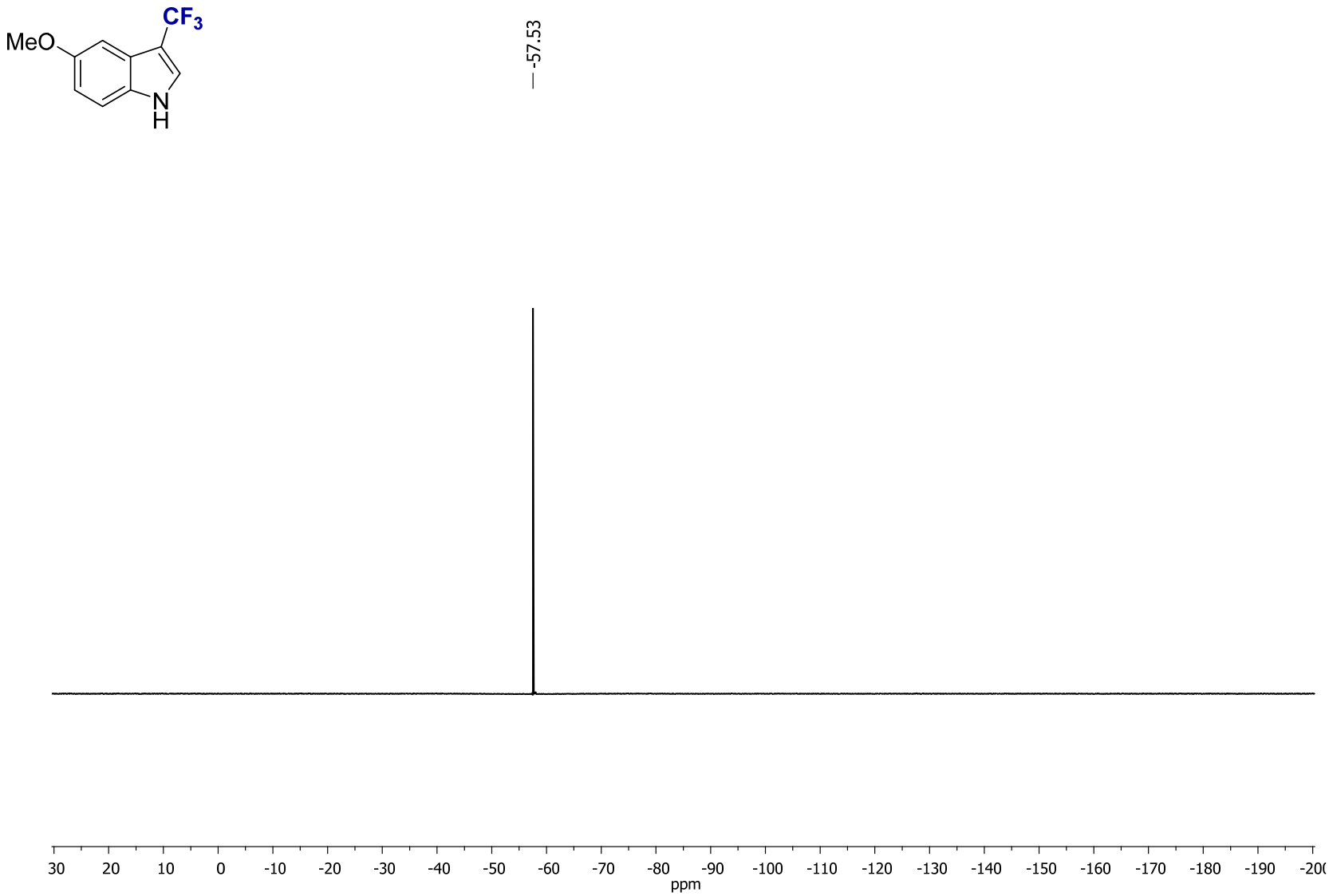

Figure S66. ^{19}F NMR ($CDCl_3$, 376.5 MHz) of **2r**

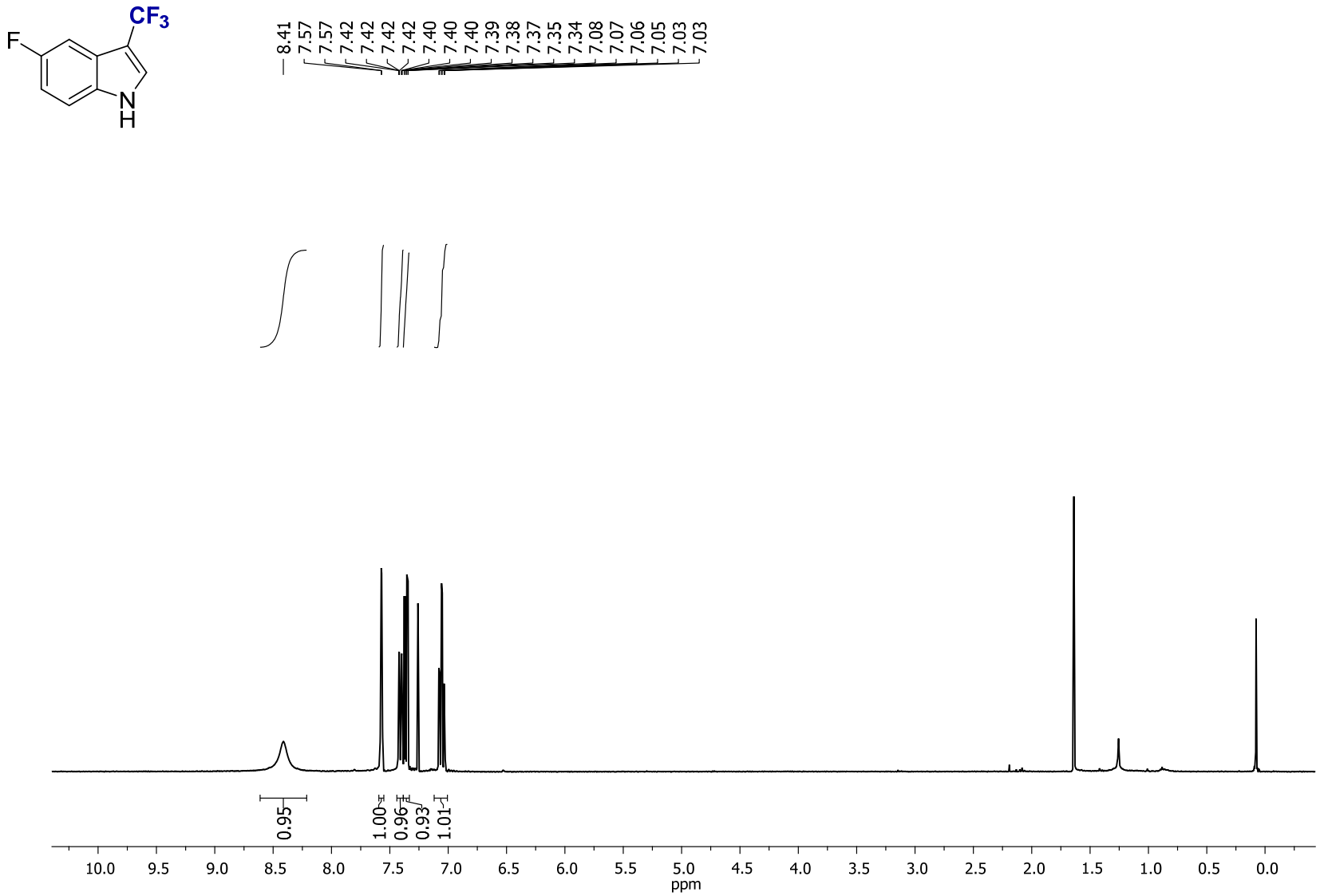

Figure S67. ^{1}H NMR ($CDCl_3$, 400 MHz) of **2s**

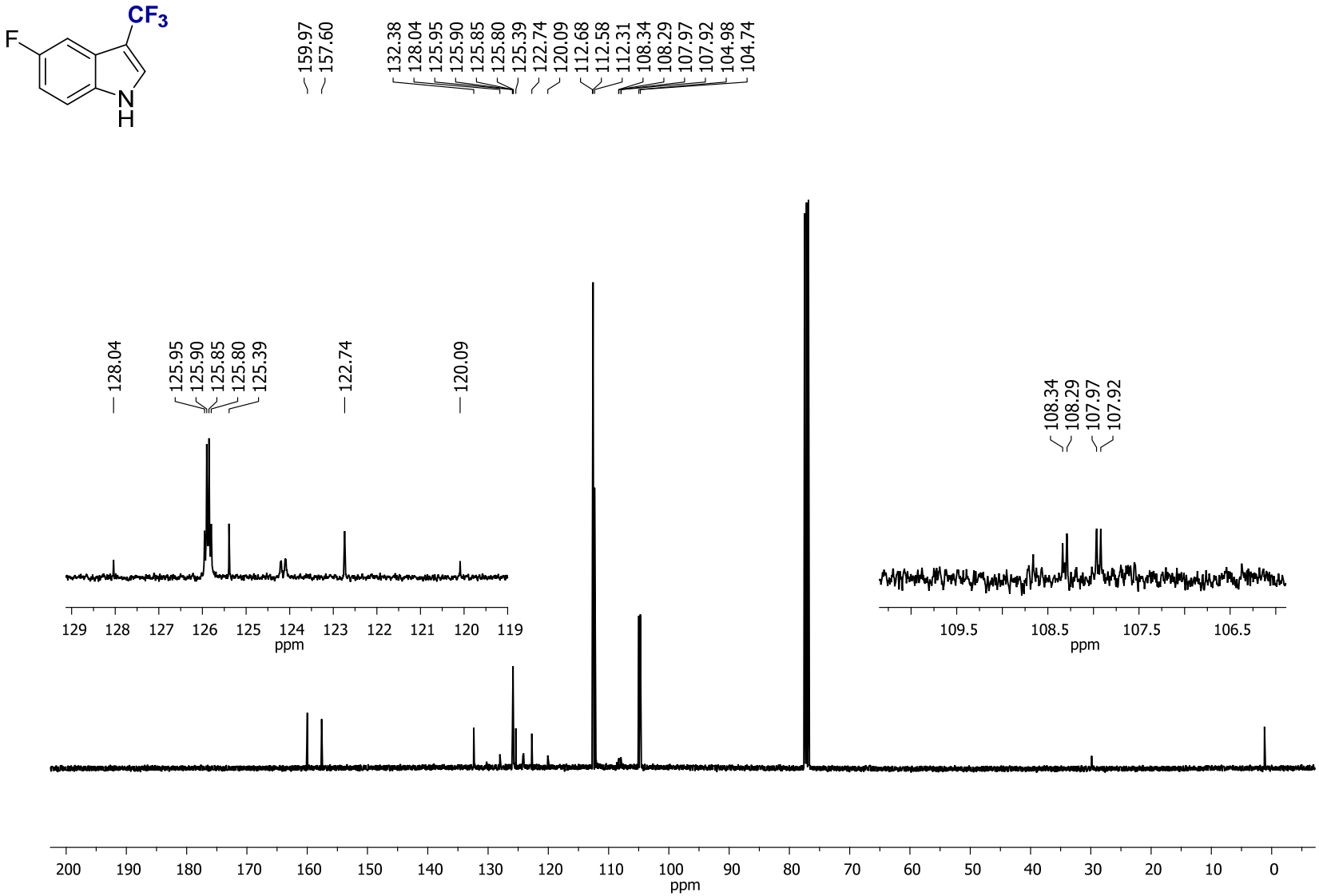

Figure S68. ^{13}C NMR ($CDCl_3$, 100.6 MHz) of **2s**

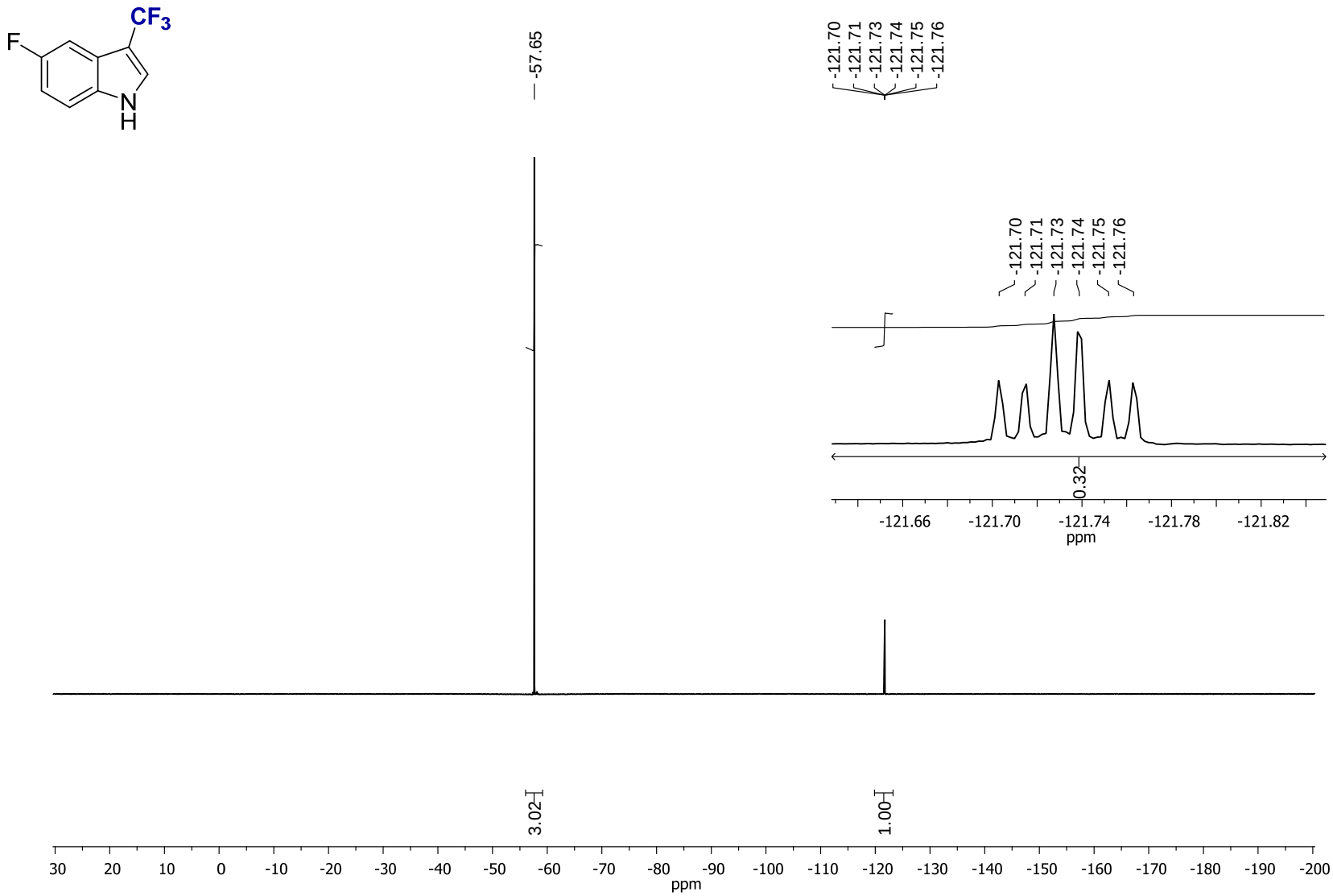

Figure S69. ^{19}F NMR ($CDCl_3$, 376.5 MHz) of **2s**

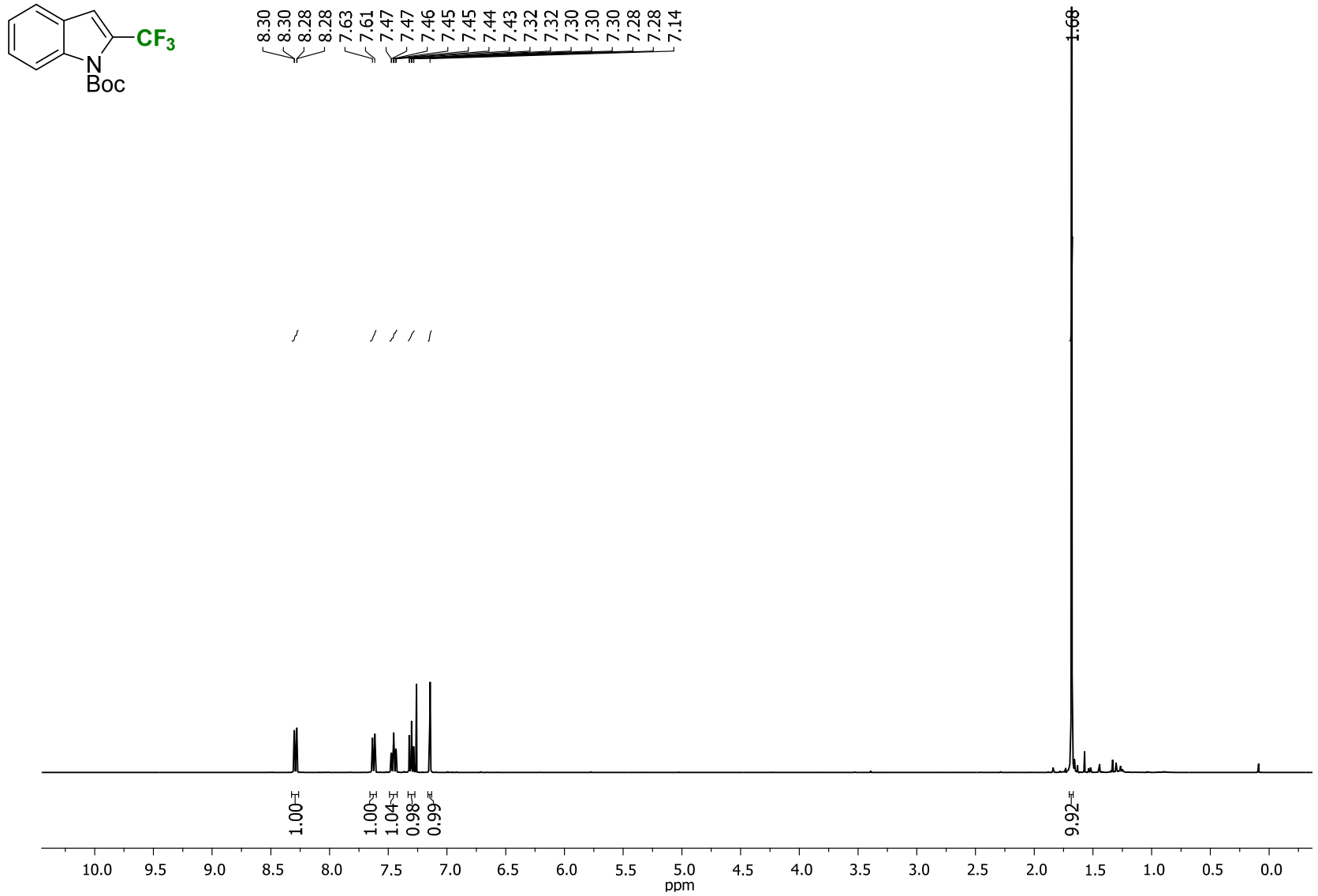

Figure S70. ^{1}H NMR ($CDCl_3$, 400 MHz) of **2t**

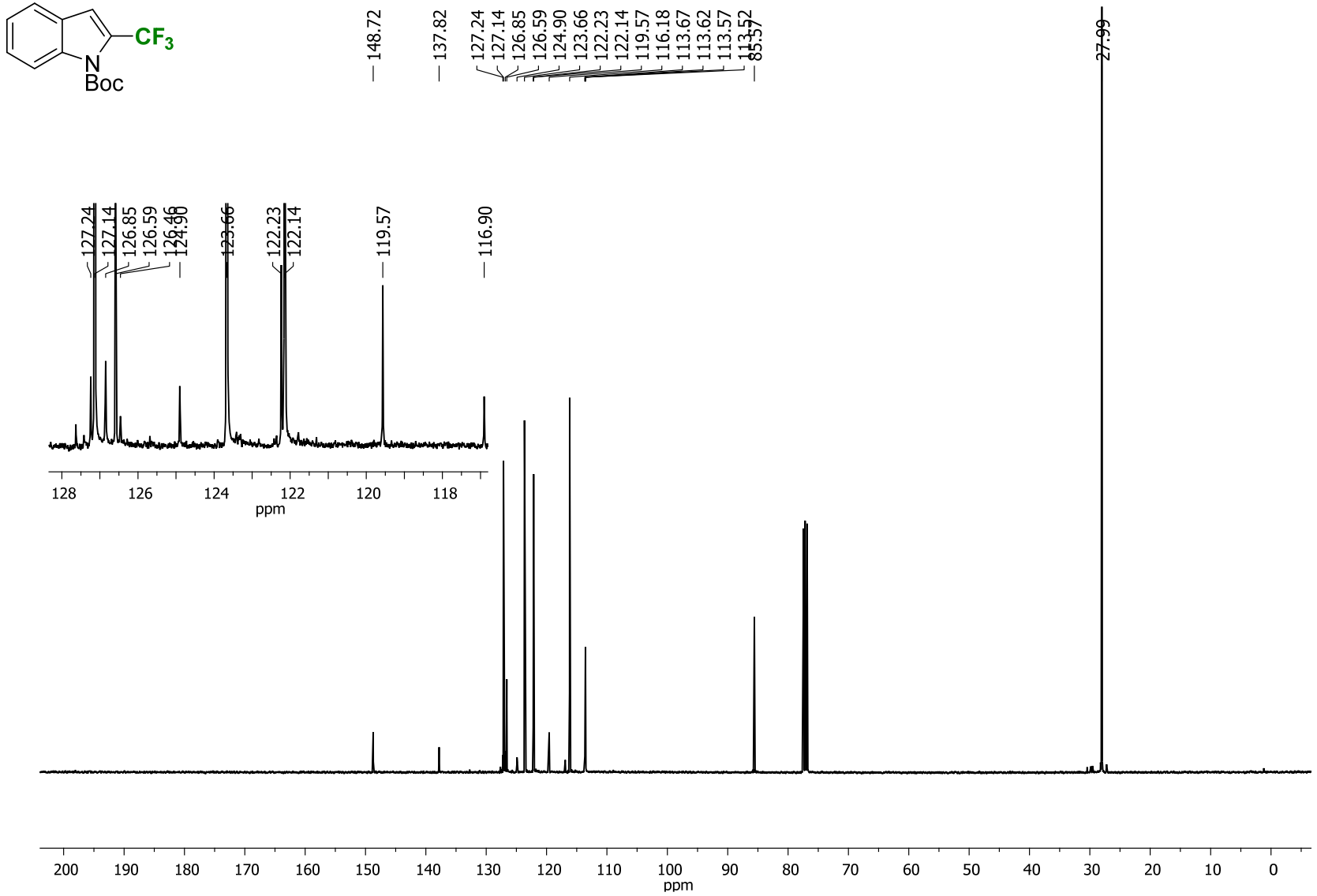

Figure S71. ^{13}C NMR ($CDCl_3$, 100.6 MHz) of **2t**

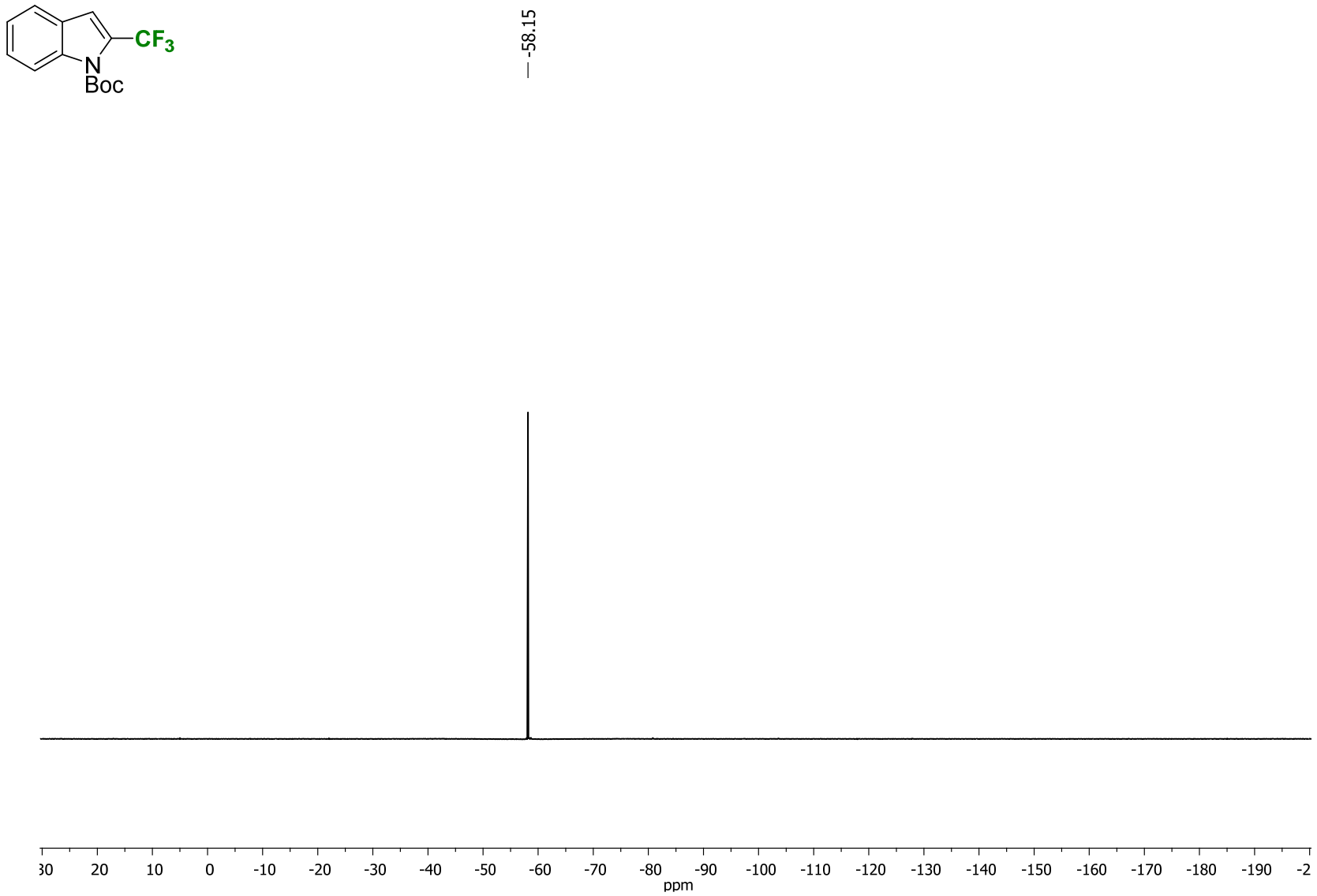

Figure S72. ^{19}F NMR ($CDCl_3$, 376.5 MHz) of **2t**

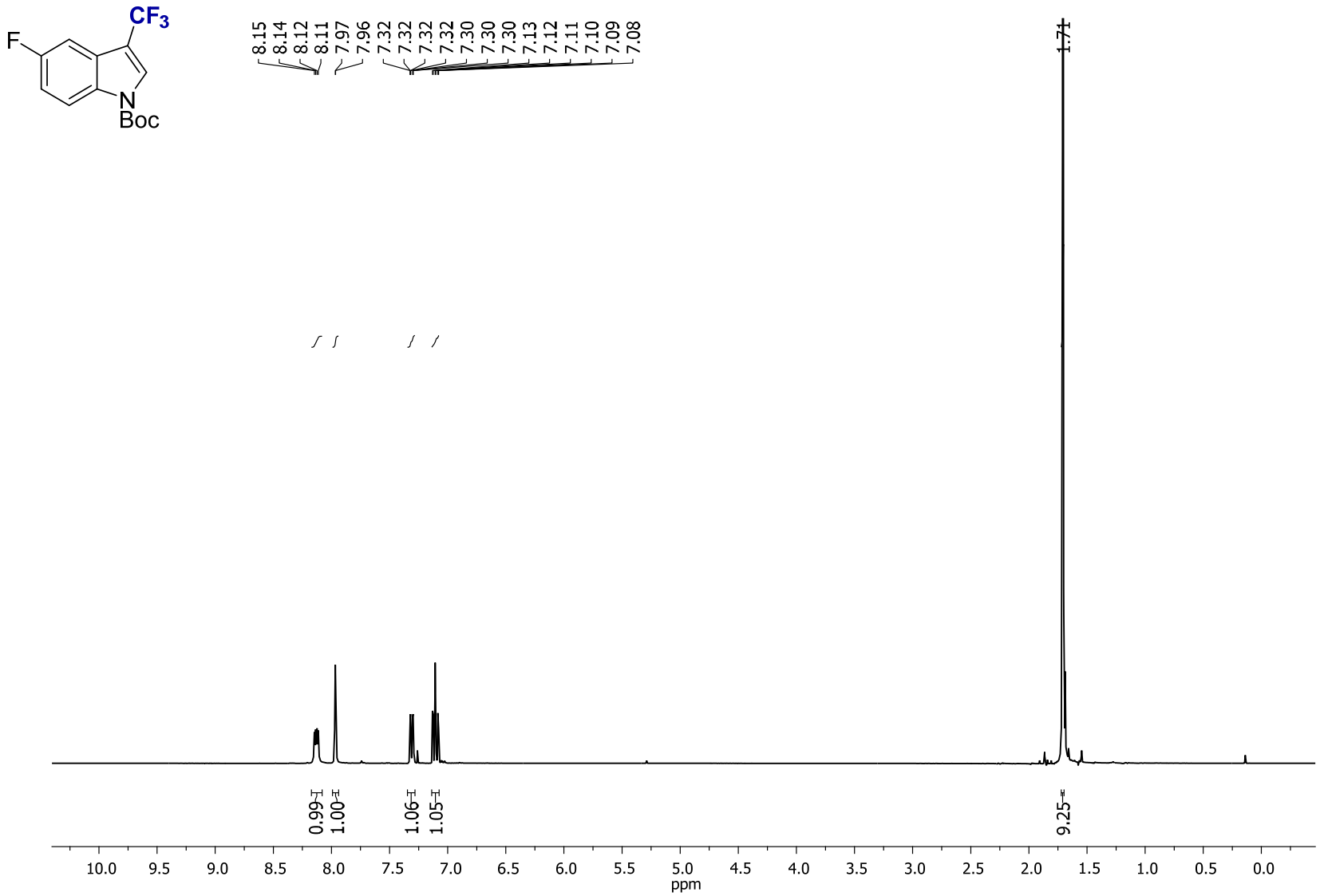

Figure S73. ^{1}H NMR ($CDCl_3$, 400 MHz) of **2u**

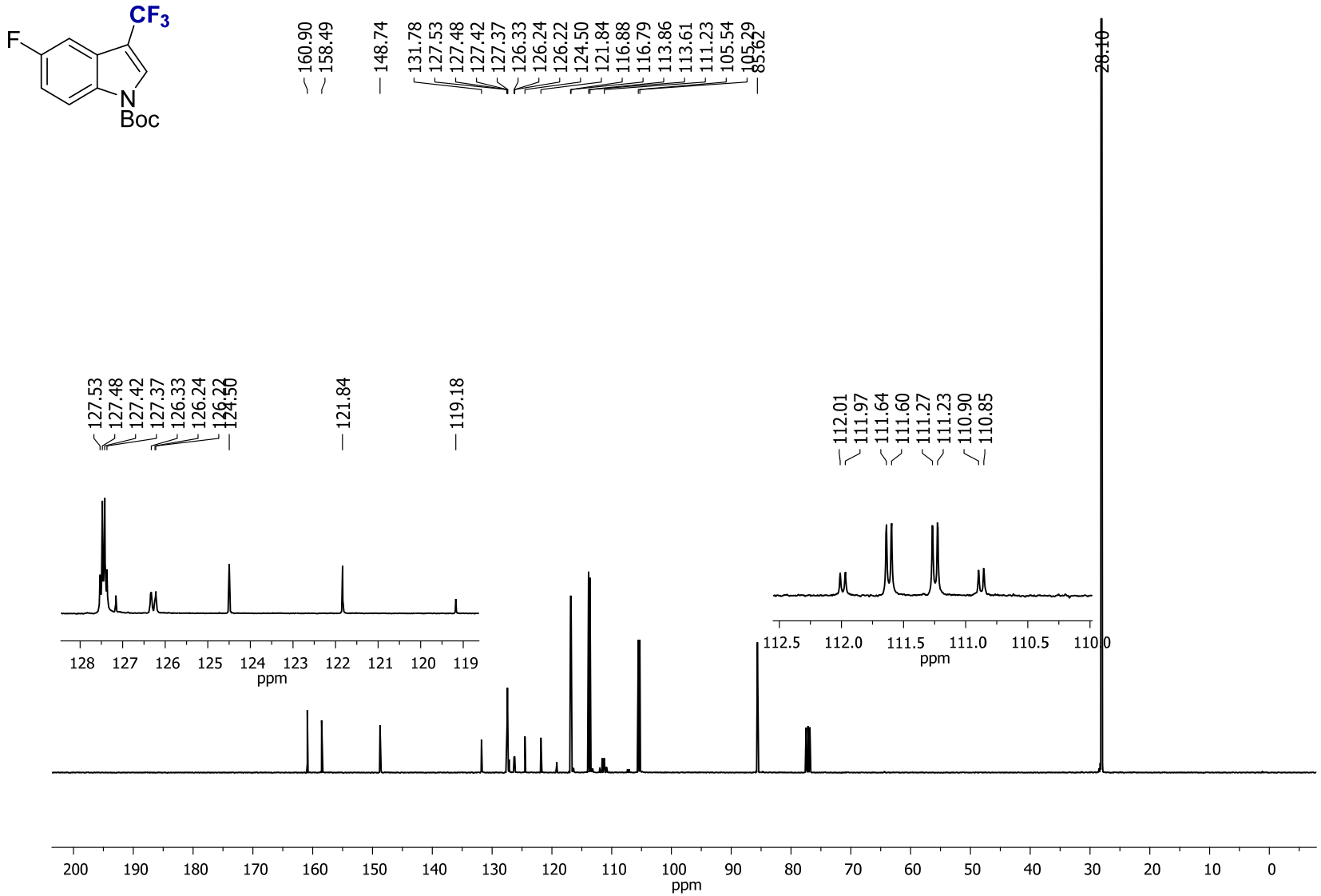

Figure S74. ^{13}C NMR ($CDCl_3$, 100.6 MHz) of **2u**

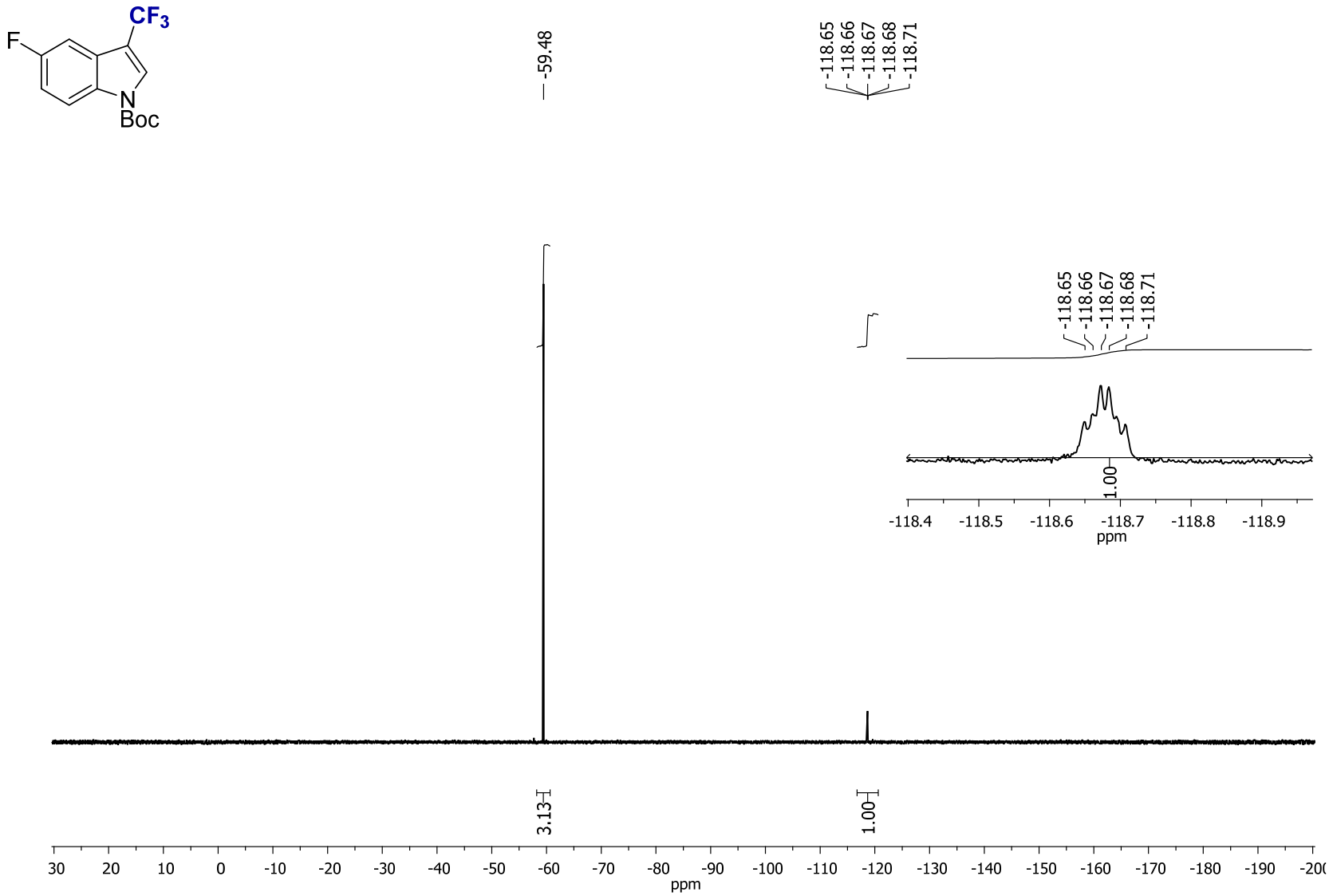

Figure S75. ^{19}F NMR ($CDCl_3$, 376.5 MHz) of **2u**

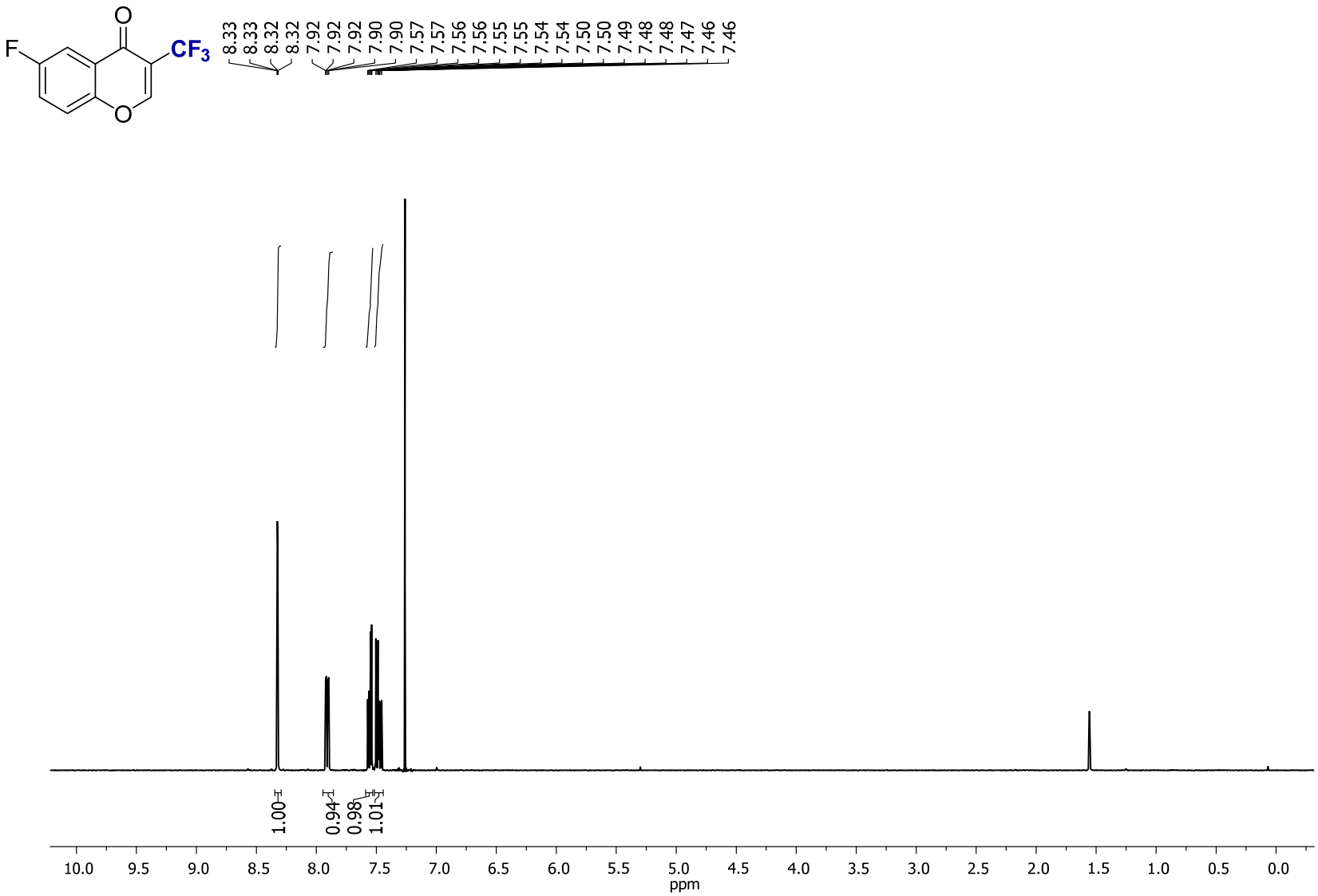

Figure S76. ^{1}H NMR ($CDCl_3$, 400 MHz) of **2v**

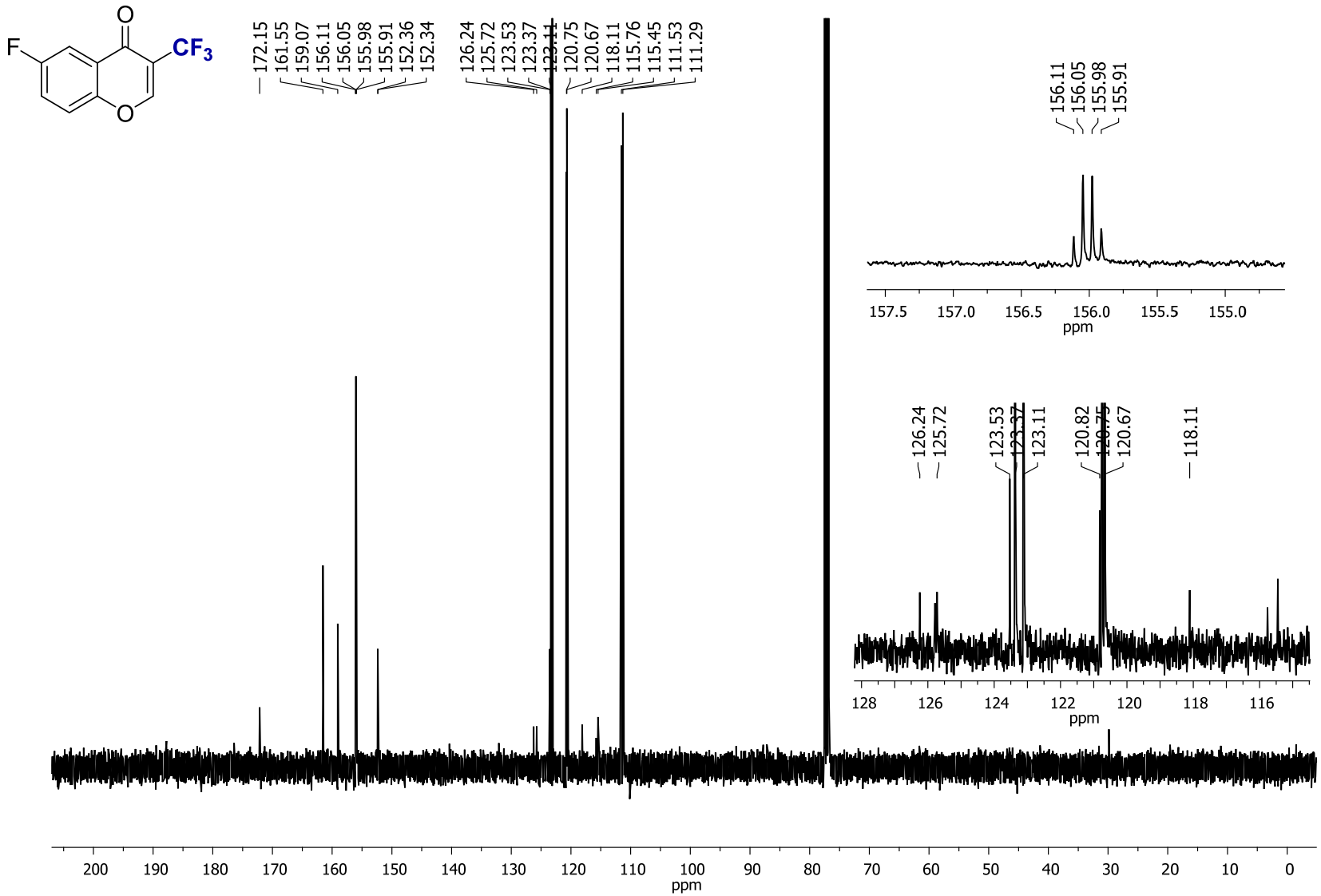

Figure S77. ^{13}C NMR ($CDCl_3$, 100.6 MHz) of **2v**

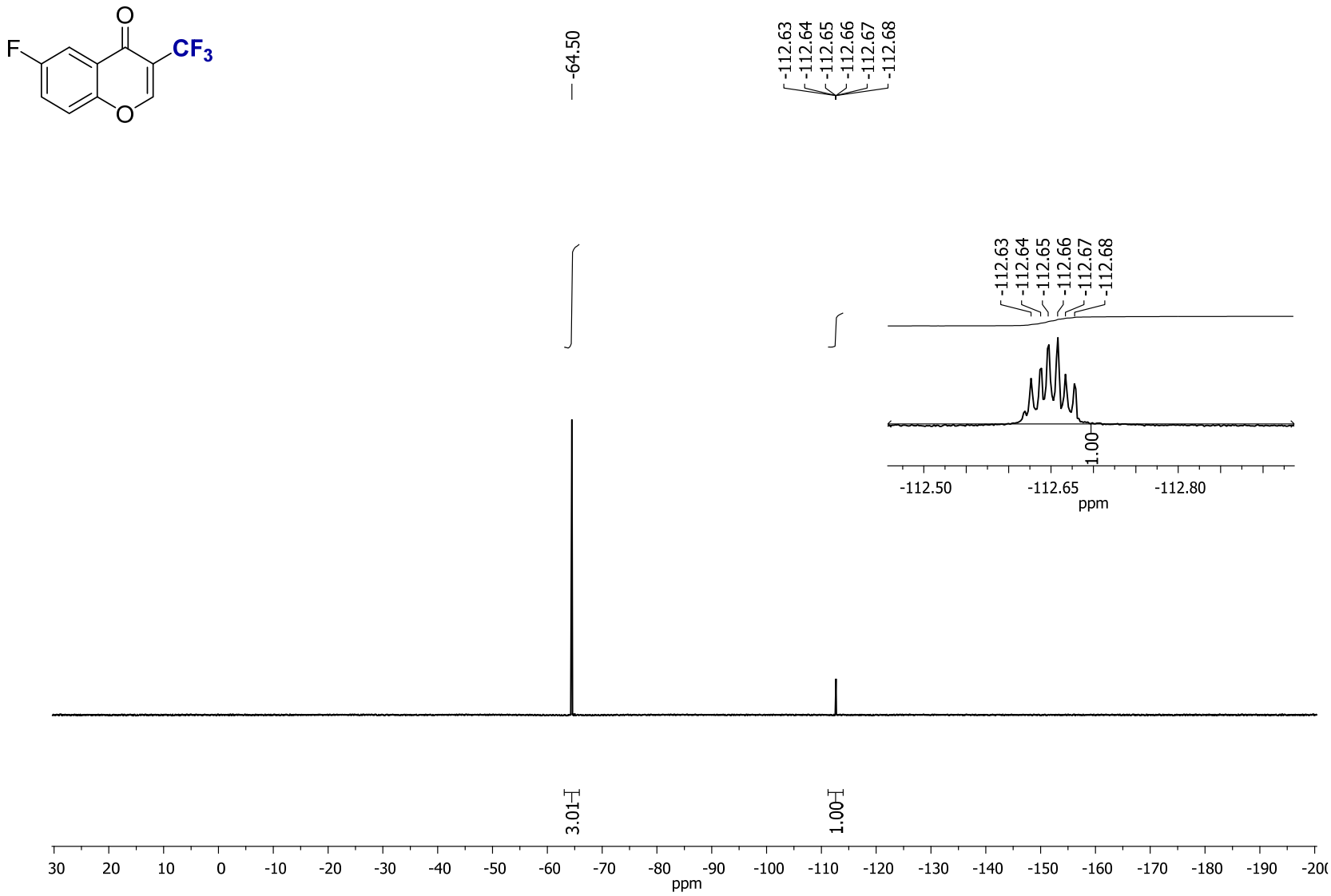

Figure S78. ^{19}F NMR ($CDCl_3$, 376.5 MHz) of **2v**

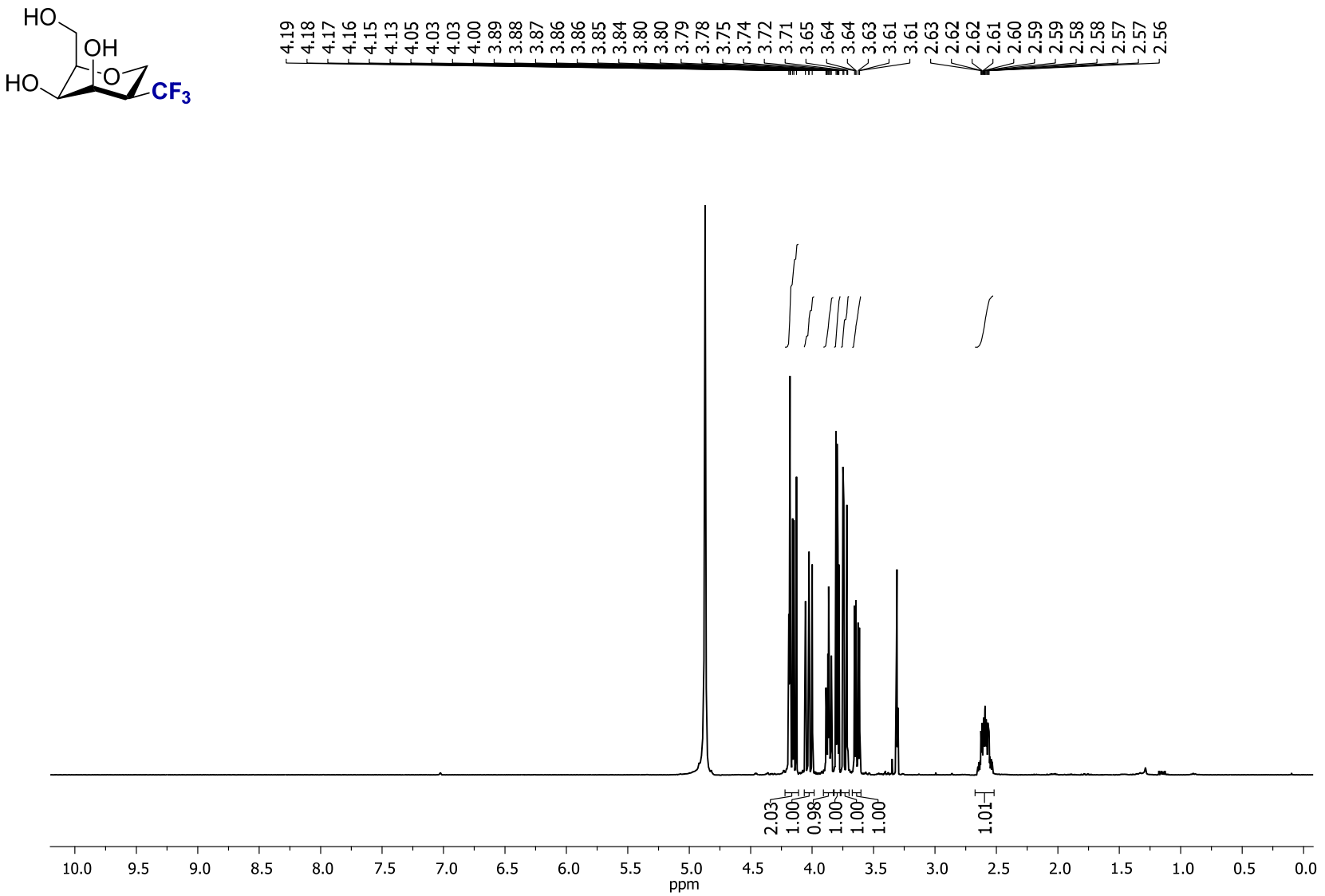

Figure S79. ^{1}H NMR (CD_3OD, 400 MHz) of **5e**

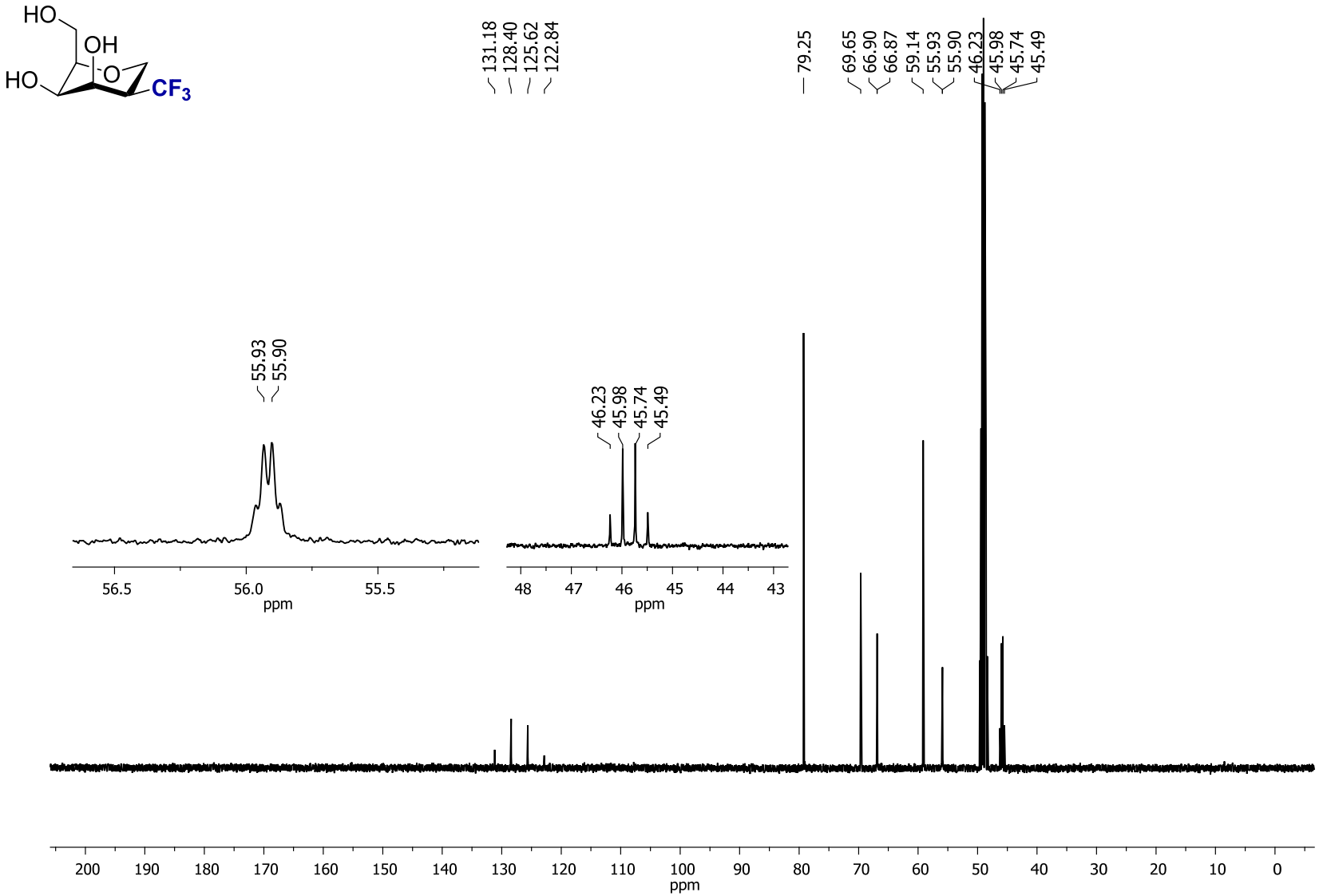

Figure S80. ^{13}C NMR (CD_3OD, 100.6 MHz) of **5e**

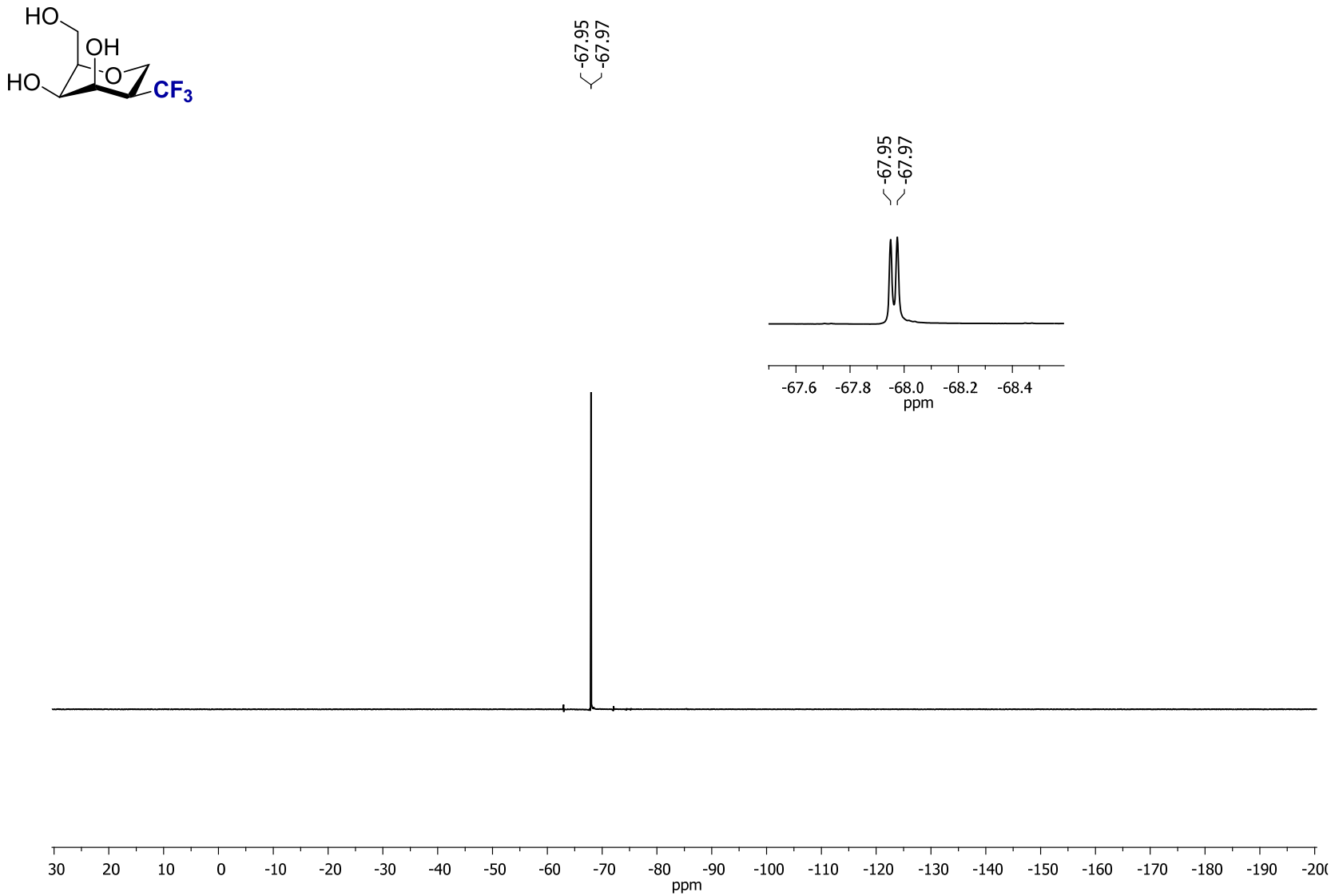

Figure S81. ^{19}F NMR (CD_3OD, 376.5 MHz) of **5e**

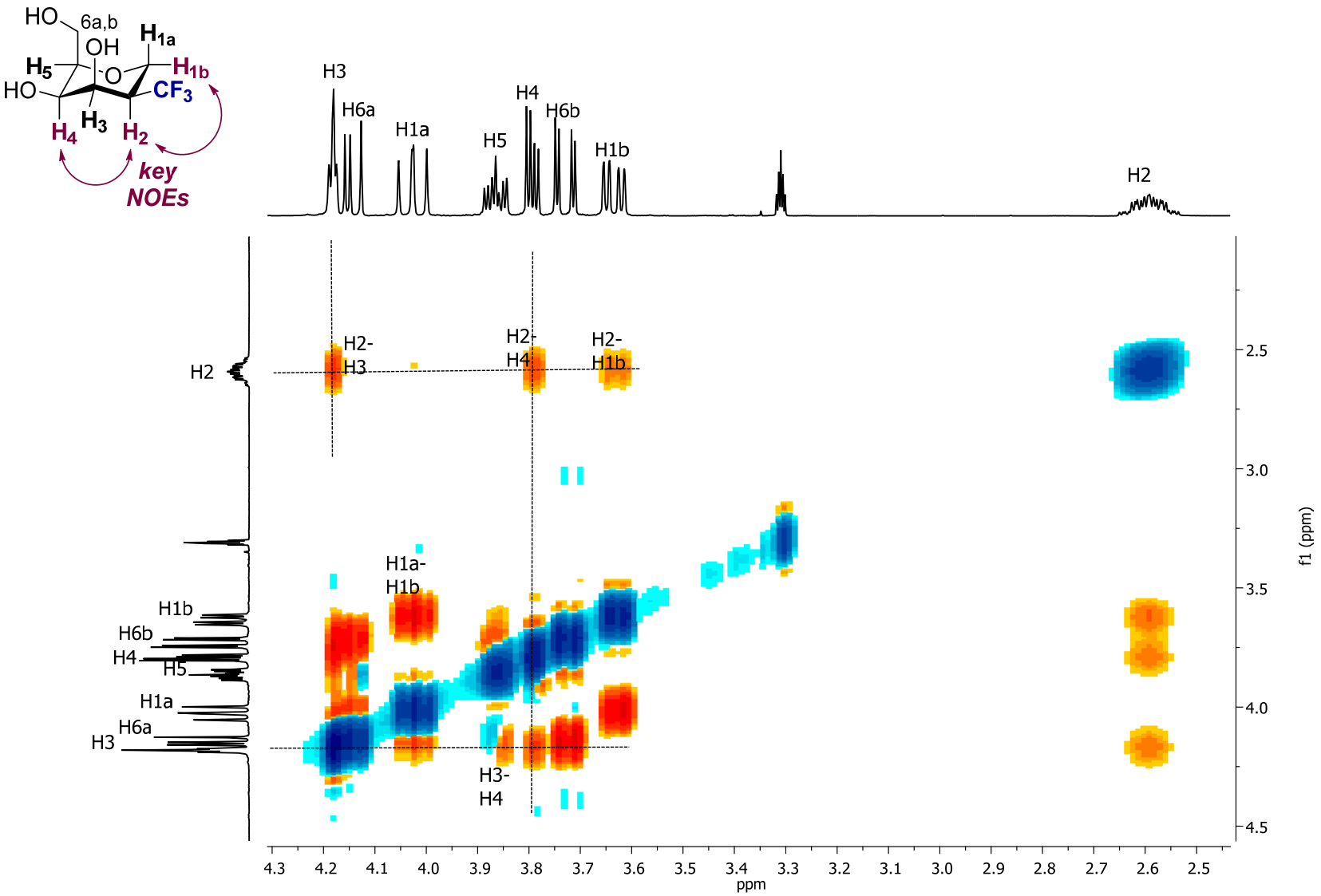

Figure S82. 2D NOESY of **5e** in CD_3OD

4. X-ray crystallographic data

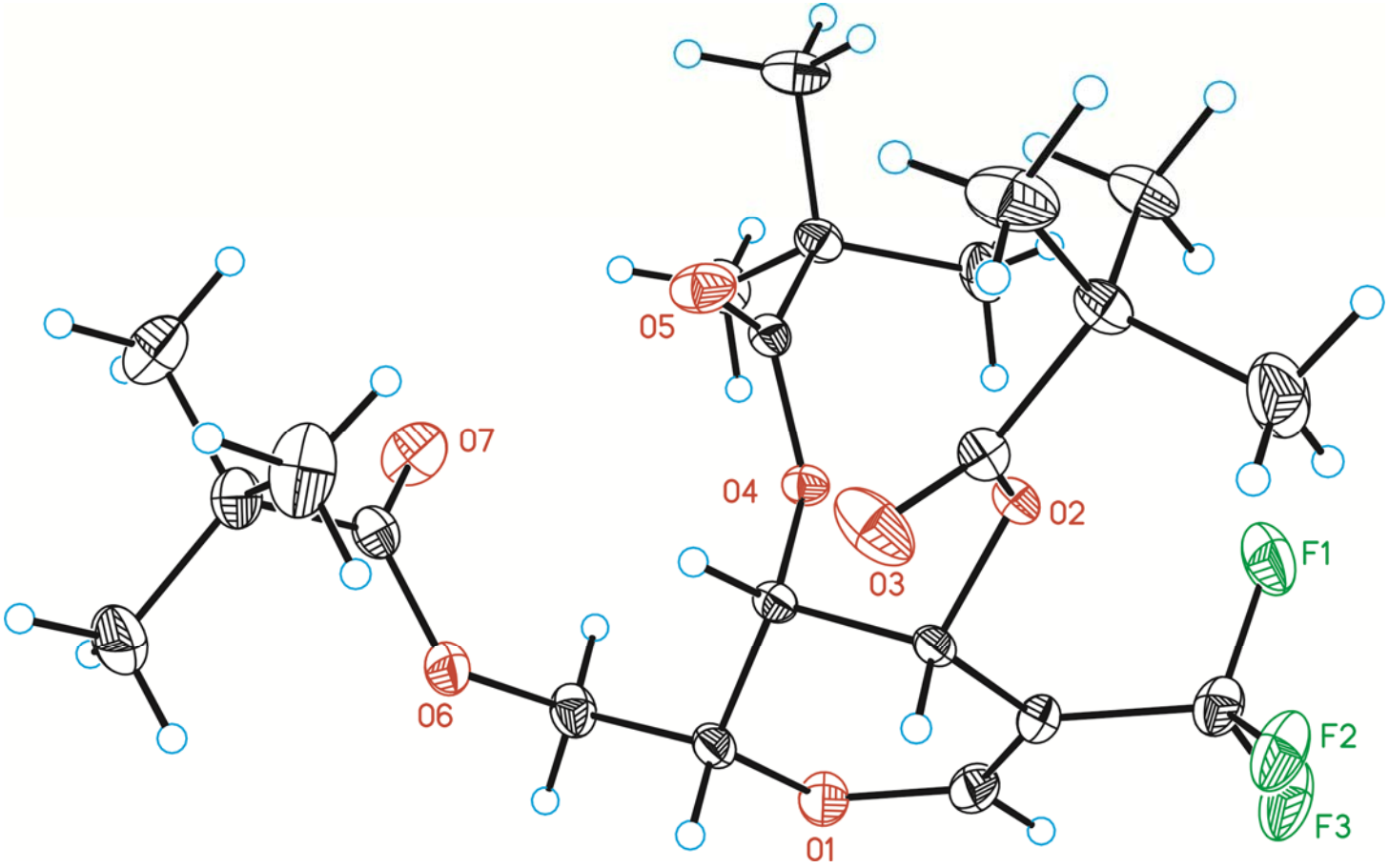

Figure S83. ORTEP diagram of compound **2c** with 50% probability ellipsoid:
Black = carbon, Red = oxygen, Blue = hydrogen, Green = fluorine

Table S2. Crystal data and structure refinement for **2c**

CCDC	1533215	
Empirical formula	C21.95 H33 F2.85 I0.05 O7	
Formula weight	469.38	
Temperature	100(2) K	
Wavelength	0.71073 Å	
Crystal system	Orthorhombic	
Space group	P2(1)2(1)2(1)	
Unit cell dimensions	a = 8.7431(3)Å	α= 90°.
	b = 10.3339(3)Å	β = 90°.
	c = 26.7833(9)Å	γ = 90°.
Volume	2419.88(14) $Å^3$	
Z	4	
Density (calculated)	1.288 Mg/m^3	
Absorption coefficient	0.171 mm^{-1}	
F(000)	996	
Crystal size	0.30 x 0.10 x 0.005 mm^3	
Theta range for data collection	1.521 to 30.573°.	
Index ranges	-12<=h<=12,-14<=k<=8,-37<=l<=29	
Reflections collected	15619	
Independent reflections	6891[R(int) = 0.0304]	
Completeness to theta =30.573°	94.700005%	
Absorption correction	Empirical	
Max. and min. transmission	0.999 and 0.95	
Refinement method	Full-matrix least-squares on F^2	
Data / restraints / parameters	6891/ 0/ 307	
Goodness-of-fit on F^2	1.053	
Final R indices [I>2sigma(I)]	R1 = 0.0333, wR2 = 0.0867	
R indices (all data)	R1 = 0.0375, wR2 = 0.0886	
Flack parameter	x =-0.14(3)	
Largest diff. peak and hole	0.268 and -0.206 e.$Å^{-3}$	

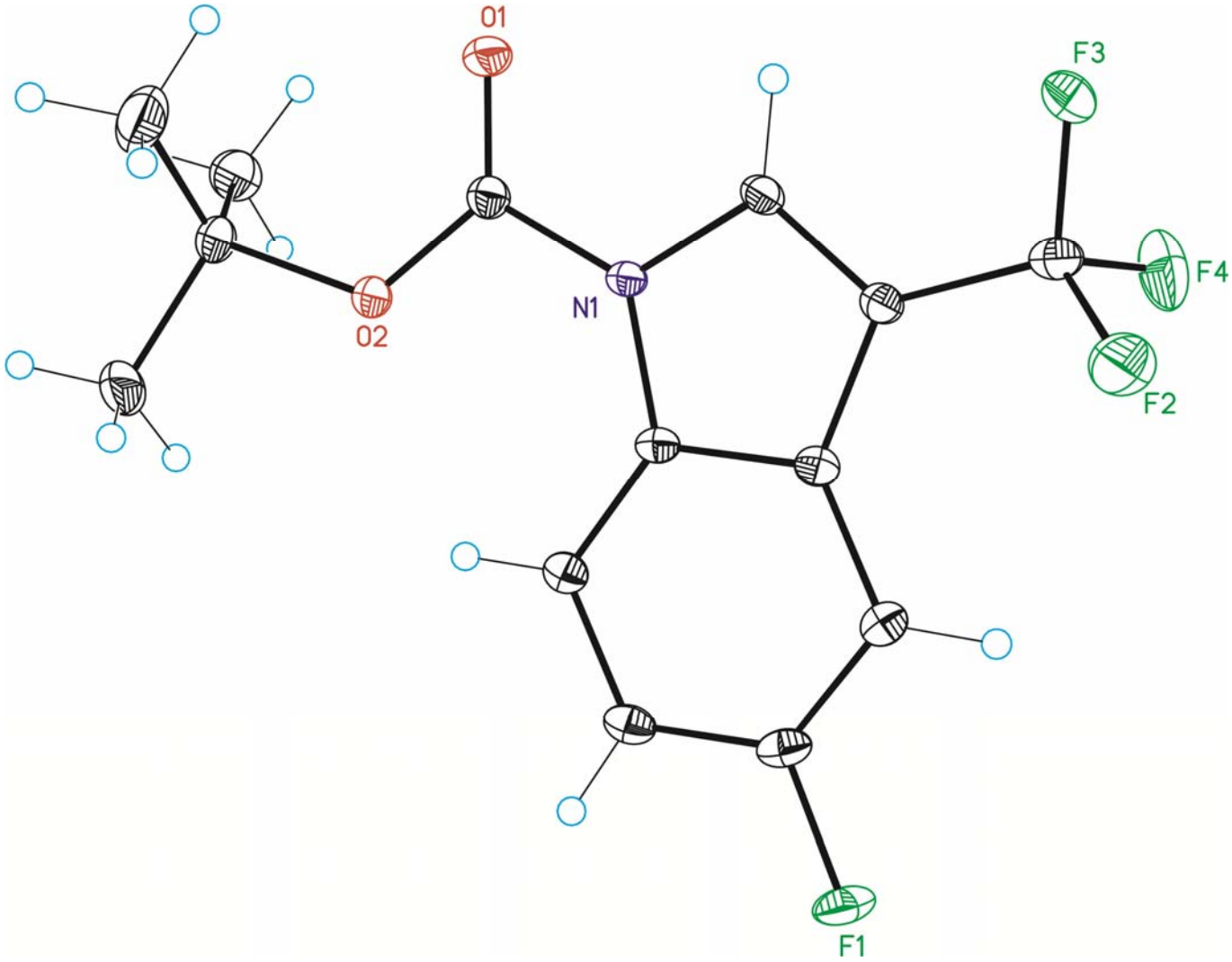

Figure S84. ORTEP diagram of compound **2u** with 50% probability ellipsoid:
Black = carbon, Red = oxygen, Blue = hydrogen, Green = fluorine, Purple = nitrogen

Table S3. Crystal data and structure refinement for **2u**

CCDC	1533216	
Empirical formula	C14 H13 F4 N O2	
Formula weight	303.25	
Temperature	100(2) K	
Wavelength	0.71073 Å	
Crystal system	Monoclinic	
Space group	P2(1)/n	
Unit cell dimensions	a = 6.9858(6)Å	α= 90°.
	b = 23.733(2)Å	β = 90.395(3)°.
	c = 8.2231(8)Å	γ = 90°.
Volume	1363.3(2) $Å^3$	
Z	4	
Density (calculated)	1.477 Mg/m^3	
Absorption coefficient	0.135 mm^{-1}	
F(000)	624	
Crystal size	0.60 x 0.25 x 0.10 mm^3	
Theta range for data collection	1.716 to 30.283°.	
Index ranges	-9<=h<=6,-33<=k<=29,-11<=l<=10	
Reflections collected	11964	
Independent reflections	3977[R(int) = 0.0308]	
Completeness to theta =30.283°	97.7%	
Absorption correction	Empirical	
Max. and min. transmission	0.987 and 0.93	
Refinement method	Full-matrix least-squares on F^2	
Data / restraints / parameters	3977/ 51/ 220	
Goodness-of-fit on F^2	1.040	
Final R indices [I>2sigma(I)]	R1 = 0.0479, wR2 = 0.1123	
R indices (all data)	R1 = 0.0634, wR2 = 0.1208	
Largest diff. peak and hole	0.488 and -0.323 $e.Å^{-3}$	

5. References

(1) (a) Cobo, I.; Matheu, M. I.; Castillón, S.; Boutureira, O.; Davis, B. G. Phosphine-Free Suzuki–Miyaura Cross-Coupling in Aqueous Media Enables Access to 2-*C*-Aryl-Glycosides. Direct C–H Trifluoromethylation of Glycals by Photoredox Catalysis. *Org. Lett.* **2012**, *14*, 1728–1731. (b) Wang, B.; Xiong, D.-C.; Ye, X.-S. *Org. Lett.* **2015**, *17*, 5698−5701. (c) Rodríguez, M. A.; Boutureira, O.; Díaz, Y.; Matheu, M. I.; Castillón, S.; Seeberger, P. H. Synthesis of 2-Iodoglycals, Glycals, and 1,1‘-Disaccharides from 2-Deoxy-2-iodopyranoses under Dehydrative Glycosylation Conditions. *J. Org. Chem.* **2007**, *72*, 8998–9001.

(2) (a) Zhang, L.; Zheng, M.; Zhao, F.; Zhai, Y.; Liu, H. Rapid Generation of Privileged Substructure-Based Compound Libraries with Structural Diversity and Drug-Likeness. *ACS Comb. Sci.* **2014**, *16*, 184−191. (b) Biswas, S.; Batra, S. One-Step Synthesis of 2-Amino-5*H*-pyrimido[5,4-*b*]indoles, Substituted 2-(1,3,5-triazin-2-yl)-1*H*-indoles, and 1,3,5-Triazines from Aldehydes. *Eur. J. Org. Chem*. **2012**, 3492–3499. (c) Kobayashi, Y.; Yamamoto, K.; Asai, T.; Nakano, M.; Kumadaki, I. Studies on Organic Fluorine Compounds. Part 35. Trifluoromethylation of Pyrimidine- and Purine-Nucleosides with Trifluoromethyl–Copper Complex. *J. Chem. Soc., Perkin Trans. 1*, **1980**, 2755–2761.

(3) Lishchynskyi, A.; Berthon, G.; Grushin, V. V. Trifluoromethylation of Arenediazonium Salts with Fluoroform-Derived $CuCF_3$ in Aqueous Media. *Chem. Commun.* **2014**, *50*, 10237–10240.

(4) (a) Lishchynskyi, A.; Novikov, M. A.; Martin, E.; Escudero-Adán, E. C.; Novák, P.; Grushin, V. V. Trifluoromethylation of Aryl and Heteroaryl Halides with Fluoroform-Derived $CuCF_3$: Scope, Limitations, and Mechanistic Features. *J. Org. Chem.* **2013**, *78*, 11126–11146. (b) Konovalov, A. I.; Lishchynskyi, A.; Grushin, V. V. Mechanism of Trifluoromethylation of Aryl Halides with $CuCF_3$ and the Ortho Effect. *J. Am. Chem. Soc.* **2014**, *136*, 13410−13425.